Theory of defect interactions in metals

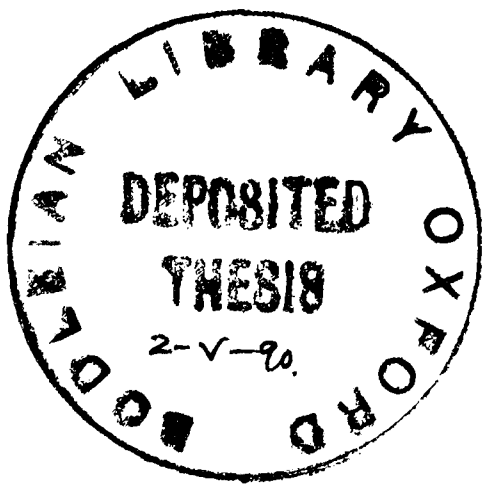

Roger Thetford
Linacre College

Thesis submitted for the degree of Doctor of Philosophy at the University of Oxford

Trinity Term 1989

Theoretical Physics Division
Harwell Laboratory

Department of Theoretical Physics
University of Oxford

September 1989

Theory of defect interactions in metals

Roger Thetford
Linacre College

Thesis submitted for the degree of Doctor of Philosophy at the University of Oxford

Trinity Term 1989

Abstract

The static relaxation program DEVIL has been updated to use N–body Finnis-Sinclair potentials. Initial calculations of self-interstitial and monovacancy formation energies confirm that the modified program is working correctly.

An extra repulsive pair potential (constructed to leave the original fitting unaltered) overcomes some deficiencies in the published Finnis-Sinclair potentials. The modified potentials are used to calculate interstitial energies and relaxations in the b.c.c. transition metals vanadium, niobium, tantalum, molybdenum and tungsten.

Further adaptation enables DEVIL to model dislocations running parallel to any lattice vector. Periodic boundary conditions are applied in the direction of the dislocation line, giving an infinite straight dislocation. The energies per unit length of two different dislocations are compared with experiment.

A study of migration of point defects in the perfect lattice provides information on the mobility of interstitials and vacancies. The possible reorientation of split dumbbell interstitials in a migration step comes under scrutiny. The total energy needed to form and migrate an interstitial is compared with that required for a vacancy.

The interaction between point defects and dislocations is studied in detail. Binding energies for both self-interstitials and monovacancies at edge dislocations are calculated for the five metals mentioned above. Formation energies of the point defects in the neighbourhood of the edge dislocation are calculated for niobium, and the extent of the regions from which the defects are spontaneously absorbed are found. For split dumbbell interstitials, the size and shape of the absorption region depends on the orientation of the dumbbell. Migration of both interstitials and vacancies into the absorption zone is studied; the presence of the dislocation has a particularly dramatic effect on vacancy migration. The results on absorption zones are related to the dislocation sink strengths vital in radiation damage theory.

Theoretical Physics Division,
Harwell Laboratory,
Didcot,
Oxon.
OX11 0RA

Department of Theoretical Physics,
1, Keble Road,
Oxford.
OX1 3NP

September 1989

CONTENTS

LIST OF FIGURES

Acknowledgements

Many people have helped me to write this thesis. Those who guided me, exchanged ideas and provided information and results include Dr. Mike Finnis, Dr. Jim Sinclair and Dr. Tony Harker of Theoretical Physics Division, Harwell, Professor David Bacon of Liverpool University and Dr. Tom van Veen of Delft University. I am grateful to Dr. Ron Bullough F.R.S. of Harwell, who had the original idea for this project, Sir Roger Elliott F.R.S. from the Department of Theoretical Physics, Oxford, (now with Oxford University Press) and Dr. Peter Savill of Linacre College, Oxford, who have all acted as mentor in some official capacity.

The production of this thesis as a document would not have been possible without Dr. Mike Hopper of Computer Science and Systems Division, Harwell, and his 'Typesetting System for Scientific Documents'. Confidently, I leave you the reader to judge its quality.

Finally, I would like to thank two friends: my Harwell supervisor Dr. Juan Matthews, and Dr. Graeme Ackland. I have worked long and often with both, and it has been a pleasure.

The work described in this thesis is part of the longer term research carried out within the Underlying Programme of the United Kingdom Atomic Energy Authority (UKAEA). I am grateful to the UKAEA for paying my university fees.

Preface

Style

I have chosen to write this thesis in the first person singular. Although this is not the traditional manner, I believe that this style is easier to read and is fast gaining both popularity and *(ergo)* acceptability. Similarly, I have used the active voice where possible.

I have tried throughout to explain my work as I would want it explained to me. The expert may find this tiresome on occasions, but I think that it is worthwhile.

Finally, I have tried to include the titles of papers in the reference list. While the initiate will know immediately that 'Peach and Miller, *P.R.B.* **99** 1234 (1989)' is the crucial paper in the field, the tyro will appreciate a title: with a larger handle to grasp, the memory's grip will be that much firmer.

Notation

The standard notation for Miller indices can be hard to understand: I for one could not find a clear statement of what was meant by the various shapes of brackets used. For the uninitiated, I therefore offer the following:

(1,1,1) denotes a particular point, in Cartesian coordinates. This form is also used for a vector of definite length.

[111] denotes a line parallel to the vector from (0,0,0) to (1,1,1).

$\langle 111 \rangle$ denotes the set of lines of type [111]: i.e. [111], [11$\bar{1}$], [1$\bar{1}$1], [1$\bar{1}\bar{1}$], [$\bar{1}$11], [$\bar{1}$1$\bar{1}$], [$\bar{1}\bar{1}$1] and [$\bar{1}\bar{1}\bar{1}$].

(111) denotes the particular set of planes that is normal to the [111] direction.

$\{111\}$ denotes the set of planes of type (111): i.e. all planes normal to one of the $\langle 111 \rangle$ lines.

The lattice parameter a is the length of the edge of the cube defining the body-centred cubic structure. The separation of nearest neighbours in the body-centred cubic (b.c.c.) lattice is therefore $\frac{1}{2}a\sqrt{3}$. For the sake of brevity, I have usually excluded the a when quoting atom positions. Occasionally its inclusion makes a phrase read better.

Contributions of Other People

Inevitably and for the sake of clarity, I have needed at times to describe the work of other people. The largest such section comes in §1.4, where I introduce the idea of the many-body potential and describe in detail the construction of the Finnis-Sinclair potential.

M.J. Norgett initiated the DEVIL program described in chapter 2 and used as a tool throughout. I am not sure that he would recognise the program in its current state, but many of his ideas are still there.

G.J. Ackland performed the calculation of the pressure-volume curves referred to in the text of chapter 3, and also constructed the revised potential (§3.1.2). Chapter 3 deals mainly with calculations using the new potential; apart from the five molecular dynamics calculations (Ackland again) in table 3.4, these are all my own work.

At various other places I refer to results produced by other people: these are identified by the appropriate references. Similarly, where I have consciously borrowed a method, I quote the originators.

I have made use of subroutines written by J.E. Sinclair to help set up dislocations in my calculational blocks and to ease the task of displaying my results; he is duly accredited when these subroutines are mentioned in the text.

1 Introduction

1.1 Metals in Nuclear Reactors

Using a nuclear reactor is an attractive way to generate electricity, without the resource and pollution problems associated with fossil fuels. However, radiation is also generated and this can affect the materials used to build the reactor. The 14 MeV neutrons produced from nuclear fusion reactions and the fast neutrons, alpha particles and fission fragments produced by nuclear fission are all capable of causing 'radiation damage' in reactors.

An energetic particle will cause a 'cascade' of damage: after knocking one atom out of its lattice site, both the original particle and the displaced atom will usually have enough energy to knock still more atoms out of position. This process of Frenkel pair production will eventually dissipate enough energy to slow each of the blitz of particles to below the Frenkel defect production energy. The resulting cascade tends to be a chaotic region, with a vacancy-rich interior and a high concentration of self-interstitial atoms round the boundary.

Some of the interstitial atoms, referred to henceforth simply as interstitials, will recombine with nearby vacancies. But the interstitials have a lower barrier to migration than do the vacancies: many interstitials migrate into undisturbed regions of lattice, and are eventually absorbed at 'sinks' of various types (see §1.2 and §6.1 for more detail). The cascade eventually anneals out, or collapses into vacancy loops, platelets, stacking faults, *et cetera.*

This process is extremely intense. In fact, the cladding of fuel pins going to high burnup in Dounreay's Prototype Fast Reactor (PFR) is experiencing doses of over 100 displacements per atom (dpa). Averaging over the pin's lifetime, each atom in the stainless steel clad is likely to be knocked out of position *over one hundred times!*

Various physical changes arise from this massive damage to the cladding material. Easiest to understand is irradiation creep: just as thermal production of defects in a stressed bar of metal will eventually lead to distortion of the bar, so metals creep under irradiation. An edge dislocation with its Burgers vector parallel to an applied tension will tend to absorb interstitials more readily than one with a perpendicular Burgers vector; the growing extra half-plane of atoms will gradually jack apart the rest of the lattice. The phenomenon of 'growth' was first seen in the uranium metal fuel of early Magnox reactors. Fuel that fitted nicely into its can when loaded into

the reactor could come out protruding by several centimetres. Again, this is due to preferential absorption of interstitials at dislocations with certain orientations.

The Canadians have had to spend several millions of dollars recently on their CANDU reactors because of a problem with anisotropic irradiation creep and growth [Field, 1987]. When the reactors were designed, the properties of the material chosen for the horizontal reactor tubes were not well known; a few years ago examination revealed that the tubes had lengthened more than expected and could expand no further. The problem was fairly easily overcome in most of the CANDU's, but a different design of those at the Bruce site led to severe difficulties. The only way to save the Bruce reactors was to cut the ends off all the tubes and re-weld them, in a delicate remote-handling operation [Jurewicz, 1987].

If a void (a cluster of vacancies) in the lattice absorbs more vacancies than interstitials 'void swelling' results. This worrying phenomenon, first observed by Cawthorne and Fulton [1966] in material from the Dounreay Fast Reactor (DFR), is a powerful limiting factor in the life of a reactor fuel subassembly.

Matthews [1989] reviews succinctly the diverse effects of bombarding metals in a reactor with neutrons.

Much effort worldwide has been expended on trying to find metals that combine good swelling behaviour with desirable mechanical properties (high tensile strength without excessive brittleness after irradiation). From fairly conventional stainless steels to high-nickel alloys to steels containing dispersions of yttrium oxide, the search continues. For all the materials so far investigated, swelling is minimal up to a certain 'incubation dose', and then takes off rapidly. Understanding the microstructure of the metal — how monovacancies cluster to produce voids, what happens to the interstitials, *et cetera* — is the key to finding a good cladding material. And this is the province of radiation damage theory.

1.2 Radiation Damage Theory

The aim of radiation damage theory is to solve the diffusion equations for the concentration of interstitials and vacancies in the complicated medium containing also dislocations, grain boundaries, interstitial platelets, vacancy loops and voids. All of these 'sinks' can absorb the point defects, and of course the radiation damage process is continually generating new pairs of defects. Some sinks (particularly dislocations) have a strong stress field; the

strains around the point defects produce an interaction energy which must be considered in the diffusion equations. Although the problem of diffusion round a single sink may be tractable, severe complications arise in a material with a random array of different sinks. The problems are excellently reviewed by Brailsford and Bullough [1981]; Brailsford, Bullough and Hayns [1976] give the solution to the basic equation for diffusion around a sink embedded in a 'lossy medium'.

Dislocations are termed 'biased sinks', in contrast to voids (for example) which are 'neutral sinks'. Dislocations are 'biased' because interstitials feel their stress field at a longer range than vacancies do; hence more interstitials than vacancies are absorbed at dislocations. The resulting slight imbalance in numbers of interstitials and vacancies arriving at voids in the lattice leads to the void swelling mentioned above.

The 'strengths' of the sinks can be rigorously defined (see §6.1) from solutions to the diffusion equations. Given these sink strengths, the problem can be recast to look like chemical rate theory: interstitials and vacancies act like chemical species, reacting with one another and with the sinks present, with rate constants determined by the sink strengths. The phenomenon of point defect absorption at sinks is thus central to understanding the behaviour of metals under irradiation.

Early work tended to use continuum elasticity theory to model defects in metals. The stress field of a dislocation, proportional to $\sin\theta/r$ in (r,θ,z) polars with the z axis along the dislocation line, is well known. Point defects can be represented by inclusions in the elastic continuum: these can have different moduli to the host medium, and can also have a size mismatch, leading to a local distortion. Bullough and Willis [1984] review in detail work on the elasticity model. The major problem arises at the dislocation core, where the expression for the stress has a singularity. All the elastic continuum theories employ some sort of fudge at this point; a realistic treatment must take into account the discrete nature of matter.

1.3 Atomistic Modelling of Radiation Damage

The model used in atomistic modelling is also an approximation, but is on a finer scale than the model of an elastic continuum described above. Each atom is treated as a neutral point mass, interacting with its neighbours via some potential. The potential will hopefully represent the effect of the electrons in the material; the electrons are not modelled separately.

The beauty of these computer experiments is that one has so much *control*

over the situation. Experimentally, any process (for example electron irradiation, neutron bombardment or plastic deformation) used to produce say vacancies, will also produce other defects. Experimentalists have devised many subtle ways of studying point defects in metals, but they are never observing a defect as 'clean' and isolated as the computer can model. Any study trying to observe monovacancies, for example, is always complicated by the presence of di- and tri-vacancies.

I have explained above the motivation for studying the behaviour of point defects in the neighbourhood of dislocations. This section aims to give an indication of how atomistic modelling works, and how early work with pair potentials has evolved to the more sophisticated methods employed today.

Once computers became widely available, many people embarked upon computer simulations of solids. The obvious way to set up a crystal was to take a set of atoms in a regular array, define an interatomic potential ϕ which is a function only of the interatomic distance $r_{ij} = |\mathbf{r}_i - \mathbf{r}_j|$ and calculate the total energy of the array by summing over the lattice:

$$U = \sum_{i,j} \phi(r_{ij}) \tag{1.1}$$

The pair potential ϕ will tend to have a finite range, usually not beyond the third or fourth shell of neighbours, so the double sum need not be taken over the whole lattice. The form of ϕ depends on the system under study. For an ionic crystal, ϕ describes just Coulomb attraction, with some sort of repulsive term at short range to model the internuclear repulsion. For a metal, many different prescriptions for ϕ were proposed: the Johnson potentials for iron [Johnson, 1964] and many variants of the Morse potential [Girifalco and Weizer, 1959; Schober, 1977; Dederichs, Lehmann, Schober, Scholz and Zeller, 1978] are just examples. Typically, the potentials were fitted to the equilibrium lattice parameter, the (unrelaxed) vacancy formation energy, and various elastic constants.

The procedure used thereafter has not changed, except perhaps in the number of atoms that can be studied. The calculation takes a block of atoms, usually cuboidal, surrounded by a boundary layer. The N_{free} atoms in the inner region are free to move, under the influence of each other and the boundary. The boundary can either be fixed (a region of atoms in fixed positions) or cyclic (a periodic boundary condition makes atoms in the boundary images of atoms from the free region, related by a fixed translation). After introducing one or more defects, a computer program relaxes the block by altering the atomic positions until a suitable convergence criterion is satisfied. Ideally, in equilibrium the forces on all the atoms would go to zero; in practice some cut-off has to be employed.

To evaluate the sum in equation (1.1), one may look at all pairs of atoms in the lattice, discarding those that are separated by more than the range of the potential. This tends to be expensive on computer time though. At the cost of storing some large arrays, a list of neighbours may be kept for each atom in the lattice: to evaluate the sum one simply considers all the neighbours of each atom in turn. Between these two extremes lies the 'link cell method': the block is divided into a number of cells, and a list defines which cells neighbour which others. The atoms in one cell are then allowed to interact with all other atoms in that cell, plus all those in neighbouring cells. Of course, in the limit of one-atom cells this procedure becomes the full neighbour list method, while if one cell spans the whole block, we have the all-feel-all method.

The method used in DEVIL to find neighbours cleverly exploits the periodicity of the lattice structure. If a perfect lattice is counted plane by plane, the neighbours of one atom will form the same pattern in the linear array as those of another atom. A given lattice vector will correspond to the same difference in ordinal numbers: the vector from atom 23 to atom 56 will be the same as that from atom 25 to atom 58, provided the boundaries are treated suitably. Section 2.2.1 discusses this topic in more detail.

The two best-known methods for relaxing the lattice are quenched molecular dynamics (MD) and static relaxation. In a quenched MD calculation, initialisation gives all the free atoms random velocities. The atoms then move according to Newton's equations, under the forces arising from the potential; the calculation proceeds with a small timestep δt. In an attempt to find the minimum (zero force), each atom has its velocity $\mathbf{v}$ zeroed when the program detects that the acceleration $\mathbf{a}$ has changed sign (in fact, a change in sign of the *scalar* $\mathbf{a}\cdot\mathbf{v}$ is the usual trigger, being much easier to implement). The initial kinetic energy is gradually quenched out of the block; the equipartition principle gives the potential energy and thus an equivalent temperature is available after every sweep through the lattice. The method is comparable in speed to other relaxation procedures, and does have two advantages: the random velocities mean that the system can escape from high-lying shallow minima in the energy; also, removing the quenching term gives immediately a useful MD program.

Static relaxation calculations have no timestep δt. Instead, the energy of the block and the forces on the atoms are evaluated for a given configuration; the atoms are then moved to a new position and the process repeated. Each step can move 'downhill' in the many-dimensional space of energy against the $3N_{free}$ atom coordinates, and convergence is guaranteed.

The simplistic method of always taking the steepest descent can sometimes hit trouble (oscillating up and down the sides of a U-shaped valley, for example). Lidiard and Norgett [1972] suggested that the method of conjugate gradients [Fletcher and Reeves, 1964] was appropriate for this type of calculation.

Norgett accordingly wrote the first version of DEVIL, using a scheme whereby each atom moves along 'search direction' $\mathbf{s}_i$. Initially, $\mathbf{s} = \{\mathbf{s}_i\}$ is just the set of forces $\mathbf{g} = \{\mathbf{g}_i\}$ on the atoms i, but thereafter the $3N_{free}$–dimensional vector $\mathbf{s}$ is modified to be perpendicular to the search directions previously employed: the energy should already have been minimised with respect to changes in those directions. The calculation continues iterating until $\mathbf{g}\cdot\mathbf{g}$ is less than a predefined limit. This can occur in a *local* minimum rather than the global minimum, and can also occur at a saddle point. While the randomness of an MD simulation will cause the system to 'fall off' the saddle, a precise static relaxation calculation may well find the flat saddle point. Symmetry frequently contributes to this problem. A static relaxation will preserve the symmetry of the starting position, unless numerical rounding error intervenes: although at first sight the ⟨110⟩ dumbbell interstitial inserted into molybdenum seems stable with the Finnis-Sinclair potential, in fact a form with the dumbbell rotated away from ⟨110⟩ has a lower energy (see chapters 2 and 3). Section 2.3 describes more completely the full implementation of the minimisation algorithm.

Figure 1 shows the progress of a typical relaxation: note that the scale is logarithmic. One iteration comprises minimising the energy in each search direction. The numbers in parentheses along the 'iterations' axis are the number of function calls made: the average number required to find the minimum in any particular search direction is somewhat less than two. $E0$ is the energy being sought; both E and $E0$ are measured in eV, while $\mathbf{g}$ is measured in the (slightly odd, but convenient) units of eV per lattice constant.

Stress can be applied to the crystal by imposing strains, calculated from elasticity theory, on the atoms in the boundary region. Similarly, as the strain field around a dislocation is known (see for example Hirth and Lothe [1968]), applying appropriate strains to the boundary atoms enables the modelling of dislocations.

The topics studied include interstitial loops in iron [Bullough and Perrin, 1968], the core structure of screw dislocations in b.c.c. metals [Vitek, Perrin and Bowen, 1970], edge and screw dislocations in copper [Norgett, Perrin and Savino, 1972], stacking faults [Bristowe, Crocker and Norgett, 1974],

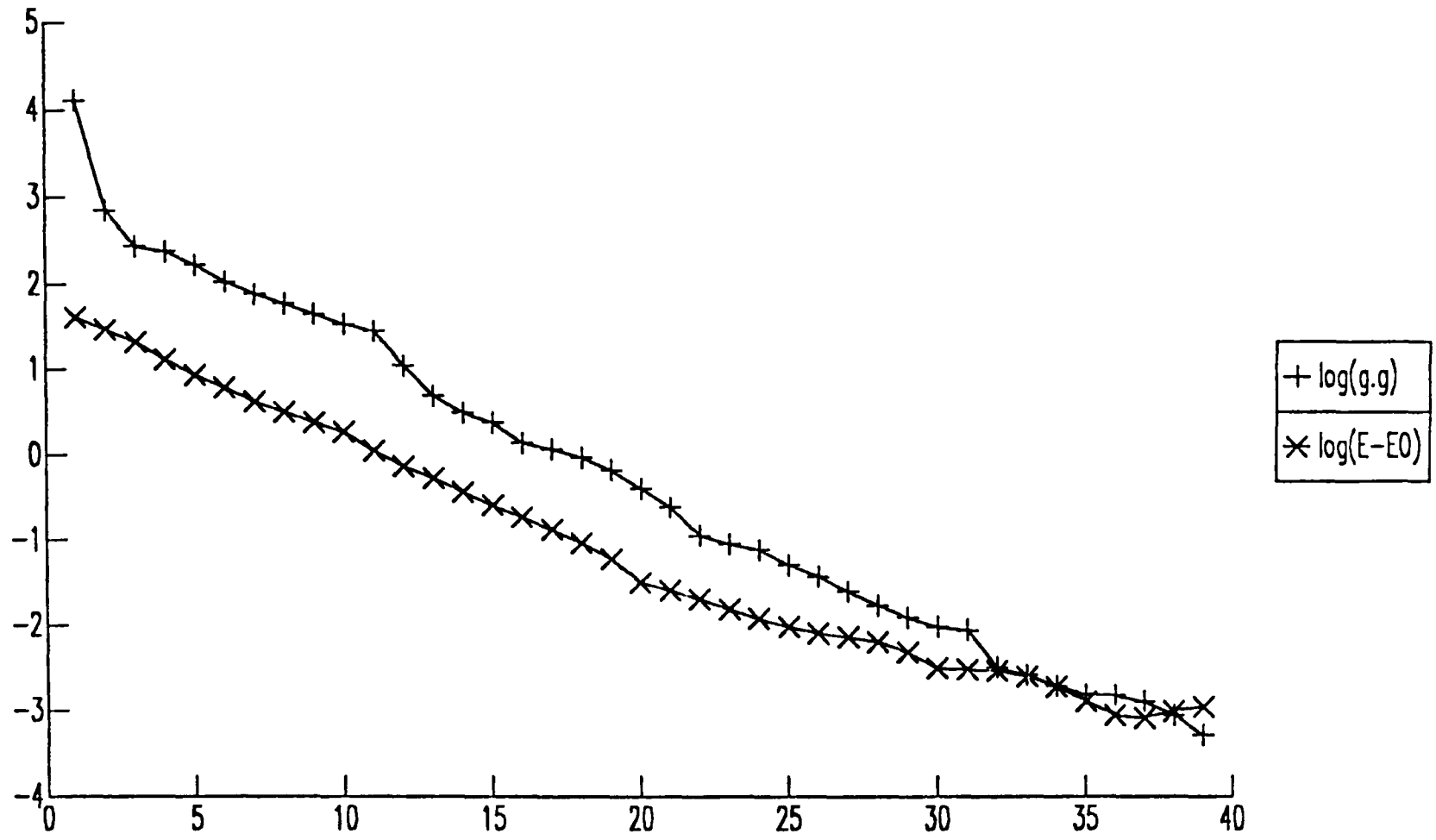

Figure 1. Progress of DEVIL minimisation

and self-interstitial diffusion in tungsten [Guinan, Stuart and Borg, 1977]. A good example of the entire procedure, from setting up a potential to calculating defect properties, is the paper by Miller [1981].

1.4 Interatomic Potentials

In the atomistic modelling of transition metals, pair potentials have been found to be insufficient to explain a number of observations. In any purely pairwise model, the relation $C_{12}=C_{44}$ (where C_{12} and C_{44} are components of the elastic modulus tensor) necessarily holds. For a real metal this is rarely the case, and one has a 'Cauchy discrepancy' or 'Cauchy pressure' of $\frac{1}{2}(C_{12}-C_{44})$. In order to keep the block of material in equilibrium, at the correct lattice parameter, 'ficticious forces' equal to the Cauchy pressure. must be applied to the surface. (For example Guinan *et al.* [1977] applied 0.2 Mb to the surface of their tungsten block.) The *free* surface of a metal shows an outward relaxation, contrary to experiment and also to intuition: if an atom sitting in the bulk were suddenly to lose about half of its neighbours, the local electron density would also drop. Trying to regain an equilibrium electron density, the surface atom would tend to move towards its undisturbed neighbours: i.e. inwards.

The advance from 2-body (pair) potentials to N–body potentials for b.c.c. transition metals enabled systems to be modelled without applying the fictitious forces that were previously necessary.

In the early 1980's, various workers proposed potentials that went beyond pair potentials. Although still simple to calculate, these 'N–body' potentials overcame some of the drawbacks afflicting pair potentials.

Stott and Zaremba [1980] proposed the idea of 'quasiatoms' for treating impurities in metallic systems. They calculated the energy of the system by applying density functional theory to the impurity ion plus its electronic screening, considered as a quasiatom in the host electron density. Similar ideas were being used by Nørskov [Nørskov and Lang, 1980; Nørskov, 1982] calculating heats of chemisorption using 'Effective Medium Theory', where a hydrogen atom, for example, sees an effective medium consisting of the electron density of a host metal.

Daw and Baskes [1984] realised that this approach could be extended, and *every* atom in a metal could be considered as being embedded in the host consisting of all the other atoms. In their embedded atom method (EAM), the electron density at the site of one atom is calculated by adding up the contributions from all of the other atoms in the lattice, each considered as a free atom. The free atom electron densities come from Hartree-Fock theory. If the summed electron density is ρ, then the energy of an atom at that site can be written as $f(\rho)$, where f is some functional called the embedding function: this will be the same for all atoms of an element, regardless of their local environments. The equation for the energy is essentially just (1.3), the same equation used by Finnis and Sinclair [1984] and which will form the basis of this thesis. Fitting the form of f to experimental quantities gives a definite prescription that can be applied to alloys for example: just sum the free-atom electron densities of the different constituent atoms at each lattice site, apply f to get the energy and sum over the whole block of alloy. This approach enables the calculation of many quantities of interest that previously caused trouble to users of pair potentials: for example surface energies and reconstructions, and the behaviour of hydrogen in metal (migration, binding to vacancies, and so on) [Daw and Baskes, 1984]. Daw [1989] provides a broad justification of the EAM in terms of the detailed behaviour of electrons, using density functional theory. His analysis is most rigorous for simple metals and for transition metals with nearly full or nearly empty d–bands.

Similar again was the work of Ercolessi, Tosatti and Parrinello [1986], who fitted their 'glue model' to lattice parameter, cohesive energy, surface tension, bulk modulus and X–point transverse phonon frequency in noble metals. The paper by Ercolessi, Parrinello and Tosatti [1988] is an example of a calculation with the glue model.

Although quite different in philosophy, the method used by Finnis and Sinclair [1984] parallels the Daw and Baskes EAM. Finnis and Sinclair assume that the function f in equation (1.3) is going to be a square root. They then fit the contributions to the electron density ρ of the neighbouring atoms by parameterising ϕ suitably. Ackland [1987] and Ackland, Finnis and Vitek [1988] describe the justification for the square root form for f. Ackland investigates three different models of the local d–electron density of states (DOS) — rectangular, Gaussian and double-Gaussian — within the second-moment approximation of tight-binding theory. In each case, the energy change caused by a local deformation comes out to be proportional to the change in the square root of the second moment of the density of states (DOS). The second moment of the DOS is a measure of the coordination of a particular atom, but so is ρ, being the sum of terms representing electron densities round neighbouring atoms. Hence the energy change is proportional to $\rho^{\frac{1}{2}}$.

The model of the energy due to Finnis and Sinclair (1984) comprises an attractive many-body term and a repulsive pair potential. The total energy of the configuration of atoms is written as

$$U_{tot} = U_N + \tfrac{1}{2}\sum_{ij} V_{FS}(R_{ij}) \qquad (1.2)$$

The second term is a conventional pair-potential summation, while the N–body term has the form

$$U_N = -A \sum_i f(\rho_i) \qquad (1.3)$$

where

$$\rho_i = \sum_j \phi(R_{ij}) \qquad (1.4)$$

and the separation R_{ij} of atoms i and j is

$$R_{ij} = |\mathbf{R}_{ij}| = |\mathbf{R}_j - \mathbf{R}_i| \qquad (1.5)$$

As discussed above, $f(\rho) = \rho^{\frac{1}{2}}$ reproduces the expression arising from tight-binding theory.

Finnis and Sinclair parameterised ϕ and V_{FS} in a purely empirical way, as

$$\begin{aligned} \phi(r) &= (r-d)^2 && r \leqslant d \\ &= 0 && r > d \end{aligned} \qquad (1.6)$$

$$\begin{aligned} V_{FS}(r) &= (r-c)^2(c_0 + c_1 r + c_2 r^2) && r \leqslant c \\ &= 0 && r > c \end{aligned} \qquad (1.7)$$

The cutoffs d and c lie between the second and third neighbour separations in the b.c.c. structure. Although the N–body term is designed to model

metallic cohesion, leaving the pair potential to cover internuclear repulsion, the nominally repulsive pair potential turns out to be slightly attractive over a small range of interatomic distance for some of the metals considered by Finnis and Sinclair. This fact is unimportant.

Ackland [1987, §2.7] describes in detail the procedure of fitting the parameters of the potential to measured values of elastic constants, cohesive energy and lattice parameter.

The method of conjugate gradients that is used in DEVIL requires, for a given configuration, the values of total energy and the forces on the atoms. The pair-potential part U_P is straightforward, giving a force

$$-\frac{\partial U_P}{\partial R_{i\alpha}} = \sum_{k \neq i} \frac{V'_{FS}(R_{ik})\, R_{ik\alpha}}{R_{ik}} \tag{1.8}$$

(with R_{ij} defined as in equation (1.5), $\partial R_{ik}/\partial R_{i\alpha} = -R_{ik\alpha}/R_{ik}$). The force on atom i due to U_N is given by (note that there is a slight error in equation (21) of Finnis and Sinclair [1984])

$$-\frac{\partial U_N}{\partial R_{i\alpha}} = -A \sum_{k \neq i} (f_i' + f_k')\phi'(R_{ik})\, R_{ik\alpha}/R_{ik} \tag{1.9}$$

where $x_{i\alpha}$ is the α–component of vector $\mathbf{x}_i$, and

$$f_i' = \left.\frac{df(\rho)}{d\rho}\right|_{\rho=\rho_i} \tag{1.10}$$

Several workers have used these N–body potentials successfully, to calculate properties of vacancies [Matthai and Bacon, 1985, Maysenhölder, 1986] interstitial clusters [Harder and Bacon, 1988] and surfaces [Ackland and Finnis 1986] in various b.c.c. transition metals.

All of the properties used by Finnis and Sinclair to produce their potential refer to the material in its *equilibrium* state: no atoms are closer than their equilibrium separation. Simply extrapolating the original potentials to small interatomic distances is unlikely to give good results, and indeed it does not. Ackland and Thetford [1987, and chapter 3 of this thesis] and Rebonato, Welch, Hatcher and Bilello [1987] both found it necessary to introduce some information on the behaviour of atoms in close proximity, and to alter the potential accordingly. Ackland and Thetford used information from electron gas potentials, and added a repulsive term to the pair potential $V_{FS}(r)$, of the form $B(r_0-r)^3 e^{-\alpha r}$ (r is the interatomic separation and r_0 the equilibrium value of r). Rebonato *et al.* added a term proportional to $(r_0-r)^3$ to the pair potential, on the basis of pressure-volume curves. Chapter 3 presents calculations using the Ackland and Thetford modification to the Finnis-Sinclair potentials.

In response to a paper pointing out that the Finnis-Sinclair potentials predict some of the thermal expansion coefficients to be negative [Marchese, Jacucci and Flynn, 1988], Rebonato [1989] has further modified the potentials. He adds a quintic polynomial to the pair potential between first and second neighbours, thus correcting the erroneous anharmonic behaviour found when the lattice parameter is increased from its equilibrium value. Sutton [1989] has found that the modified Finnis-Sinclair potentials reproduce satisfactorily the average Grüneisen parameter.

Owing to the different approach of Finnis and Sinclair compared to Daw and Baskes, the Finnis-Sinclair potentials are not immediately applicable to alloys. With a fixed (square root) form for f, any influence of the type of the neighbours on the cohesive part of the energy must be included in the $\phi(r)$ term. (Unlike in the EAM where the ϕ's are fixed from single atom electron densities, and the f is parameterised.) Rebonato [1989] gives one possible way for extending the treatment to model alloys; Ackland and Vitek [1989] give another. Both involve some extra fitting to alloy potentials. While *in principle* the EAM need not be refitted, Maarleveld, Kaars, Weeber and Bakker [1986] found that in practice the unmodified form of the EAM gave poor results in alloys. Foiles, Baskes and Daw [1986] have now produced versions of the EAM functions for application to alloys, by including the alloy heats of solution in their fitting procedure.

1.5 Scope of this Thesis

I have updated the static relaxation program DEVIL to handle N–body potentials of the Finnis-Sinclair type. Chapter 2 deals with the modifications to DEVIL, and the early calculation of interstitial and vacancy formation energies to check that the program was working correctly.

However, Ackland and Thetford [1987] found the original FS potentials to be suspect in their behaviour at short distances. Chapter 3 describes some of the problems encountered, and how a new repulsive core was added to enable meaningful modelling to be carried out. The new potentials are then applied to the calculation of interstitial energies and relaxations.

Dislocations are vitally important in determining the behaviour of metals. Chapter 4 describes how dislocations can be modelled using DEVIL, and presents some results on the stability of dislocations and the effect of the position of the dislocation line with respect to the atoms in the unit cell.

DEVIL is easily adapted to model migration of point defects, and many experimental results exist for quantities such as vacancy migration energies.

Chapter 5 presents the results of DEVIL calculations on interstitial and vacancy migration, and where possible compares the results with measurements. In the light of the DEVIL calculations, the discussion considers the controversy over whether interstitials or vacancies are migrating during 'stage III recovery' of irradiated metals.

The main motivation for this work was to study in detail the absorption of point defects at dislocations. With the framework for modelling point defects and dislocations in place, chapter 6 studies the interaction between interstitials and dislocations, concentrating on absorption and migration behaviour.

In Appendix 1 I provide a user manual for DEVIL, with details of how to use the program, the various options available and some information on the inner workings of the code.

Appendix 2 collects all the point defect formation, migration, and binding energies and presents them together, with information on the sizes of blocks and boundary conditions used to calculate them.

2 Validating DEVIL with N–body Potentials

2.1 Introduction

The DEVIL code was written in the early 1970's at Harwell, to undertake static relaxation of crystals containing defects. Early applications included studying the splitting of dislocations in copper into partial dislocations [Norgett, Perrin and Savino, 1972]; twin boundaries in b.c.c. metals [Bristowe, Crocker and Norgett, 1974]; and a comparison of the diffusion of silver in lithium with that of gold in sodium [Schober, Taylor, Norgett and Stoneham, 1975].

DEVIL is a suitable program for investigating the properties of crystal defects (point defects and dislocations), employing a new type of interatomic potential proposed by Finnis and Sinclair [1984] and described in chapter 1. The important feature of this potential is that it is not a pair potential, so DEVIL needed considerable modifications in the subroutines that calculate crystal structure. Instead of performing just one pass through the crystal to calculate energies and forces, two passes became necessary. The changes to DEVIL are described below. As DEVIL has not hitherto received extensive documentation, some notes on how the code works, and how the user should set about performing a run, are included as Appendix 1.

2.2 Description of DEVIL

2.2.1 Basic pair-potential version

The atoms over which calculation takes place are divided into two regions: 'inner' and 'outer'. The size of the former is that specified by the user, and is that over which the relaxation takes place. The latter is the boundary region, which can be either fixed or cyclic (i.e. a translated image of the main crystal). The size of this boundary region is determined by the range of the potential.

An algorithm based on an index function is used to determine a neighbour list which applies to each atom in the inner region. This is efficient in both storage and execution time. An example of the neighbour list for a b.c.c. metal is given in table 2.1; it extends to second neighbours only. Throughout the calculation, set of 'Δ index' values is added to the index of atom i to give the indices of its neighbours k. The index function is calculated so that the difference in index is the same for any pair of atoms that are linked by the same lattice vector.

For illustration, suppose that the base atom to which the displacements in table 2.1 are applied is at (0, 0, 0), and has an index value of I. Neighbour 2 is then at ($-\frac{1}{2}$, $-\frac{1}{2}$, $-\frac{1}{2}$) and has a vector ($-\frac{1}{2}$, $\frac{1}{2}$, $\frac{1}{2}$) to neighbour 1 at (−1, 0, 0). The indices of these two atoms are $I-114$ and $I-212$ respectively: the second is obtainable from the first by subtracting 98. Similarly neighbour 10 is at ($\frac{1}{2}$, $-\frac{1}{2}$, $-\frac{1}{2}$) and has index $I+98$; subtracting 98 produces, I, the index of the atom at (0, 0, 0) which is once more a vector ($-\frac{1}{2}$, $\frac{1}{2}$, $\frac{1}{2}$) away. Neighbours 6 (index $I-14$) and 3 ($I-112$), 7 ($I-2$) and 4 ($I-100$), 11 ($I+100$) and 8 ($I+2$), 12 ($I+112$) and 9 ($I+14$), 14 ($I+212$) and 13 ($I+114$), and the original atom (I) and neighbour 5 ($I-98$), are all related by the same vector ($-\frac{1}{2}$, $\frac{1}{2}$, $\frac{1}{2}$) and have the same difference in index. Of course, this scheme applies to the whole lattice and not just the neighbours of one particular atom.

No.	Neighbour displacements			Δ index
1	−1.00	0.00	0.00	−212
2	−0.50	−0.50	−0.50	−114
3	−0.50	−0.50	0.50	−112
4	−0.50	0.50	−0.50	−100
5	−0.50	0.50	0.50	−98
6	0.00	−1.00	0.00	−14
7	0.00	0.00	−1.00	−2
8	0.00	0.00	1.00	2
9	0.00	1.00	0.00	14
10	0.50	−0.50	−0.50	98
11	0.50	−0.50	0.50	100
12	0.50	0.50	−0.50	112
13	0.50	0.50	0.50	114
14	1.00	0.00	0.00	212

Table 2.1 Neighbour list for a b.c.c. lattice.

DEVIL relaxes the lattice by using the method of conjugate gradients, which appears to work well [Norgett *et al.*, 1972] for atomistic modelling calculations. The original minimisation routine, DEV3, is a slightly modified version of the Harwell subroutine VA08A.

The conjugate gradients method demands both energies and gradients, and a user subroutine (POTEN) provides these. The FUNC subroutine steps through the lattice, calling POTEN to calculate the interaction between each pair of atoms. To avoid double-counting and because a pair-potential is symmetric over both atoms, each atom has, on average, only half of its neighbour list investigated: say all those atoms with a number higher than itself. The force on atom k due to atom $i<k$ is just the negative of that on i due to k, which will have been calculated already and added to the gradients of both. The interaction energy for that pair of atoms must be counted only once. This fairly trivial point is emphasised because it is in contrast to the case described in §2.2.2 below.

Interstitial atoms, henceforth called just 'interstitials', fall outside the method used to construct the neighbour list, which works on regions of perfect crystal. FUNC treats them separately, and assumes that they may in principle interact with any other atoms in the crystal — though of course only those within the range of the potential will actually contribute. A vacancy is modelled simply by flagging an atomic site as vacant, setting all of its interactions to zero, and thereafter ignoring it. Extended defects have to be modelled either by large numbers of point defects, or by giving each atom in the perfect crystal an initial displacement. The application to a fixed boundary region of displacements corresponding to, for example, a dislocation should force the inner region into a relaxed dislocation structure. Chapter 4 discusses this procedure in more detail.

2.2.2 Version to handle N–body potentials

There is an important difference between the N–body potential and a pair potential. To perform the N–body sum of forces in equation (1.8), we require to know f_k' for all $k \neq i$: i.e. we need already to have summed the cohesive potential ϕ over the other atoms k of the lattice. It is this point which forces the modifications to DEVIL which are described below.

In the modified FUNC, the full neighbour list of each atom needs to be investigated. The atom number i is stepped downwards from the top of the 'free' inner region, and possible neighbours k are located. If k is beyond the range of the potential, the next possible neighbour is considered. If not, two cases arise.

(i) $k<i$. Calculate only the cohesive energy $\phi(R_{ij})$ and add it to the running sum ρ_i.

(ii) $k>i$. ρ_k will already be available, so a full calculation of the gradient in equation (1.9) may be carried out. To do the term involving f_i in both

$\partial U_N/\partial R_{i\alpha}$ and $\partial U_N/\partial R_{k\alpha}$, the value of $\phi'(R_{ik})R_{ik\alpha}/R_{ik}$ is stored and added to a running total. A flag is set so that when f_i' becomes available, at the end of the summation for this particular atom, the appropriate terms can be added to the gradient of the correct k atom, as well as to atom i. In addition, the value and gradients of the pair potential are calculated.

Interstitials are treated separately, but in essentially the same manner. No neighbour list is constructed as they are not part of the perfect crystal structure, so they are left free to interact — possibly — with all other atoms. The cases $k<i$ and $k>i$ are dealt with as above, and $k=i$ is excluded.

Unlike the original case, some calculation needs to be done for atoms in any fixed boundary region. For atoms in this boundary, a flag is set when POTEN is called. This flag results in only the value of $\phi(R_{ik})$ being calculated; f_i is then accumulated. The value of f_i is needed because as the inner atoms move, the sum of cohesive potentials for the boundary atoms will vary, and this in turn affects the forces on the 'free' atoms via equation (1.9). Problems can arise in calculating the total cohesive energy at a boundary atom, as some of its neighbours may not lie in the calculation region at all. For example, if an atom is in the $+x$ boundary layer, no information is likely to be available on its (100) neighbour. In this case, DEVIL uses the equilibrium separation for a (100) neighbour in the perfect crystal.

2.3 The Relaxation Calculation

Originally DEVIL used the Harwell subroutine VA08A to minimise the energy of the lattice. In order to get more information on how the calculation was going, Norgett used a modified version with extra printing. Moving away from the library routine has the disadvantage that advances in numerical methods used in the Harwell subroutine library are not included in the code as they happen, but it has the advantage that the algorithm can be optimised to make it more suitable for the problem in hand. The modified VA08A, now called DEV3, incorporates some tuning which I shall now describe.

The method of conjugate gradients [Fletcher and Reeves, 1964] moves downhill in an N–dimensional space, in directions which are orthogonal to each other. For a particular search direction $\mathbf{s}$, DEV3 aims to satisfy the condition

$$\mathbf{g}\cdot\mathbf{s} = 0 \qquad (2.1)$$

Rather than waste a lot of time trying to satisfy this condition precisely, the

search is deemed satisfactory if $\mathbf{g}\cdot\mathbf{s}$ is reduced to less than a tenth of its value at the start of the step: that is, if

$$\mathbf{g}\cdot\mathbf{s} < 0.1(\mathbf{g}\cdot\mathbf{s})_{initial} \tag{2.2}$$

After each new choice of $\mathbf{s}$, a step length in that direction must be chosen; I improved the old algorithm for choosing such a step to a form more suited for the N–body potential problem. I also simplified the method of interpolation used when the initial step along $\mathbf{s}$ fails to satisfy (2.2), taking advantage of the form of the potentials. Once the calculation has made a few iterations, it will often satisfy the inequality (2.2) at the first attempt; a second estimate nearly always satisfies (2.2), usually with $\mathbf{g}\cdot\mathbf{s}\sim 0.001(\mathbf{g}\cdot\mathbf{s})_{initial}$. Finally, because the conjugate gradient algorithm never quite satisfies equation (2.1), some 'slack' develops in the method: after a certain number of iterations, a greater decrease in energy can be obtained by returning to the steepest descent rather than continuing in yet another conjugate direction. I have investigated the effect of altering the number of iterations taken before restarting in the steepest descent direction, and modified DEV3 accordingly.

I also tried the routine VA14A, which is meant to be a more modern version of VA08A. In fact VA14A ran more slowly than VA08A for cases where large relaxations were required, so I did not try to produce a tuned-up version of VA14A.

2.4 Results

With the modifications to the original version described above, I ran the code on a series of test cases, using the Finnis and Sinclair molybdenum potential. The aim of this section of work was to check that the code, in its modified form, was giving the correct answers; and to try to optimise its performance.

2.4.1 Single vacancy

My first test was to calculate the formation energy of a vacancy and compare the answer with that obtained by Matthai and Bacon [1985], who used the Finnis-Sinclair potential and quenched molecular dynamics. At this stage I was interested in whether the code converged properly, and what influence the boundary conditions and block size had on the vacancy formation energy obtained.

The reader should note that the cohesive energy of the crystal, 6.82 eV per atom, has to be subtracted from the value actually printed out by DEVIL

to get the vacancy formation energies given below. This is due to the fact that the vacancy formation energy E_v^f is usually defined as the energy difference between an assembly of atoms in the perfect crystal configuration and that same number of atoms in a structure containing a vacancy. DEVIL, on the other hand, calculates a perfect crystal energy E_p, removes one atom from the lattice, and computes the relaxed energy of this new structure relative to E_p.

The unrelaxed value of E_v^f obtained by DEVIL is 2.579 eV, agreeing with 2.58 eV obtained analytically by Finnis and Sinclair [1984]. The relaxed values for various sizes of crystal are given in table 2.2, which quotes the energies to more accuracy than the data warrant in order to show convergence; Matthai and Bacon [1985] give 2.54 eV.

The DEVIL formation energy is not quite the fully-relaxed energy. The block is constrained to have a certain volume, either by its fixed boundary or because the periodic boundary conditions have a fixed period. A full minimisation could be carried out by giving the boundary layer various displacements, but this process seems rather complicated for a preliminary work, and the 'constant volume formation energy' is in itself a useful concept. (For reference, Catlow, Corish, Jacobs and Lidiard [1981] collect together a set of relationships between quantities measured at constant pressure and those evaluated at constant volume.)

size	boundary type	E_v^f/eV
6×6×6	cyclic	2.555
6×6×6	fixed	2.552
8×8×8	cyclic	2.551
10×10×10	cyclic	2.550
10×10×10	fixed	2.550

Table 2.2 Molybdenum vacancy formation energies: various block sizes.

Note that a lattice which is ten lattice planes in each direction contains only 250 atoms as not all 'mesh sites' (see appendix by Norgett in Thetford [1985]) are occupied; however a block of this size appears quite capable of giving a reasonable result for the vacancy formation energy. Though less accurate, a calculation with cyclic boundary conditions executes faster than one of the same size with a fixed boundary region. The fixed-boundary case runs more slowly because it requires the cohesive energies of all the atoms in

the outer region. Even with just a second-neighbour interaction, a $10\times10\times10$ inner region implies a $14\times14\times14$ outer region; the number of boundary atoms can easily exceed those in the 'free' region.

The calculation with periodic boundaries is less accurate because it models a relaxation region that is in some sense smaller than that of the corresponding fixed calculation: for consider a vacancy in a $10\times10\times10$ block. In the cyclic case, the tenth plane of atoms will tend to see the eleventh moving away from it — it is just an image of the first plane, which moves inwards. In the fixed case, the eleventh plane remains stationary. Hence the inward relaxation will be less for a block with cyclic boundaries. To obtain a given accuracy most cheaply, use cyclic boundaries wherever possible; this will not be possible, though, for defects requiring a particular displacement to be applied to a fixed boundary.

Of course, using periodic boundary conditions in all three directions is equivalent to modelling an infinite 3-dimensional array of defects. As the block size increases, the concentration of these defects decreases.

2.4.2 Single interstitial

Once the code was working as desired for a vacancy, I used it to calculate the relaxation round an interstitial. Various changes had to be made to FUNC to cope with all the interactions of interstitials with the rest of the lattice and with each other. With these made, I tried two ways of modelling the dumbbell interstitial. The first was simply to insert an interstitial at a point near to the origin, such as (0.5, 0.25, 0.0), and relax the crystal from there. The second was to create a vacancy at the origin, then insert two interstitials nearby. As the interstitials can be inserted close to their equilibrium positions, the structure should relax in fewer iterations; and as we may be able to use a shorter neighbour list, each iteration can take less computer time.

In fact I found that, for the dumbbell interstitial which ends up close to (±0.32, ±0.19, 0.00), (the 'bent' interstitial referred to in chapters 3 and 4) the atoms originally at (0.5, 0.5, ±0.5) and (-0.5, -0.5, ±0.5) move far enough to interact with atoms such as (1.5, 0.5, 1.5): originally a third neighbour. Thus I needed to choose between making the search distance exceed $\sqrt{2}$ (the third-neighbour distance), or inserting six interstitials and five vacancies. The latter approach proved to give faster running times particularly as the 'interstitials' could be inserted close to their equilibrium positions.

Table 2.3 gives calculated values of the interstitial formation energy, using

the unmodified version of the Finnis-Sinclair potential. The CPU (processor) times are for the six-interstitial method mentioned above, run on a Cray X-MP and with ACC1 (see Appendix 1) set to 5×10^{-5}. They are shown merely to indicate how the execution time increases as a larger region is considered. The number of iterations (search directions) needed is also shown, to explain the apparently disproportionate increase in CPU time as the block size increases. The relaxation propagates outwards and in a large region will take many iterations to reach the outside.

The irregular increase of the number of iterations is due to a number of factors: how the positions of the inserted interstitials compare with the final positions, whether the convergence criterion is just met on a certain step or comfortably exceeded on the following one, how well the line search is performing, *et cetera*.

size	boundaries	E_i^f/eV	CPU time /s	iterations
10×10×10	cyclic	6.987	10.1	38
12×12×12	cyclic	6.967	14.9	38
12×12×12	fixed	6.964	17.6	33
14×14×14	cyclic	6.957	17.2	37
14×14×14	fixed	6.955	26.9	34
16×16×16	cyclic	6.951	26.1	37
16×16×16	fixed	6.950	51.8	51
18×18×18	cyclic	6.946	64.9	70
20×20×20	cyclic	6.944	83.9	67

Table 2.3 Formation energies for molybdenum interstitials, in various blocks.

Again, as for vacancy formation energies, an allowance had to be made for the changed number of atoms in the assembly; here, 6.82 eV had to be added to the value printed out by DEVIL.

When performing these calculations, care must be taken to avoid certain pitfalls. The major one is symmetry: if a pair of interstitial atoms is put in at say $\pm(0.2,\ 0.2,\ 0.2)$ bracketing a vacant site at $(0,\ 0,\ 0)$ and the rest of the crystal is symmetric, the dumbbell will always retain its $x=y=z$ symmetry as it relaxes. The resulting metastable position actually has an energy of about 0.3 eV above the true minimum. The apparently strange initial positions

shown in the input data in Appendix 1 break the symmetry and prevent this happening.

A second pitfall concerns boundaries. If these are too close to the defect (i.e. the relaxation region is not large) then they can distort an expected symmetry. In the b.c.c. examples above, periodicity requires an even number of lattice planes in directions where a cyclic boundary condition is to be applied. For comparability, the fixed-boundary calculations also have an even number of lattice planes, but this means that a vacancy, for example, cannot be placed precisely in the centre of the block.

A third is that the range of the potential is longer than it may seem at first sight. Suppose that the cohesive potential reaches out to the second neighbours of atom i, for example to atom k at a displacement of (1, 0, 0) in a b.c.c. lattice. Then as the force on atom i depends on the value of ρ_k (see equations (1.8) and (1.9)), it will depend on all second neighbours of k and in particular on the one which is (2, 0, 0) from i: its sixth neighbour. Thus an impurity at (0, 0, 0) in a 7×7×7 lattice with fixed boundaries will interact with all boundaries; even in an 8×8×8 block, it will still feel the closest boundary.

The larger distortions produced by an interstitial are reflected in the higher formation energy. A consequence of this is that a larger block is required before the energy approaches that of an interstitial in an infinite lattice: perhaps twice as large as the block needed for a vacancy.

While working on this problem, I took the opportunity to tune some of the parameters mentioned in §2.3 that control the relaxation: initial step length, execution of the line search and the number of conjugate steps taken before returning to the steepest descent.

2.5 Conclusions

The value obtained above for the molybdenum vacancy formation energy agrees well with that of 2.54 eV given by Matthai and Bacon [1985], providing evidence that the code is working properly when relaxing a vacancy. The relaxation calculated from the Finnis-Sinclair potential is not large, but this has also been observed with other potentials. For example, van Haughten, Berg, Caspers and van Veen [1978] have calculated vacancy formation energies with two different molybdenum pair potentials, and get relaxation from 3.60 eV to 3.20 eV, and from 4.80 eV to 4.58 eV (all figures ±0.05 eV). By way of comparison, the experimental vacancy formation energy quoted by Herzig and Köhler [1981] is 3.0 to 3.25 eV.

For molybdenum interstitials, the calculated relaxed formation energy is 6.94 eV. This energy is harder to calculate, and much harder to measure, than the vacancy formation energy. Van Heughten *et al.* give 9.26 eV for a molybdenum pair potential fitted to elastic constants, and 4.39 eV for the potential fitted to phonon spectra. Miller [1981] calculates 4.71 eV for the ⟨110⟩ split dumbbell interstitial. The DEVIL result falls well within this range; but note that the modification to the potentials to be introduced in chapter 3 will increase the calculated value slightly.

In this thesis I do not intend to investigate in detail the validity of the Finnis-Sinclair potentials, but their molybdenum potential at least seems to give reasonable results. The method of fitting used by Finnis and Sinclair to derive it gives little consideration to the form of the short-range repulsion, so it is gratifying to see the molybdenum interstitial formation energy coming out well. However, interatomic spacings around a single interstitial atom are not much less than the equilibrium value; chapter 3 considers the shortcomings that become evident at considerably reduced interatomic distances, and for interstitials in some of the other metals.

In conclusion, I have resurrected the DEVIL program, set it up to deal with an N–body potential, and have produced good results. While further refinements and generalisations are desirable, primarily the extension to parallelepiped blocks and dislocations running in directions which are not cube edges, DEVIL provides a useful tool for the study of lattice defects.

3 Point Defects and the new Core Potential

3.1 Introduction

3.1.1 Problems with the Finnis-Sinclair potential

Although the Finnis-Sinclair potentials described in §1.4 are a considerable advance on pair potentials, Ackland and Thetford [1987] found some difficulties with them. Finnis and Sinclair [1984] fitted the original parameters to elastic moduli of the metals in an equilibrium state: i.e. with the interatomic separation at the perfect-lattice value. Using these parameters for the metals vanadium, niobium, tantalum, molybdenum and tungsten led to anomalies in properties for which atoms are forced close together, such as the compressibility at high pressure. Two of the potentials (vanadium and niobium) were actually attractive at short range, causing atoms in molecular dynamics calculations to tend to fall together.

3.1.2 Modifying the potential

Any modification to the form of the potential must not change the fitting at equilibrium separation. Any extra terms must therefore vanish at the nearest-neighbour separation b_0, as must their first and second derivatives. Ackland and Thetford [1987] chose to add a term to the repulsive pair potential part of the Finnis-Sinclair potential, $V_{FS}(r)$ in equation 1.1. This term has roughly exponential form and is fitted to the electron gas potentials for dimers. The short range repulsion is increased, overcoming the anomalies mentioned above, without changing the equilibrium fitting to elastic constants.

The fitting procedure is described in detail in Ackland and Thetford [1987]. Several different functional forms were tried, and the one which best fitted the data while satisfying all the criteria was a product of a cubic and an exponential term:

$$V(R_{ij}) = V_{FS}(R_{ij}) + B(b_0 - R_{ij})^3 \, e^{-\alpha R_{ij}} \qquad (3.1)$$

The parameters B and α, determined from fitting in the region $0.4 < R_{ij}/b_0 < 1.0$, are shown in table 3.1, together with the nearest-neighbour distances b_0.

Ackland and Thetford [1987] used the modified potentials to calculate revised pressure-volume curves, finding much better agreement with experiment. The rest of this chapter describes interstitial calculations made with the revised potentials. Where possible, I compare the results obtained using the original with those from the modified potentials.

metal	B/eV Å^{-3}	α/Å^{-1}	b_0/Å
V	23.0	0.5	2.6320
Nb	48.0	0.8	2.8585
Ta	91.0	1.05	2.8629
Mo	1223.0	3.9	2.7255
W	90.3	1.2	2.7411

Table 3.1 Parameters of the core function in equation (3.1).

Rebonato, Welch, Hatcher and Bilello [1987] also felt compelled to add an extra repulsive term to the Finnis-Sinclair potential. They fitted to pressure-volume curves, and calculated interstitial configurations. Table 3.2 includes their values for interstitial formation energies; although their absolute values differ from mine, the pattern of stability is the same.

3.2 Calculations on Interstitials

Interstitials are the defects most likely to be affected by a change in the form of the potential at small separations. Using the new cores described above, I made DEVIL relaxation calculations for interstitials in vanadium, niobium, tantalum, molybdenum, and tungsten. No stable structure could be found with the potentials for vanadium and niobium as originally published, but the addition of the core term led to stable interstitial configurations for these metals.

3.2.1 Procedure for constraining dumbbell direction

In some of the work described in the following sections, the atoms forming the interstitial dumbbell have to obey certain constraints. For example, figures 3 to 6 all show interstitial formation energy plotted against dumbbell orientation, while figure 2 shows the region considered.

Such constraints are easily applied within DEVIL. Suppose that a particular atom i needs to lie on the line of a unit vector $\mathbf{n}$ from the origin. In the method of conjugate gradients described in §2.5, a search direction $\mathbf{s}_i$ is defined for each atom i, at each minimisation step. By redefining $\mathbf{s}_i$ to $\mathbf{s}_i'$, where

$$\mathbf{s}_i' = (\mathbf{s}.\mathbf{n})\mathbf{n} \tag{3.2}$$

atom i will move only on a line parallel to $\mathbf{n}$.

Making atoms conform to a constraint will impose residual forces. These

residual forces should be removed from the set of forces $\{\mathbf{g}_j\}$, otherwise the convergence criterion (which puts a limit on $\sum_j \mathbf{g}_j^2$) may be unreachable. For the 'line' constraint above, $\mathbf{g}_i$ must also lie along $\mathbf{n}$, so before calculating $\sum_j \mathbf{g}_j^2$ to compare with the desired accuracy, we replace $\mathbf{g}_i$ with

$$\mathbf{g}_i' = (\mathbf{g}_i \cdot \mathbf{n})\mathbf{n} \tag{3.3}$$

Equally easily, an atom may be constrained to move in a particular plane. If the plane is perpendicular to the unit vector $\mathbf{n}$, then s_i and $\mathbf{g}_i$ need only be replaced by

$$\mathbf{s}_i' = \mathbf{s}_i - (\mathbf{s}_i \cdot \mathbf{n})\mathbf{n} \tag{3.4}$$

and

$$\mathbf{g}_i' = \mathbf{g}_i - (\mathbf{g}_i \cdot \mathbf{n})\mathbf{n} \tag{3.5}$$

This approach may also be used to keep an atom at a fixed distance from a certain point $\mathbf{x}_{ref}$ (to within second-order terms in the step length): $\mathbf{n}$ is simply recalculated at each step to be the unit vector parallel to the line from $\mathbf{x}_{ref}$ to $\mathbf{x}_i$: i.e.

$$\mathbf{n} = (\mathbf{x}_i - \mathbf{x}_{ref}) / |\mathbf{x}_i - \mathbf{x}_{ref}| \tag{3.6}$$

I have written a new subroutine CONSTT to apply such constraints: given an atom position $\mathbf{x}_i$ and a vector ($\mathbf{s}_i$ or $\mathbf{g}_i$) that must obey a constraint, CONSTT will return a suitably modified vector to the minimisation routine DEV3.

3.2.2 Molybdenum and the bent interstitial

One feature of the old potential that persists with the new is the apparently strange relaxed configuration of the dumbbell interstitial in molybdenum. Calculation of interstitial formation energies for the various possible symmetry positions (octahedral, tetrahedral, crowdion; ⟨100⟩, ⟨110⟩, and ⟨111⟩ split dumbbells) of the defect in a b.c.c. lattice suggested that the ⟨110⟩ split dumbbell was energetically favoured [Zeper 1986, Harder and Bacon 1986]. But by starting the relaxation from a configuration which was asymmetric, and using the potentials in their original form, I found a relaxed structure with the atoms of the dumbbell at approximately (±0.32, ±0.19, 0.00) (see chapter 2). This has an energy lower by about 0.05 eV than that of the ⟨110⟩ interstitial, and other workers [Zeper 1986, Harder and Bacon 1986] have since found the same phenomenon.

A block of size $7a \times 7a \times 7a$, with faces parallel to the cube faces of the b.c.c. structure, consists of 14 lattice planes in each direction, and is referred

to as a 14^3 block. A 14^3 block of perfect lattice contains 686 atoms; 16^3 contains 1024 atoms, and 18^3 contains 1458 atoms.

When the core described in §3.1.2 was included in the molybdenum potential, I found two relaxed minima. In a 14^3 block with cyclic boundary conditions, one of the minima has the dumbbell atoms at ($\pm$0.3166, $\pm$0.1978, $\pm$0.0235) and formation energy 6.983 eV; the other dumbbell is positioned at ($\pm$0.2653, $\pm$0.2630, $\pm$0.0559) and has energy 6.991 eV. Which of the two is obtained depends on the starting configuration. For a 16^3 block, it is possible to relax to $\langle 110 \rangle$, but only by starting very nearby. I find an energy of 7.033 eV for the dumbbell at ($\pm$0.2658, $\pm$0.2658, $\pm$0.0001), compared with 6.974 eV for ($\pm$0.3182, $\pm$0.1958, $\pm$0.0182).

The $\langle 110 \rangle$ dumbbell is at a very shallow minimum in the potential energy. To try to elucidate how this situation arises, I have considered the effect of rotation of the dumbbell in 3-space. It is sufficient to consider the tetrahedron bounded by the origin and the three principal directions $\langle 100 \rangle$, $\langle 110 \rangle$ and $\langle 111 \rangle$: see figure 2. The energy can then be plotted against orientation projected onto the 'stereographic triangle' shaded in figure 2.

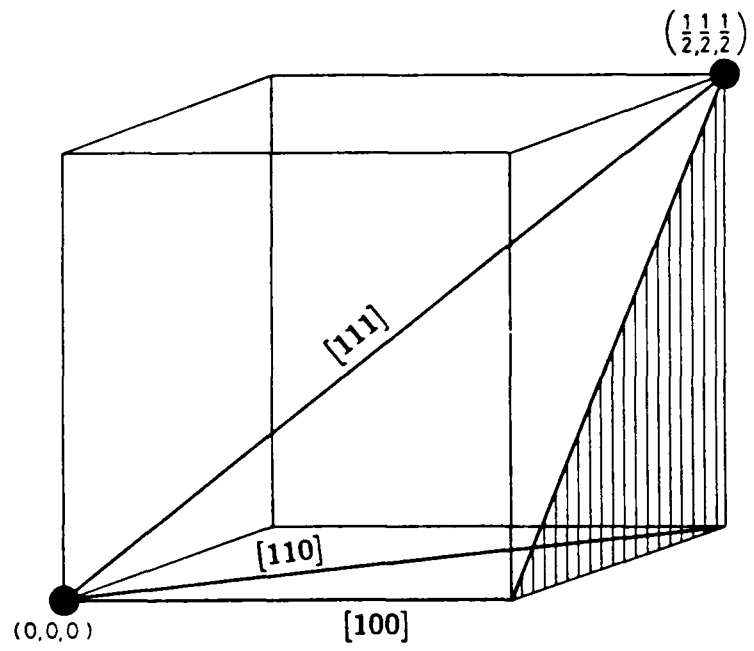

Figure 2. Calculation region for the b.c.c. structure.

DEVIL relaxed a 14^3 block of molybdenum atoms, with cyclic boundary conditions. The results, tabulated in table 3.2, compare well with the results given by Zeper [1986]. The energy of the stable configuration agrees with the one experimental number available [van Veen, 1986] of 8$\pm$1 eV. Figure 3 is an energy contour plot of the region round $\langle 110 \rangle$. Although there is a

metal	configuration	E_i^f/eV	core?	block	Rebonato[a]
V	⟨1 0 0⟩	4.936	yes	14^3	3.73
V	⟨1 1 0⟩	**4.163**	yes	14^3	3.23
V	⟨1 1 0⟩	**4.155**	yes	16^3	
V	⟨1 1 1⟩	4.608	yes	14^3	
V	crowdion	4.600	yes	14^3	
V	crowdion	4.592	yes	16^3	3.50
Nb	⟨1 0 0⟩	4.821	yes	14^3	4.13
Nb	⟨1 1 0⟩	**4.485**	yes	14^3	3.99
Nb	⟨1 1 0⟩	**4.472**	yes	16^3	
Nb	⟨1 1 1⟩	4.795	yes	14^3	
Nb	crowdion	4.857	yes	14^3	4.10
Ta	⟨1 0 0⟩	8.068	yes	14^3	6.12
Ta	⟨1 1 0⟩	**6.847**	yes	14^3	5.34
Ta	⟨1 1 0⟩	**6.828**	yes	16^3	
Ta	⟨1 1 1⟩	7.157	yes	14^3	
Ta	crowdion	7.158	yes	14^3	5.43
Ta	⟨1 0 0⟩	4.103	no	14^3	4.08
Ta	⟨1 1 0⟩	3.968	no	14^3	3.95
Ta	⟨1 1 1⟩	3.933	no	14^3	
Ta	crowdion	**3.806**	no	14^3	3.78
Mo	⟨1 0 0⟩	7.207	yes	14^3	7.92
Mo	⟨1 1 0⟩	7.042	yes	14^3	7.73
Mo	⟨1 1 0⟩	7.033	yes	16^3	
Mo	bent[b]	**6.983**	yes	14^3	
Mo	bent[b]	**6.974**	yes	16^3	
Mo	⟨1 1 1⟩	7.223	yes	14^3	
Mo	crowdion	7.187	yes	14^3	8.02
W	⟨1 0 0⟩	9.815	yes	14^3	
W	⟨1 1 0⟩	9.641	yes	14^3	
W	⟨1 1 1⟩	8.919	yes	14^3	
W	⟨1 1 1⟩	8.908	yes	16^3	
W	crowdion	**8.893**	yes	14^3	
W	crowdion	**8.881**	yes	16^3	
W	crowdion	**8.875**	yes	18^3	

[a] From Rebonato, Welch, Hatcher and Bilello [1987]. They use 'up to 256 atoms', which corresponds to a 12^3 block.
[b] See text for explanation of this.
All blocks have cyclic boundary conditions.

Table 3.2 Interstitial formation energies.

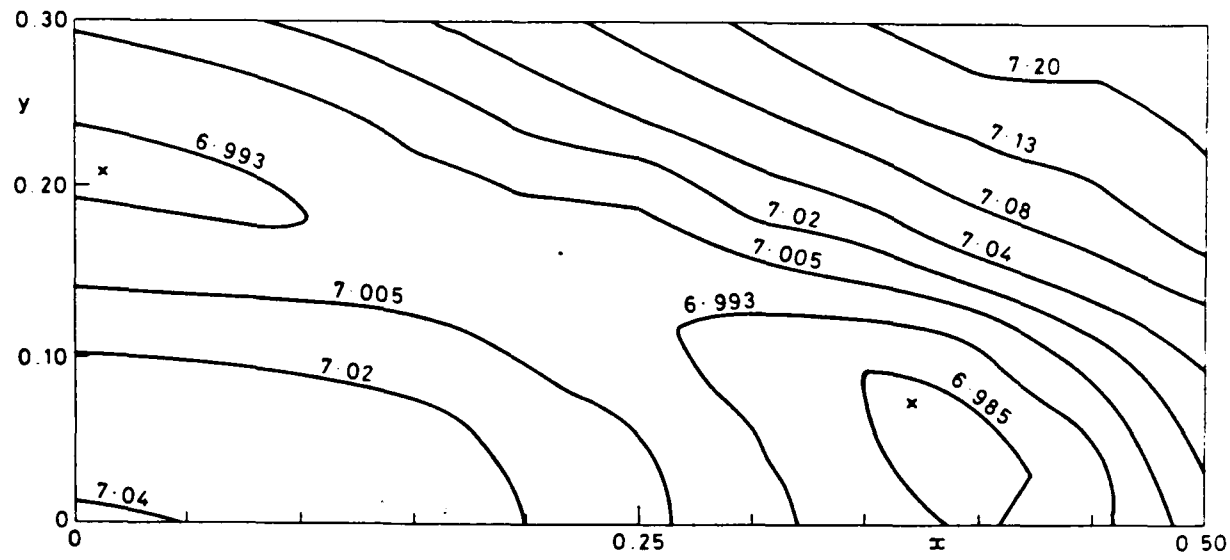

Dumbbell orientation is $\langle 1 \;\; 1-x \;\; y \rangle$.

Contour levels are chosen to highlight the structure.

The two minima are marked X.

Figure 3. Energy contours (eV) for molybdenum dumbbell.

general tendency for the dumbbell to sit near the $\langle 110 \rangle$ direction, there is a 'moat' running round a slight rise in the energy at that point.

The energy barrier to rotation around the moat is approximately 16 meV, compared to the 'knoll' height of about 50 meV. At room temperature thermal motion would lead to a mean alignment in the $\langle 110 \rangle$ direction. If this surface represents the true potential energy, it may be difficult to distinguish it experimentally from one with a global minimum at $\langle 110 \rangle$.

The experimental results available [Ehrhart, 1978; Okuda and Mizubayashi, 1981] confirm that the $\langle 110 \rangle$ split dumbbell is the favoured interstitial configuration.

3.2.3 Tantalum: the effect of the core

The effect of introducing the core of the potential is most dramatic for tantalum. Figure 4 plots formation energy against orientation for the tantalum dumbbell, before the core was included. To aid interpretation, the energy surface has been reflected in the line joining the points labelled $\langle 100 \rangle$ and $\langle 111 \rangle$: certain features can be clearer in the reflected portion than in the original. The values obtained (see table 3.2) are broadly in line with those calculated for the principal dumbbell orientations by Harder and Bacon [1986]; the slight differences in energy probably arise from the use of different boundary conditions. The configurations with minimum energy are picked out in bold type.

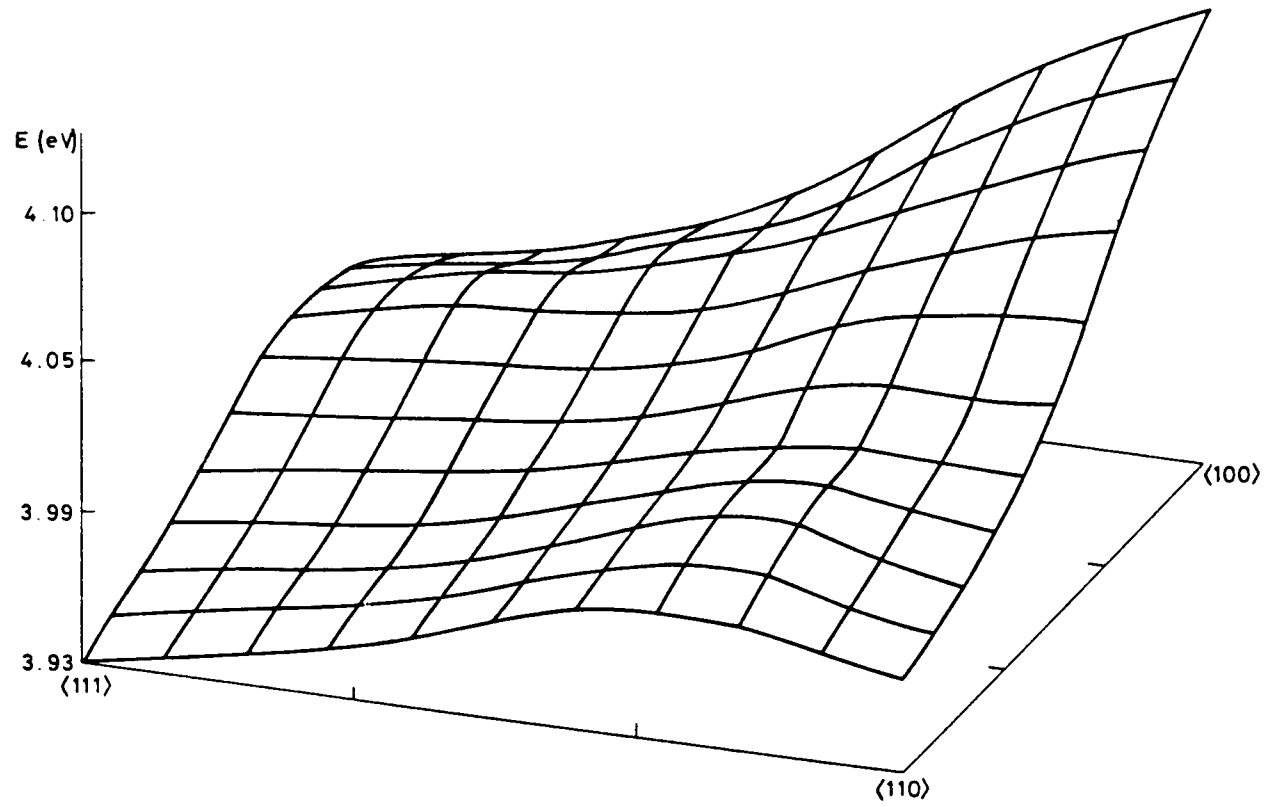

Figure 4. Tantalum without core: interstitial formation energy against orientation.

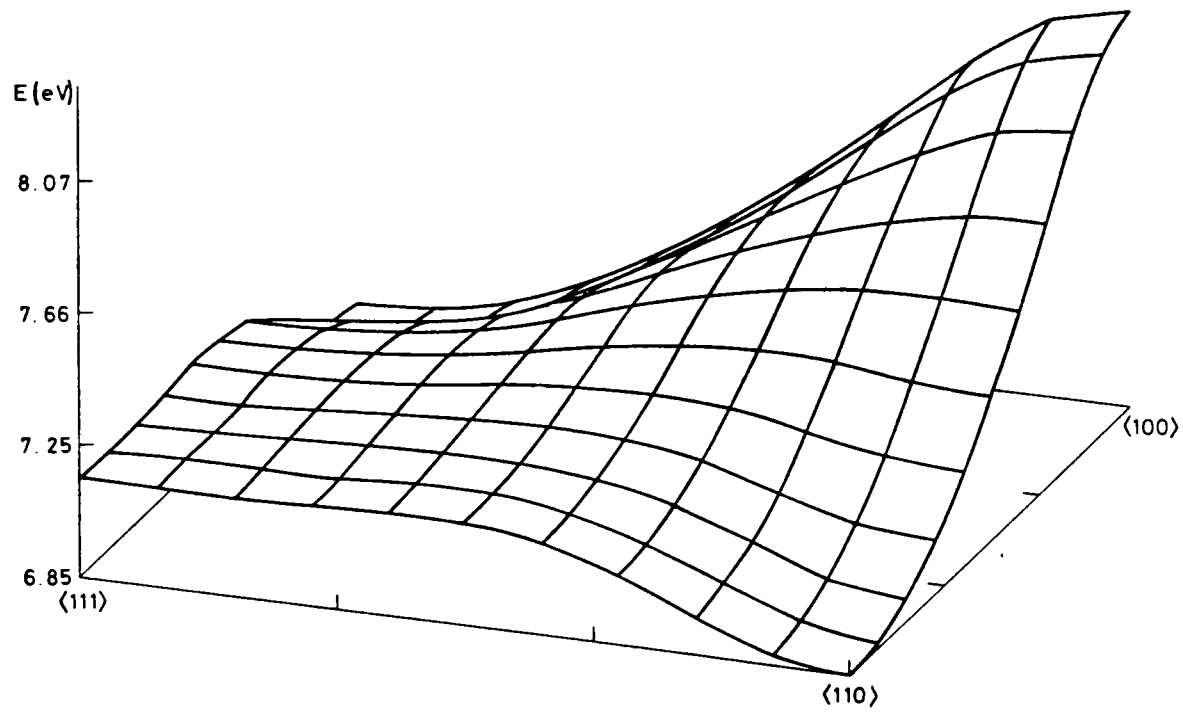

Figure 5. Tantalum with core: interstitial formation energy against orientation.

When the core is included, total energies rise considerably for all interstitial configurations, as can be seen by comparing the two tantalum sections in table 3.2. The two ⟨111⟩ defects (the ⟨111⟩ crowdion and the ⟨111⟩ split dumbbell interstitial) now have almost the same energy, and the minimum is shifted to the ⟨110⟩ orientation. Figure 5 plots the formation energy against orientation once the core has been introduced. The new relaxed positions lead to a change in shape of the contribution to the energy from the cohesive part of the potential. This now dominates, and a stable ⟨110⟩ configuration arises.

3.2.4 Vanadium and niobium: the effect of the core

As mentioned earlier, the potentials for vanadium and niobium as originally published lead to an instability in a lattice structure. Hence the absence of these metals from the work of Harder and Bacon [1986], and the difficulties experienced earlier when trying to perform relaxations with DEVIL. The inclusion of the core allows calculations to be carried out, and the results obtained with DEVIL are given in table 3.2. For both metals, a plot of interstitial formation energy against dumbbell orientation looks similar to that for tantalum given in figure 5, though in niobium the $\langle 111 \rangle$ energy is approximately equal to the $\langle 100 \rangle$ energy. Both have deep minima at $\langle 110 \rangle$, and relax quickly to this configuration from anywhere nearby.

I carried out one relaxation for vanadium with the atoms starting very near to the positions used to generate the crowdion, but with a slight asymmetry. After about 120 lattice energy evaluations, compared to the 30 or 40 usually required for convergence, the lattice had relaxed to the $\langle 110 \rangle$ split dumbbell configuration. I also made a crowdion calculation on a 16^3 block, for comparison with the usual 14^3 region. The crowdion, as the most extended defect, is most likely to be constrained by a small block. As table 3.2 shows, the energy was reduced by only 8 meV, indicating that the 14^3 calculation gives acceptable results. In fact, I have found that, for an interstitial in a general b.c.c. metal, a good rule of thumb is that the energy difference between 16^3 and 18^3 is approximately half that between 14^3 and 16^3, and keeps halving as the block size is increased in steps of two lattice planes. For vanadium, this suggests that the formation energy of the crowdion in an infinite block is about 4.584 eV.

3.2.5 Tungsten: a stable crowdion and 1-d migration

All of the metals so far described have a stable dumbbell in the $\langle 110 \rangle$ direction, or near to it, once the core has been included. Tungsten, however, is different. Although a $\langle 111 \rangle$ dumbbell is a minimum of the energy, and the lattice will relax into this configuration if started near to it, the absolute energy minimum is that of the crowdion.

Unfortunately, experimental evidence [Mizubayashi and Okuda, 1981] points to the fact that the stable interstitial configuration in tungsten is the $\langle 110 \rangle$ dumbbell, just as for the other refractory b.c.c. transition metals. I think that the tungsten results should therefore be regarded as a model of what would happen to any $\langle 111 \rangle$ defects produced by irradiation at very low temperature and 'frozen-in' by a lack of thermal energy. Alternatively, the prediction of the $\langle 111 \rangle$ crowdion can be taken as an example of the diversity of behaviour possible from an apparently simple model.

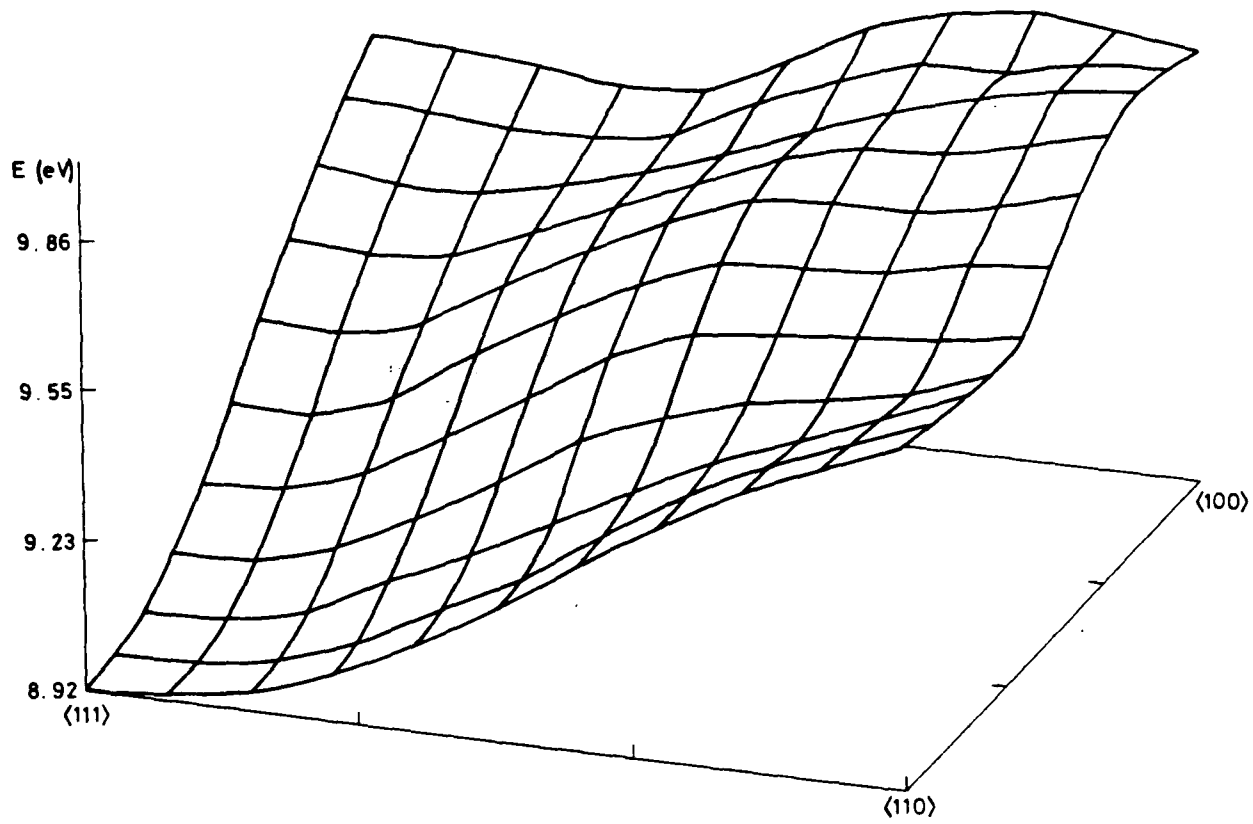

Figure 6. Tungsten: interstitial formation energy against dumbbell orientation.

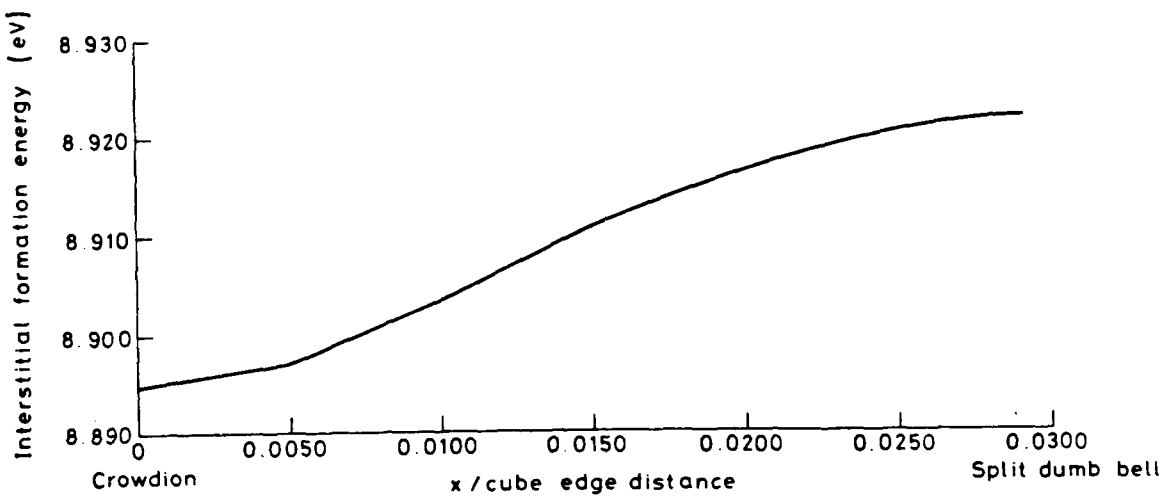

Figure 7. Energy of migration in the ⟨111⟩ direction for a tungsten interstitial.

The fact that the crowdion configuration is close to that of the ⟨111⟩ dumbbell suggests that interstitial migration along the ⟨111⟩ direction should be the preferred route in tungsten. (For a more detailed discussion, see §5.1.1.) For a dumbbell to rotate from [111] to [11$\bar{1}$] via [110] (the lowest-energy path), an activation energy of 0.72 eV (table 3.2 and figure 6) must be overcome. For the interstitial to move from the crowdion position to the split dumbbell pointing in the same direction, requires only 0.027 eV (figure 7).

Block size has an effect on the stability of certain configurations in tungsten. A 14^3 lattice with periodic boundary conditions allows the $\langle 111 \rangle$ split dumbbell to be stable, as does a 16^3 block with fixed boundaries, but a relaxation starting very near to the $\langle 111 \rangle$ dumbbell in a 14^3 block with fixed boundaries will yield the crowdion. The extremely shallow energy minimum at $\langle 111 \rangle$ in figure 6 does not show up because of the coarse grid employed for the calculations.

The cohesive part of the tungsten potential has a relatively long range, thus causing a few modelling problems. Table 3.3 gives the ranges of the two parts of the potential in terms of the cube edge distance a: the range of the cohesive part in tungsten comes close to the third-neighbour distance of $a\sqrt{2} \simeq 1.414a$. A small distortion of the lattice can therefore bring the third neighbours into range, causing problems for a program like DEVIL which works on the neighbour-list principle. I had to write a module, CHECK, to go through the relaxed configuration of the lattice, check for any extra interactions which had not previously been considered, and write appropriate warning messages. This indicated that many third-neighbour interactions were present, and the search distance for constructing the neighbour-list had to be increased to encompass all such interactions.

metal	a/Å	r_{coh}/a	a_{rep}/a
V	3.0399	1.214766	1.250
Nb	3.3088	1.186183	1.272
Ta	3.3058	1.233281	1.270
Mo	3.1472	1.307456	1.033
W	3.1652	1.390188	1.027

Table 3.3 Range of the cohesive and repulsive parts of the potential.

3.2.6 Molecular dynamics

Ackland [Ackland and Thetford 1987] has made quenched molecular dynamics (MD) simulations, with periodic, constant pressure boundary conditions, for interstitials in all of the metals studied in this chapter. The molecular dynamic cell is constrained merely to be a parallelepiped, thus allowing both volume and shear stresses to relax. In the calculation of interstitial formation it is quite important that these degrees of freedom are available. For a typical 16^3 block, they lower the energy by about 0.03 eV,

compared with constant-volume, zero-shear configurations. A molecular dynamics program is also more likely to locate the global minimum, rather than relax to a local minimum. The paper by Ackland and Thetford [1987] gives more details of the molecular dynamics program.

The lowest energy configurations found by MD are given in table 3.4, and are compared with the values obtained by static relaxation extracted from table 3.2. In all cases the energies predicted by MD are slightly lower, but the equilibrium configurations are the same. This gives confidence that the static relaxations are not converging to a merely local minimum.

metal	configuration	formation energy /eV	
		MD	DEVIL
V	⟨1 1 0⟩	4.140	4.155
Nb	⟨1 1 0⟩	4.447	4.472
Ta	⟨1 1 0⟩	6.788	6.828
Mo	bent	6.957	6.974
W	crowdion	8.871	8.881

All of the MD calculations have a 16^3 block with dynamic boundary conditions, carried out at constant pressure, with the MD block constrained only to remain a parallelepiped. Cores are included.

Table 3.4 Comparison between interstitial formation energies and configurations obtained by molecular dynamics, and energies from DEVIL.

A typical DEVIL relaxation of a 16^3 block to give the energy correct to 10^{-4} eV, needs about 40 calls of the function which evaluates the lattice energy, and 16 seconds of CPU time on a Cray X-MP. A similar calculation using quenched MD requires about 100 timesteps and 90 seconds CPU. The expansion of the block delays convergence, because the absolute positions of the atoms are dependent upon the block size.

3.2.7 Elastic deformations and interstitial energies

The introduction of an interstitial induces stresses in a lattice. In calculating the formation energy of a relaxed interstitial it is important to allow this stress to relax as much as possible. With the DEVIL program the volume of the block was fixed at the perfect-lattice value. The calculations using the MD program were initially for a block free to expand and shear,

but when a constant volume constraint was introduced the results were identical to DEVIL. This is expected since periodic boundary conditions are used in both cases, and the discrepancy between DEVIL and MD results can thus be attributed entirely to elastic strain energy.

An analysis based on continuum elasticity theory [Ackland and Thetford 1987] calculates the effect of relaxing the shear and volume strains. Such a relaxation accounts very well for the differences between the simulation energies in table 3.4.

3.3 Conclusions

Fitting repulsive cores to the pair-potential part of the FS potentials is necessary if meaningful atomistic simulations are to be carried out. The cores presented above for the five b.c.c. metals vanadium, niobium, tantalum, molybdenum and tungsten seem to lead to sensible properties of the metals. (Although Finnis-Sinclair potentials were also derived for Fe and Cr, their stability has not yet been investigated.) The pressure-volume curves shown in Ackland and Thetford [1987] appear to be realistic, and simulation of vanadium and niobium has become possible.

I have obtained formation energies for various interstitial configurations, and compared them with the theoretical work of other authors. Inclusion of the core has a significant effect in some cases, altering which of the possible symmetry positions has the lowest energy. The results of selected static relaxations have been compared with those from a molecular dynamics program.

The results obtained from the many-body potential suggest that one-dimensional migration of interstitials will take place in tungsten, along the $\langle 111 \rangle$ direction. This conclusion is based on the rather sparse migration calculations so far carried out, with only a small region round the $\langle 111 \rangle$ migration path so far investigated. Further migration calculations are presented in chapter 6.

4 Dislocations

4.1 Introduction

I have previously reported [Thetford 1985, and chapter 2] the modification of the DEVIL program to handle *N*–body potentials developed by Finnis and Sinclair [1984]. Chapter 3 describes how the cores of the potentials needed modification, and presents some results for interstitial and vacancy formation energies.

The aim of this work is to investigate the interaction between point defects and dislocations. DEVIL must therefore be able to model dislocations running in various directions: the original program needed some modification to be able to do this. Further changes enabled DEVIL to take advantage of the arrival of a Cray-2 computer at Harwell. I rewrote FUNC, the CPU-intensive routine that evaluates the energy of a block. Not only can the Cray compiler vectorise much of the new FUNC, but the new subroutine uses more of the vast Cray storage in a bid to save processor time. I describe these changes in §4.2 below, and then go on to present some results on dislocations in §4.3.

The DEVIL program is more fully discussed in chapter 2 and Appendix 1, but briefly the calculation considers a block of 'free' atoms, surrounded by boundary layers. The boundary layers can be fixed, or they can be cyclic images of the free block. The energy of the block, which is to be minimised, is given by equation (1.2) (reproduced here for easy reference) as

$$U_{tot} = U_N + \tfrac{1}{2}\sum_{ij} V(R_{ij}) \tag{4.1}$$

Indices i and j index the atoms in the block, and R_{ij} is the separation of atoms i and j. The terms in this equation are defined in more detail in §1.4.

If equation (4.1) is rewritten as

$$U_{tot} = \sum_i E_c(i) + \sum_i E_r(i) \tag{4.2}$$

we can identify E_c as the 'cohesive' *N*–body energy of atom i and E_r as the repulsive pair potential contribution. Equations (4.1) and (1.2) show that

$$E_c(i) = -A\,(\sum_j \phi(R_{ij}))^{\frac{1}{2}} \tag{4.3}$$

$$E_r(i) = \tfrac{1}{2}\sum_j V(R_{ij}) \tag{4.4}$$

These definitions will be referred to later.

4.2 Changes to DEVIL

The DEVIL code used for the calculations described in previous chapters worked perfectly satisfactorily, but did not run very fast and could perform only a few types of calculations. Wishing to investigate migrating defects (requiring many relaxations per migration step) and dislocations (requiring distorted boundaries and blocks aligned in arbitrary directions), I realised that I would have to rewrite much of DEVIL. The sections below describe these modifications.

4.2.1 Vectorisation

Cray supercomputers are able to 'vectorise' loops of code to speed up execution. For example a loop that added together two vectors of length 64 would take 256 floating point operations on a scalar computer (128 'load' operations, 64 additions and 64 stores to memory). Each floating point operation takes about six clock periods. A Cray in vector mode, on the other hand, must first set up the two vectors; but it can then produce one result per clock period. The speed-up factor can be up to six, depending on the vector length. Certain types of loop will not vectorise: for example those containing subroutine calls, or if later iterations of the loop depend on the results of earlier calculations. Figure 8 shows an example program containing five loops, of which two vectorise and three do not.

Norgett wrote the original DEVIL program in the early 1970's. He used a clever algorithm based on an index function to find neighbours: see §2.2.1 for a full description. This method avoided having to store neighbour lists for each atom in the structure, and so enabled DEVIL to model quite large structures without running out of storage space. However, the program ran slowly enough to make the cost of my proposed defect migration calculations prohibitive.

The advance in the size of main memory in recent computers has meant that a neat addressing strategy is unnecessary, and full neighbour lists can be stored for each atom. In fact, the complicated old way of finding the neighbours of an atom meant that the Cray compiler could not vectorise the FUNC subroutine. (FUNC evaluates energies and forces for a block of atoms.) My first attempt to make DEVIL run faster was to rewrite FUNC so that the compiler could vectorise it.

The expression for the force between atoms i and j depends on both $E_c(i)$ and $E_c(j)$, so FUNC must perform two passes through the lattice. On the first, FUNC calculates the cohesive energies E_c; on the second, it calculates values of E_r and uses the E_c's to determine the forces.

```
      PROGRAM VTEST
*
*     Test program to investigate vectorisation
*     cft77 compiler (release 2.0) on Cray-2, 14 July 1988
*
      DIMENSION A(10), B(10), C(10)
      DIMENSION L(10), M(10)
*
*
* Vectorises:
      DO 10 I=1,N
        IF (I.GT.4) THEN
            L(I) = L(I)+I
        ELSE
            L(I) = L(I)+I+I
        ENDIF
        B(2*I) = A(I)
        SUM = SUM + A(I)
        K   = K   + I
  10  CONTINUE
*
* Vectorises:
      DO 20 I=1,N
        X = A(I)*B(I)
        C(J) = C(J) + X
  20  CONTINUE
*
* Does not vectorise (scalar updated more than once):
      DO 30 I=1,N
        IF (I.GT.4) THEN
            K = K+I
        ELSE
            K = K+I+I
        ENDIF
  30  CONTINUE
*
* Does not vectorise (recurrence on L,M; store to array
* reference that is not a vector on M):
      DO 60 I=1,N
        IF (I.GT.4) THEN
            M(K) = M(K)+I
        ELSE
            L(K) = L(K)+I+I
        ENDIF
  60  CONTINUE
*
* Does not vectorise (subscript conditionally incremented):
      DO 70 I=1,N
        IF (I.GT.4) THEN
            K = K+I
        ENDIF
  70  CONTINUE
*
      STOP
      END
```

Figure 8. Tests of vectorisation.

The 'subscript conditionally incremented' problem is flagged 'not yet implemented'. Presumably Cray intends to enable such constructions to be vectorised by a later release of the compiler.

The Cray-2 compiler is rather temperamental, and I found that it would refuse to vectorise constructions in large code blocks that it would happily vectorise in smaller test programs. FUNC was therefore split into four sections.

The first calculates the contributions to the E_c's from interactions between 'regular' (free and fixed) atoms; the second completes the calculation of the E_c's by considering interactions between interstitials and free atoms and among interstitials. With all of the E_c's calculated, the third section can accumulate the repulsive interactions E_r for 'regular' atoms and calculate the forces on them, and the fourth section deals once more with the interstitials.

By postponing the calculation of certain totals and accumulating vectors of intermediate results, almost all of the FUNC calculation can be made to vectorise.

The new method for finding neighbours meant that I was able to adapt DEVIL to deal with blocks of atoms that were general parallelepipeds, and not just cuboids. The user can now define any three (non-coplanar) vectors for his block edges: I shall refer to the 'block edge' vectors as $\mathbf{b}_1$, $\mathbf{b}_2$ and $\mathbf{b}_3$. DEVIL will set up a block of the relevant shape and locate all the atom sites, before proceeding with the energy minimisation. In about 1976 Norgett dubbed this generalised version of DEVIL 'DEVIL-2', but the program was never developed.

4.2.2 Distortion

The next task for DEVIL was to set up a block of atoms, then distort it. I wrote a new subroutine DSTORT, which can be used in several ways. DSTORT can move a single atom to a specified position, but most importantly it can set up a dislocation.

Given the Burgers vector of the desired dislocation and the position and direction of the dislocation line, a strain field can be calculated. If the block of atoms is set up so that the dislocation line is parallel to $\mathbf{b}_3$ and if a periodic boundary condition is applied in this direction, an infinitely long dislocation can be modelled.

Sinclair provided a subroutine based on work by Stroh [1962], which uses anisotropic elasticity theory to produce the strain field round a dislocation. These strains are applied to atoms in the fixed boundary; the atoms in the free region should then relax into a structure that exhibits a dislocation. To help the minimisation on its way, the strain field is applied to the free atoms too.

Inserting an edge dislocation is akin to cutting halfway through the block of material along the dislocation glide plane, displacing one part relative to the other by the Burgers vector $\mathbf{b}$, and repairing the cut. Assume for the time being that the dislocation line lies along the z axis, and the glide plane is the

xz plane. Transforming from (x,y,z) coordinates into (r,θ,z) polars, there is a discontinuity of **b** in the strain field across $\theta=0$.

This discontinuity can cause problems with the neighbour lists, as some neighbours may be taken out of range and new ones appear. One solution is to define a large number of atoms as interstitials (DEVIL assumes that interstitials are free to interact with any other atom in the lattice); another is to increase the volume of lattice that is scanned for neighbours by increasing the search radius; the third is to perform an extra survey of all atoms that are near the cut, redefining the neighbour lists as appropriate. The first two approaches will cause a large increase in execution time, but the third can get very complicated when skew blocks are distorted by strain fields. I found that the simplest solution was a combination of the first two methods: a moderate increase in search radius, allied to some judicious redefining of atoms as interstitials.

Introducing interstitials close to the boundary of the crystal meant a further change to DEVIL: if periodic boundary conditions are in operation, these interstitials will have cyclic images on the other side of the block. Care must be taken to ensure that FUNC picks up all the interactions involving the cyclic images.

After suffering from many problems with neighbour lists, I wrote another new DEVIL subroutine. Called CHECK, this subroutine simply goes through the whole lattice to see whether any pairs of atoms that are not defined as neighbours are interacting. To prevent the wastage of large amounts of Cray time on invalid runs, CHECK is called periodically (at a user-controlled interval), and aborts the run if any errors are found. A useful extension to CHECK would be a block of code that automatically redefined the neighbour lists, then carried on the minimisation.

4.2.3 Other new features of DEVIL

To avoid having to set up and relax a dislocation every time I wanted to model a point defect interacting with a dislocation, I needed a dumping facility. DEVIL can now pick up the coordinates of a relaxed dislocation, introduce one or more point defects, and proceed from there: the atoms away from the disturbance caused by the point defect will already be in their relaxed positions. As this process is really just a redefinition of atom positions, it is handled by the DSTORT routine.

The increasing complexity of the calculations made some sort of graphical output vital: I had to be able to *see* what the atoms were doing. A standard DEVIL run will now produce a plot of atom positions, with displacement

vectors indicating how the atoms have relaxed from their initial positions. DSTORT can also read in a set of atom coordinates and select a certain slice of them for display.

The GHOST80-based plotting routine, PLOT, is another Sinclair subroutine: it will plot atoms in Eulerian coordinates (in terms of the normalised block vectors), always looking along the dislocation line. PLOT will also size the circles representing the atoms according to how close to the 'eye' they are, giving some impression of depth.

A few minor changes to DEVIL enable the code to be more flexible: several values that were previously written into the program can now be read as input. One of the new input parameters controls how DSTORT behaves: whether it reads in coordinates from a dump, sets up a dislocation, simply plots an input file without relaxing, plots without displacement vectors, or some combination of these options. Appendix 1 gives full details.

4.3 Results

4.3.1 The position of the dislocation line

To establish a base of experience with DEVIL, I have made a number of calculations on blocks of crystal containing just edge dislocations. A vital test of the program was that it should correctly predict the orientation of the dislocation that has minimum energy.

The first set of calculations introduced dislocations with two different Burgers vectors into blocks of V, Nb, Ta, Mo and W. For all of the calculations described here, I set the accuracy ACC1 (see Thetford [1985] or Appendix 1) to 5×10^{-4}. This value seems sufficient to give energies accurate to three decimal places, or 1 meV.

One parameter that may be varied by the user is the position of the dislocation line in the crystal. As distortions of the fixed boundary layer atoms are determined by their coordinates relative to this line, the line position (*dislx*,*disly*) will have an effect on the energy of the block. For simplicity, (*dislx*,*disly*) is defined in Cartesian coordinates, and is the point where the dislocation line intersects the $z=0$ plane.

Figures 9 and 10 show the effect of varying the line position on the structure of the dislocated block. Two adjacent layers of atoms (the large and the small circles) have been plotted. Moving the position of the dislocation line by one layer of atoms gives a different structure, and causes a step change in the energy. The cause is the arrangement of the atoms at the

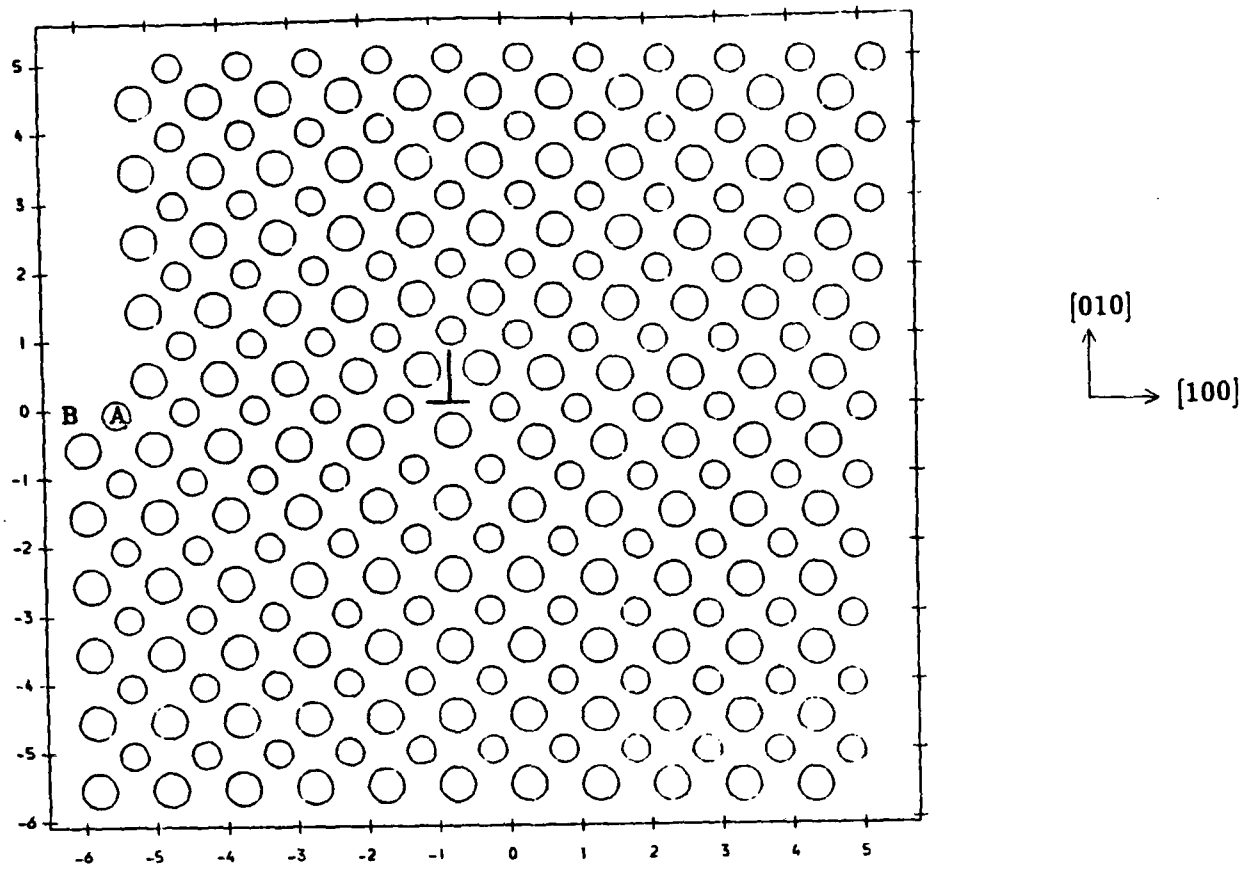

Figure 9. Tantalum [100] dislocation, dislocation line at (0.00, 0.00).

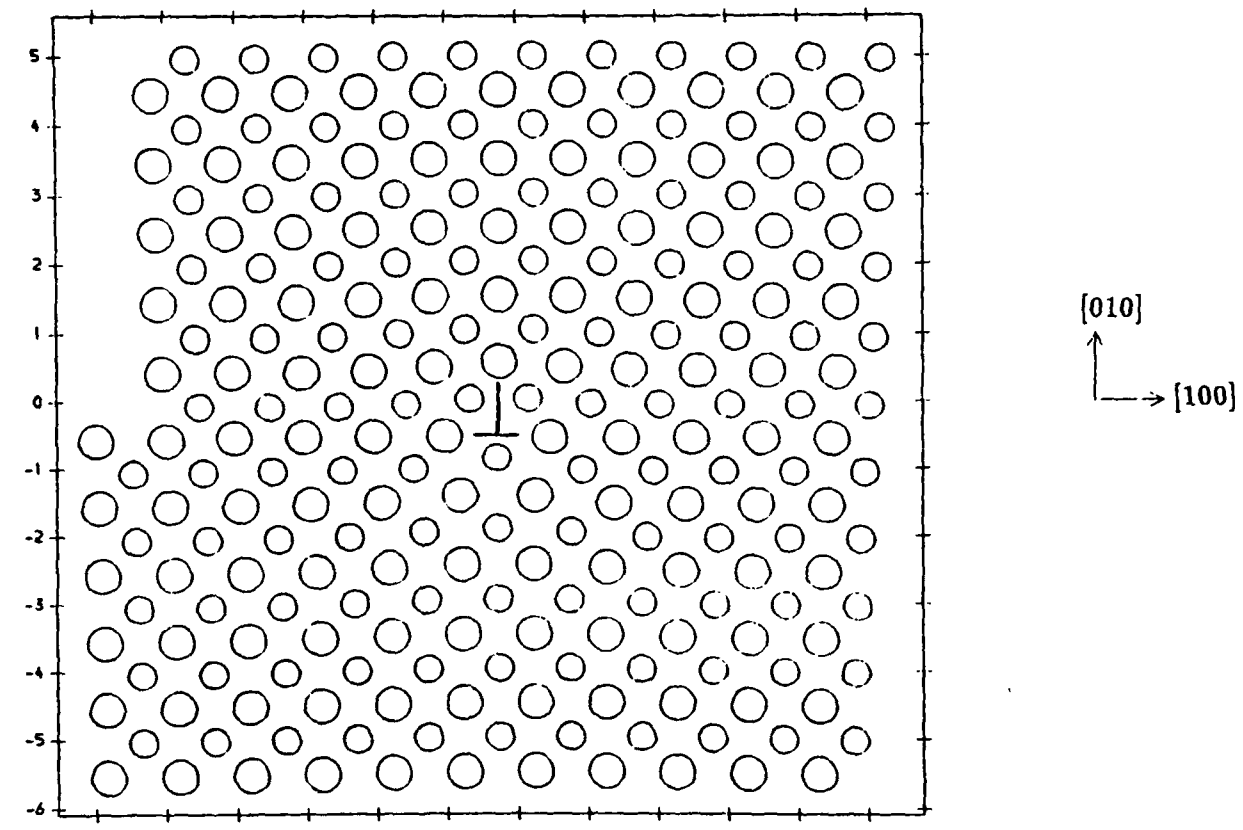

Figure 10. Tantalum [100] dislocation, dislocation line at (0.50, –0.50).

left-hand edge of the figures: in particular, the presence or absence of the atom plotted at (–5.5, 0.0): call it *A*. Of course, *A* really represents a whole row of atoms. In figure 9, the atom at (–6.0, –0.5) (*B*, say) feels the presence of *A*, which is in the correct equilibrium location (according to elasticity theory). In figure 10, *A* is missing so the calculation of the cohesive energy of *B* simply assumes that the $(\frac{1}{2}, \frac{1}{2}, \pm\frac{1}{2})$ neighbours are at the *perfect-lattice* separation (see §2.2.2). This artificial value upsets the calculation, and so raises the energy of the assembly. (The energies of the fixed atoms must be included in the block energy, for they will alter as the free atoms move.) The arrangement of figure 9 has an energy that is lower by 8 eV.

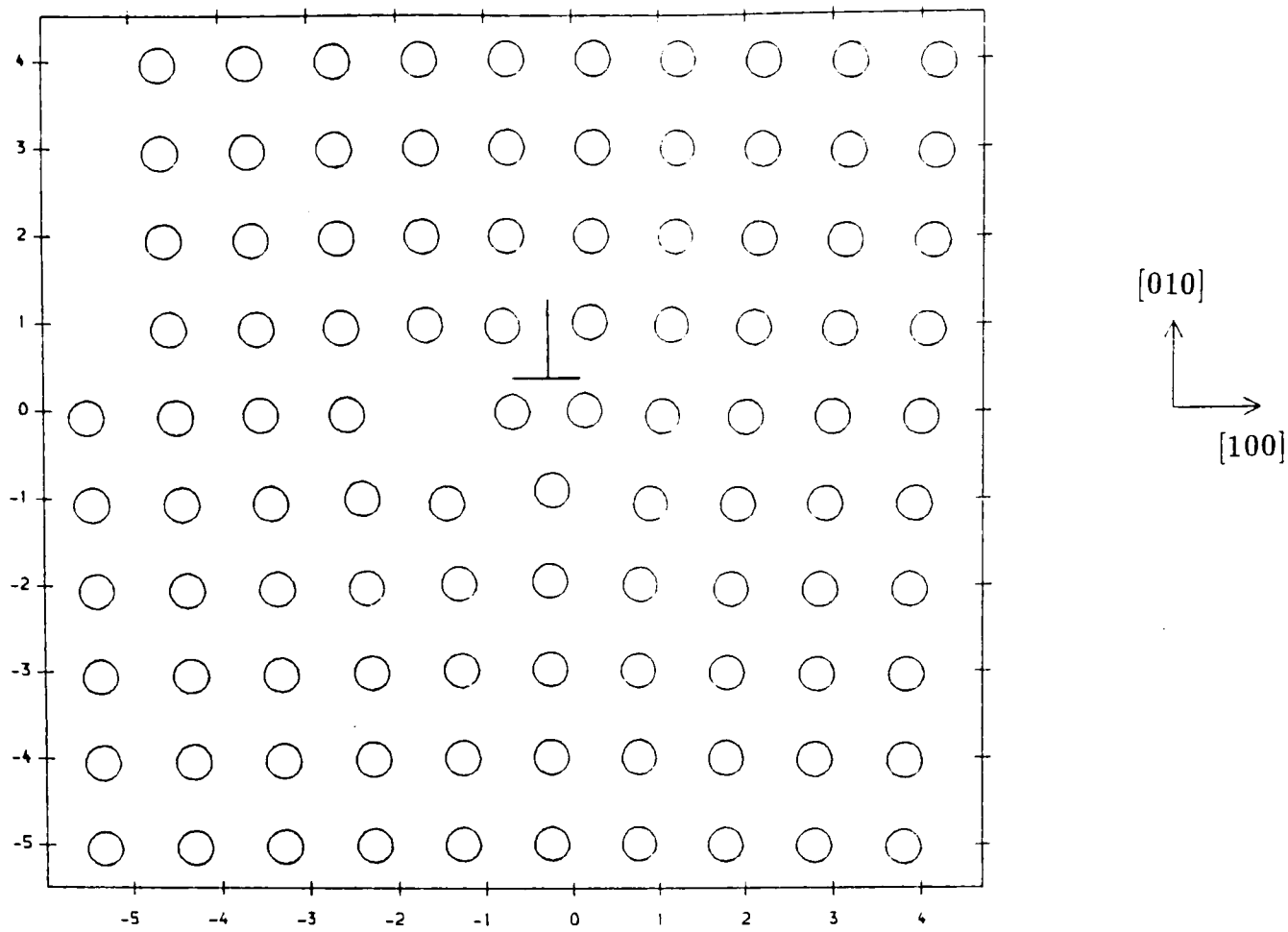

Figure 11. Tantalum [100] dislocation: relaxation to a local minimum.

Figure 11 shows another effect of the dislocation line position: the starting position chosen has relaxed to a configuration that has an energy higher than the minimum. Because the conjugate gradients minimisation used by DEVIL is a monotonic procedure and does not include any random fluctuations, DEVIL sometimes finds such local minima or metastable states. Being able to plot atom positions makes spotting these anomalies quite easy, and they are easily cured (redefine the errant atom as an interstitial and insert it closer to its 'true' relaxed position).

The position of the dislocation line affects the block energy in a more subtle way. A dislocation produces a stress field. The energy contained in a particular block of atoms depends on the position of that block relative to the dislocation line: i.e. what region of the stress field is sampled by the block. As the energy density is highest closest to the dislocation line, a block placed centrally will have a higher energy than one that only just includes the dislocation line. I tested this expectation using a $\frac{1}{2}[111](1\bar{1}0)$ edge dislocation (i.e. a dislocation with Burgers vector $\frac{1}{2}[111]$ and glide plane $(1\bar{1}0)$ — usually abbreviated to just '$\frac{1}{2}[111]$ dislocation') in a block of molybdenum atoms with width 7[111]. The dislocation line now runs in the $[11\bar{2}]$ direction. Moving the dislocation line towards the edge of the block by 3[111] reduced the energy by about 10 eV [Thetford, 1988].

Putting the axes of a discontinuous displacement field through lines of atoms seems to be inviting instabilities, so all calculations henceforth have dislocation lines as far away from atoms as possible, and in the middle of the block. Provided the same coordinates are used for all sets of comparable

calculations, no difficulties should arise. In the rest of this thesis, I have used (*dislx*,*disly*) = ($\frac{1}{4}$,$-\frac{1}{8}$) for the $\frac{1}{2}\langle 111\rangle$ dislocation, and (*dislx*,*disly*) = ($\frac{1}{4}$,$\frac{1}{4}$) for $\langle 100\rangle$.

4.3.2 Varying the Burgers vector

Elasticity theory suggests that the energy per unit length of a dislocation should be proportional to $\mathbf{b}^2$, the square of the Burgers vector. In a b.c.c. lattice, the two dislocations with shortest Burgers vector are $\frac{1}{2}\langle 111\rangle$ and $\langle 100\rangle$. In each of the five metals studied, I have calculated the dislocation energy per unit length for these two Burgers vectors. Calculations on blocks of different sizes also give an idea of how many atoms are needed to reduce edge effects to an acceptable level.

Metal	$\frac{1}{2}\langle 111\rangle$ dislocation			$\langle 100\rangle$ dislocation		
	N_{free}	E /nJm^{-1}	Theory[a]	N_{free}	E /nJm^{-1}	Theory[a]
V	1152 2560	2.59 2.72	1.37	686 1024	3.30 3.34	1.82
Nb	1152	2.88	1.07	686 1024	3.83 3.88	1.44
Ta	1152	3.80	3.27	686 1024	4.84 4.90	4.35
Mo	1152	4.27	3.41	686 1024	5.15 5.26	4.55
W	1152	5.58	5.22	686 1024	6.73 6.89	6.95

[a] from equation (4.5)

Table 4.1 Energy E per unit length (nJm^{-1}) for $\frac{1}{2}\langle 111\rangle$ and $\langle 100\rangle$ dislocations.

Table 4.1 gives dislocation energies per unit length for $\frac{1}{2}\langle 111\rangle$ and for $\langle 100\rangle$ dislocations. To enable comparison with the $\langle 100\rangle$ case, two layers of a relaxed block of tantalum atoms containing a $\frac{1}{2}\langle 111\rangle$ dislocation are shown in figure 12. I have modelled $\langle 100\rangle$ dislocations in blocks of two different sizes: 14×14×14 and 16×16×16 atom planes. Because the calculation is expensive, I have made only one run (vanadium, 32×16×30 atom planes) on

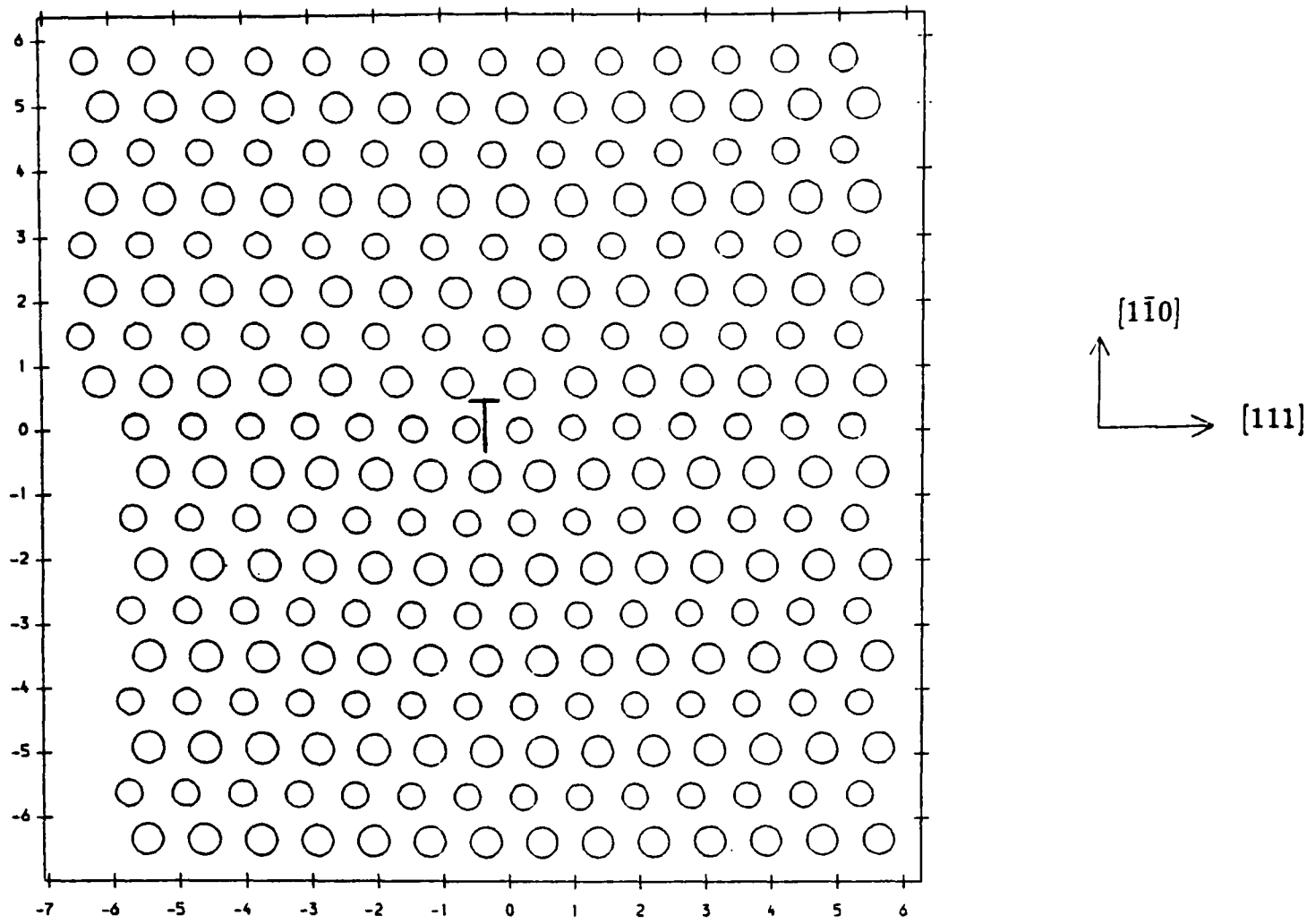

Figure 12. Two planes of atoms, ½[111] dislocation in tantalum.

a large block containing a $\frac{1}{2}\langle 111\rangle$ dislocation. In contrast to the situation for point defects, the larger blocks give larger energies.

There is a difference between the point defect case and the dislocation calculations. For the point defects, the boundary atoms are fixed at their perfect lattice positions. As the size of the block increases, more volume is available to relax the defect strain. Because the strain field falls off as r^{-2}, the energy contained in a spherical shell of radius r and thickness δr is proportional to $r^{-2}\delta r$. The energy for an infinite block integrates to say E_∞, and the modelled energy E reduces gradually to E_∞ as the artificial constraint of making the strains vanish at a boundary of finite radius becomes less important.

For a dislocation, the strain field is proportional to r^{-1} so the energy contained in a cylindrical shell of radius r and thickness δr is proportional to $r^{-1}\delta r$. Integrating outwards from the core radius r_0 to a boundary radius r_1, the energy of a dislocation (in isotropic elasticity theory) is

$$E(r_1) = \frac{b^2\mu}{4\pi(1-\nu)} \ln(r_1/r_0) + E_{core} \qquad (4.5)$$

where μ is the shear modulus, ν the Poisson ratio, $b=|\mathbf{b}|$, and E_{core} is the contribution from the core. Hence $E(r_1)\rightarrow\infty$ as $r_1\rightarrow\infty$, and boundary conditions cannot be neglected. The anisotropic treatment is fraught with complicated mathematics, and deeper theoretical investigation mined with pitfalls. I desire only a rough comparison, so the 'theory' columns in table 4.1 assume that $\ln(r_1/r_0) = 3$ for the DEVIL blocks, take $\nu=C_{12}/(C_{11}+C_{12})$, $\mu=C_{44}$ (with the C's from Finnis and Sinclair [1984]), and allow $0.1\mu b^2$ for

E_{core} [Hirth and Lothe 1968, p63]. The table gives assurance that the values predicted by DEVIL are not wildly inaccurate, though they do tend to be higher than the crude theoretical estimates, particularly for vanadium and niobium.

One interesting anomaly appeared during this work. To help the relaxation, the atoms along the line $x=y=0$ are redefined as interstitials. As these atoms are in the core of the dislocation they are likely to have relatively large displacements from their equilibrium positions, and so can start interacting with atoms that were originally out of range of the potential. By redefining them as interstitials, DEVIL assumes that they may interact with any other atom in the block; were they still normal free atoms, they (and hence the rest of the lattice) would require excessively long neighbour lists. Figure 13, extracted from the DEVIL output for $\langle 100 \rangle$ dislocations in a 16^3 block, shows the relaxed coordinates of these 'interstitial' atoms for the five metals. The interstitials in vanadium, niobium, tantalum and tungsten form straight lines parallel to the z axis, while the line of molybdenum interstitials seems to bend. No such phenomenon appears for the $\frac{1}{2}\langle 111 \rangle$ dislocation. Although the deviation from the straight line is not large, this result together with the previously reported 'skew dumbbell' in molybdenum [Thetford 1985, Ackland and Thetford 1987, Zeper 1986, Harder and Bacon 1986], suggests that the Finnis-Sinclair potential for molybdenum can behave strangely.

4.4 Conclusions

The original DEVIL program has been extended in several ways.

- The block of atoms can now be a general parallelepiped, not just a cuboid.
- The kernel of the code (the FUNC subroutine that calculates energies and gradients) has been entirely rewritten in a vectorisable form.
- Dislocations can be introduced into the modelled region, with boundary displacements determined from anisotropic elasticity theory.
- A set of relaxed coordinates from a previous run can be used as a starting position for a subsequent run.
- Slices across the modelled block can be plotted, making errors and anomalies easy to spot.

A survey of dislocation line position shows that moving this line can lead to unexpected energy differences, particularly if the origin of coordinates

Interstl coords:	-1.571995E-02	1.602255E-02	-4.000003E+00
V	-1.572741E-02	1.602961E-02	-2.999993E+00
	-1.572809E-02	1.604703E-02	-2.000000E+00
	-1.572168E-02	1.603708E-02	-1.000005E+00
	-1.573229E-02	1.602807E-02	1.476892E-06
	-1.572020E-02	1.603305E-02	1.000000E+00
	-1.571422E-02	1.602877E-02	2.000002E+00
	-1.572202E-02	1.602933E-02	2.999998E+00
Interstl coords:	-3.553268E-02	9.758391E-03	-3.999999E+00
Nb	-3.553851E-02	9.762876E-03	-3.000000E+00
	-3.554621E-02	9.767615E-03	-2.000000E+00
	-3.553880E-02	9.760494E-03	-1.000000E+00
	-3.553009E-02	9.751679E-03	-1.132269E-06
	-3.552854E-02	9.743302E-03	1.000001E+00
	-3.553181E-02	9.738675E-03	2.000000E+00
	-3.553256E-02	9.745560E-03	3.000000E+00
Interstl coords:	-2.211577E-02	1.057990E-02	-4.000000E+00
Ta	-2.210885E-02	1.057989E-02	-3.000005E+00
	-2.210222E-02	1.056983E-02	-2.000002E+00
	-2.210932E-02	1.057445E-02	-9.999922E-01
	-2.211539E-02	1.058466E-02	1.931026E-06
	-2.211109E-02	1.056634E-02	9.999950E-01
	-2.209894E-02	1.055113E-02	2.000001E+00
	-2.210473E-02	1.056348E-02	3.000002E+00
Interstl coords:	1.605121E-03	-3.561035E-03	-3.999953E+00
Mo	1.439313E-03	-3.719946E-03	-3.000037E+00
	1.425994E-03	-3.770032E-03	-2.000057E+00
	1.500548E-03	-3.750704E-03	-1.000005E+00
	1.378008E-03	-3.902172E-03	3.152945E-06
	1.254697E-03	-3.996169E-03	9.999824E-01
	1.317753E-03	-3.821220E-03	2.000032E+00
	1.544836E-03	-3.586376E-03	3.000037E+00
Interstl coords:	-4.218298E-02	-4.757536E-02	-3.999998E+00
W	-4.218202E-02	-4.757752E-02	-3.000002E+00
	-4.218356E-02	-4.757529E-02	-1.999997E+00
	-4.218380E-02	-4.757455E-02	-1.000003E+00
	-4.218156E-02	-4.757754E-02	1.669890E-06
	-4.218458E-02	-4.757498E-02	9.999994E-01
	-4.218620E-02	-4.757514E-02	2.000000E+00
	-4.218409E-02	-4.757758E-02	2.999999E+00

Figure 13. Comparison of positions of atoms in dislocation cores.

crosses a plane of atoms. Keeping the dislocation line well away from lines of atoms seems to provide a stable basis for making comparisons.

Reference values for the energies of various dislocations in the five transition metals vanadium, niobium, tantalum, molybdenum and tungsten are presented in table 4.1. The $\frac{1}{2}\langle 111 \rangle$ dislocation is more stable than the $\langle 100 \rangle$ dislocation, as would be expected from simple elasticity theory. The energies are the same order of magnitude as theoretical values.

None of the dislocations modelled seem susceptible to dissociation into partials. This is not surprising: the $\frac{1}{2}\langle 111 \rangle$ Burgers vector is the shortest possible in the b.c.c. lattice, and as the energy of the $\langle 100 \rangle$ dislocation is only about 30% higher, any reaction such as

$$[100] \rightarrow \tfrac{1}{2}[111] + \tfrac{1}{2}[1\bar{1}\bar{1}] \qquad (4.6)$$

will increase the total energy.

The molybdenum potential continues to show some interesting behaviour: a dislocation that is expected to be straight is found to relax to a slightly bowed position. This phenomenon is likely to be connected with the existence of the low-energy 'bent interstitial' found only in molybdenum (§3.2.2).

The development of DEVIL has been aimed at modelling the interaction of dislocations and point defects. Interactions involving stationary defects can now be handled immediately, and migration calculations will require only a small modification.

5 Defect Migration in Perfect Lattices

5.1 Introduction

Before considering the migration of interstitials towards dislocations, it is useful to investigate migration in perfect crystals. This work not only provides a comparison for the migration steps towards the dislocation cores to be considered in §6.8 and §6.9; it also provides experience in using DEVIL, produces some results for comparison with experiment, and studies a problem that is important in its own right. I have already touched (in §3.2.5) upon interstitial migration in tungsten, but more detailed work for the other metals is required.

Considerable controversy surrounds self-diffusion in radiation-damaged metals, and what mechanism is responsible for the so-called 'stage III recovery'. Figure 14, taken from Young [1978], shows a typical curve for the behaviour of the resistivity of a radiation-damaged metal. As the metal is annealed, different defects become mobile at different temperatures; eventually all the vacancies and interstitials are mobile, annihilate one another and the resistivity attains its pre-damage value. Balluffi [1978] and Young [1978] present details of the controversy, and Wollenberger [1983] gives a sober review. Proponents of the one-interstitial model (OIM) maintain that the stage III recovery is due to vacancy migration, while the advocates of the two-interstitial model (TIM) invoke motion of the stable interstitial state.

Table 5.1 lists the various stages of the resistivity recovery, and how each of the models explains them. (For an idea of the intensity of the debate on this issue, see Schüle [1981], Jacques and Robrock [1981] and Frank [1981], particularly the discussion on this last paper. The battle recommenced at the next 'Point Defects' conference in Berlin: see, for example, the flatly contradictory statements in van Veen [1986] and Frank and Seeger [1986].) Any work that throws some light on this problem, although likely to be hailed by one set of protagonists and assailed by the other, must be useful.

Many different migration paths can be considered, but intuitively, the step to the nearest neighbour appears to be most likely: hence for these b.c.c. metals, I have looked at the $\langle 111 \rangle$ route. Sections 5.1.1 and 5.1.2 of this introduction describe the interstitial migrations studied here. §5.2 details the calculational procedure used, and §5.3 gives the results of the interstitial migrations.

Unlike the interstitial migration enthalpy, measurements do exist for the

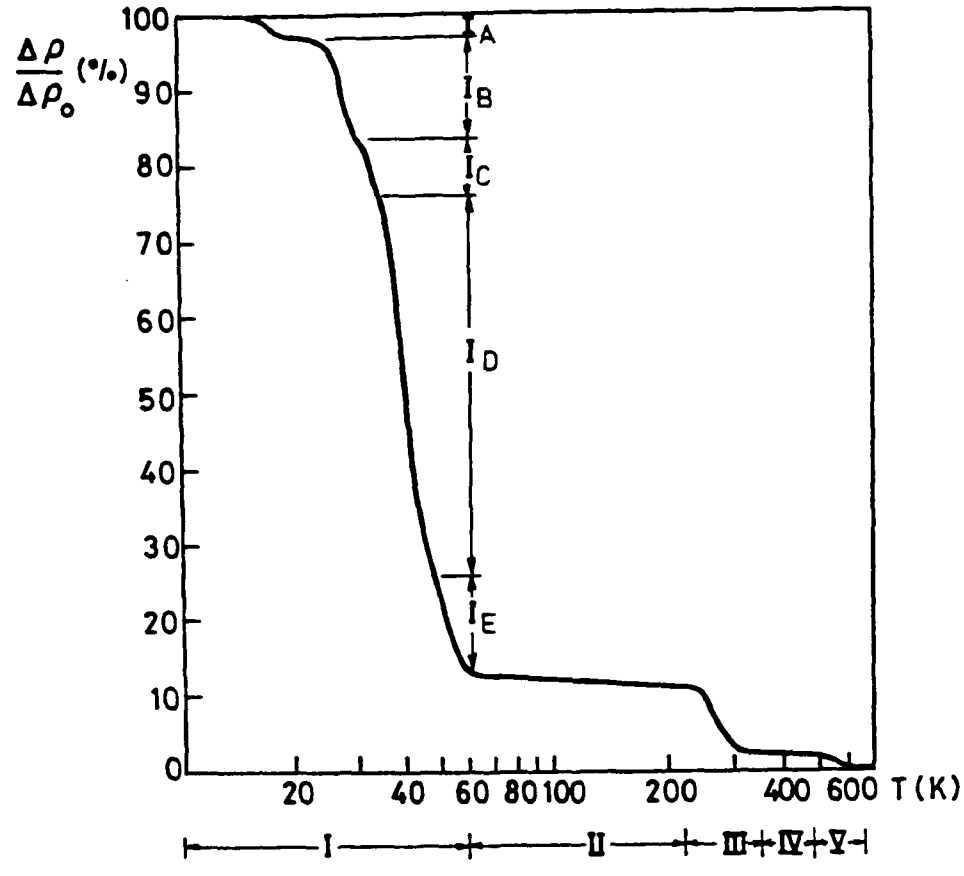

Figure 14. Isochronal recovery curve of electrical resistivity of copper electron-irradiated at 4 K.

vacancy migration enthalpy (see, for example, Phillipp, Saile and Urban [1981] and Tietze, Takaki, Schwirtlich and Schultz [1981]). As DEVIL can calculate migration energies very easily, I have done the calculations and §5.4 presents the results.

As all the calculations in this chapter are performed at constant lattice parameter (constant volume), the calculated quantities are *energies (E)* of migration and formation. Experiments carried out at constant pressure will measure *enthalpies* (*H*), and while the difference is not large for these metals (there being little change in the volume of the block as a vacancy migrates, for example), I have made the distinction throughout.

5.1.1 Migration of ⟨111⟩ crowdions and dumbbell interstitials

Consider for a moment a metal in which the interstitial forms a ⟨111⟩ dumbbell or a ⟨111⟩ crowdion. For reasons explained below (§5.3.5), consider migration in the [11$\bar{1}$] direction. Let the dumbbell have length $2l_d a$ and be centred on (0, 0, 0). The two atoms forming the dumbbell are then at $(\pm l_d/\sqrt{3})(1, 1, -1)$; typically l_d is 0.38 in a b.c.c. lattice, giving dumbbell positions of ±(0.219, 0.219, −0.219)

Suppose now that for a crowdion centred at $(\frac{1}{4}, \frac{1}{4}, -\frac{1}{4})$ the distance to the nearest neighbours is $2l_c a$. The 'nearest-neighbour' atoms will then be at $(\frac{1}{4}, \frac{1}{4}, -\frac{1}{4}) \pm 2l_c(1, 1, -1)$. In particular, if l_c takes the tungsten value of 0.382, one of these atoms is at (−0.192, −0.192, 0.192).

Stage	One Interstitial Model	Two Interstitial Model
I_A–I_C	Close pairs of interstitials and vacancies recombine.	Close pairs of interstitials and vacancies recombine.
I_D	'Correlated recombination' of freely-migrating interstitial with its own vacancy.	Close pair recombination, plus annihilation of vacancies by 'on-line' crowdions (vacancy lies on migration line of crowdion).
I_E	Free long-range migration of stable interstitials ($\langle 110 \rangle$ dumbbells in b.c.c. metals), annihilating frozen-in vacancies and forming interstitial and interstitial-impurity clusters.	Long-range migration of metastable interstitials ($\langle 111 \rangle$ crowdions or dumbbells in b.c.c. metals)
II	Interstitial clusters coarsen; more frozen-in vacancies are annihilated. Some detrapping from clusters.	Detrapping from interstitial clusters, plus conversion of mobile metastable interstitials to sessile stable interstitials.
III	Vacancies mobile, annihilating interstitials at interstitial clusters, forming vacancy clusters and being absorbed at fixed sinks.	Stable interstitials ($\langle 110 \rangle$ dumbbells in b.c.c. metals) free to migrate.
IV	Various rearrangements and coarsening.	Vacancies mobile.
V	Vacancy clusters dissociate thermally, all excess defects eliminated by self-diffusion.	Vacancy clusters dissociate thermally, all excess defects eliminated by self-diffusion.

Table 5.1 Stages of resistivity recovery, according to the OIM and the TIM.

Clearly then, the $\langle 111 \rangle$ crowdion and $\langle 111 \rangle$ dumbbell have atoms in very similar positions. Figure 15, a view of the $(1\bar{1}0)$ plane, shows the two configurations. Moving an atom from (–0.219, –0.219, 0.219) to (–0.192, –0.192, 0.192) and another from (0.219, 0.219, –0.219) to (0.25, 0.25, –0.25) (or vice versa) is unlikely to cost a lot of energy: the distance involved is only $0.05a$, and the relaxed configuration of the rest of the lattice ought to be similar in the two cases.

Hence for metals where both the $\langle 111 \rangle$ dumbbell and the $\langle 111 \rangle$ crowdion

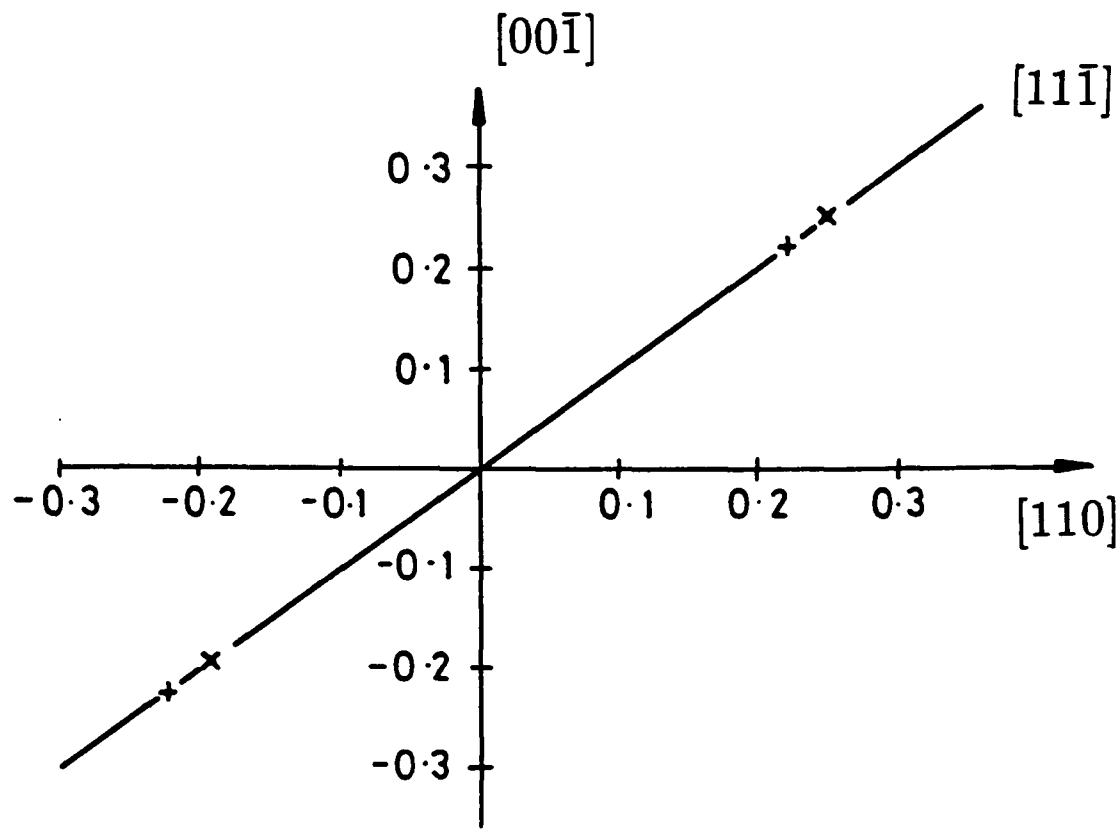

Figure 15. Closeness of the ⟨111⟩ crowdion (x) and the ⟨111⟩ split dumbbell (+).

are at least metastable, I expect the interstitial formation energies to be similar. Moreover, migration in any of the ⟨111⟩ directions should be energetically favourable.

5.1.2 Migration of ⟨110⟩ dumbbell interstitials

Consider now a metal in which the stable interstitial configuration is a ⟨110⟩ split dumbbell. Once more, let the dumbbell have length $2l_d a$ and be centred on (0, 0, 0). The two atoms forming the dumbbell are then at $(\pm l_d/\sqrt{2})(1, 1, 0)$; typically $l_d = 0.377$ so the dumbbell atoms are at $\pm(0.267, 0.267, 0.00)$.

The shortest migration along $-[11\bar{1}]$ is to a split dumbbell centred at $(-\frac{1}{2}, -\frac{1}{2}, \frac{1}{2})$. This dumbbell can be aligned in any of the six ⟨110⟩ directions, but the ones of interest here are [110], $[01\bar{1}]$ and $[10\bar{1}]$: the others are not favourably oriented for migration from the given start position. As $[01\bar{1}]$ and $[10\bar{1}]$ are related symmetrically by an interchange of the x and y axes, and as this transformation keeps the starting dumbbell [110] unchanged, we need consider migration to only one of this pair. Figure 16 shows the initial position of the dumbbell centred at (0, 0, 0), and the two possible final positions studied.

Step A is the migration to a parallel dumbbell. The 'migrating' atom of the dumbbell pair typically moves from (–0.267, –0.267, 0.0) to (–0.233, –0.233, 0.50): a step that is very close to [001]. Jacques and

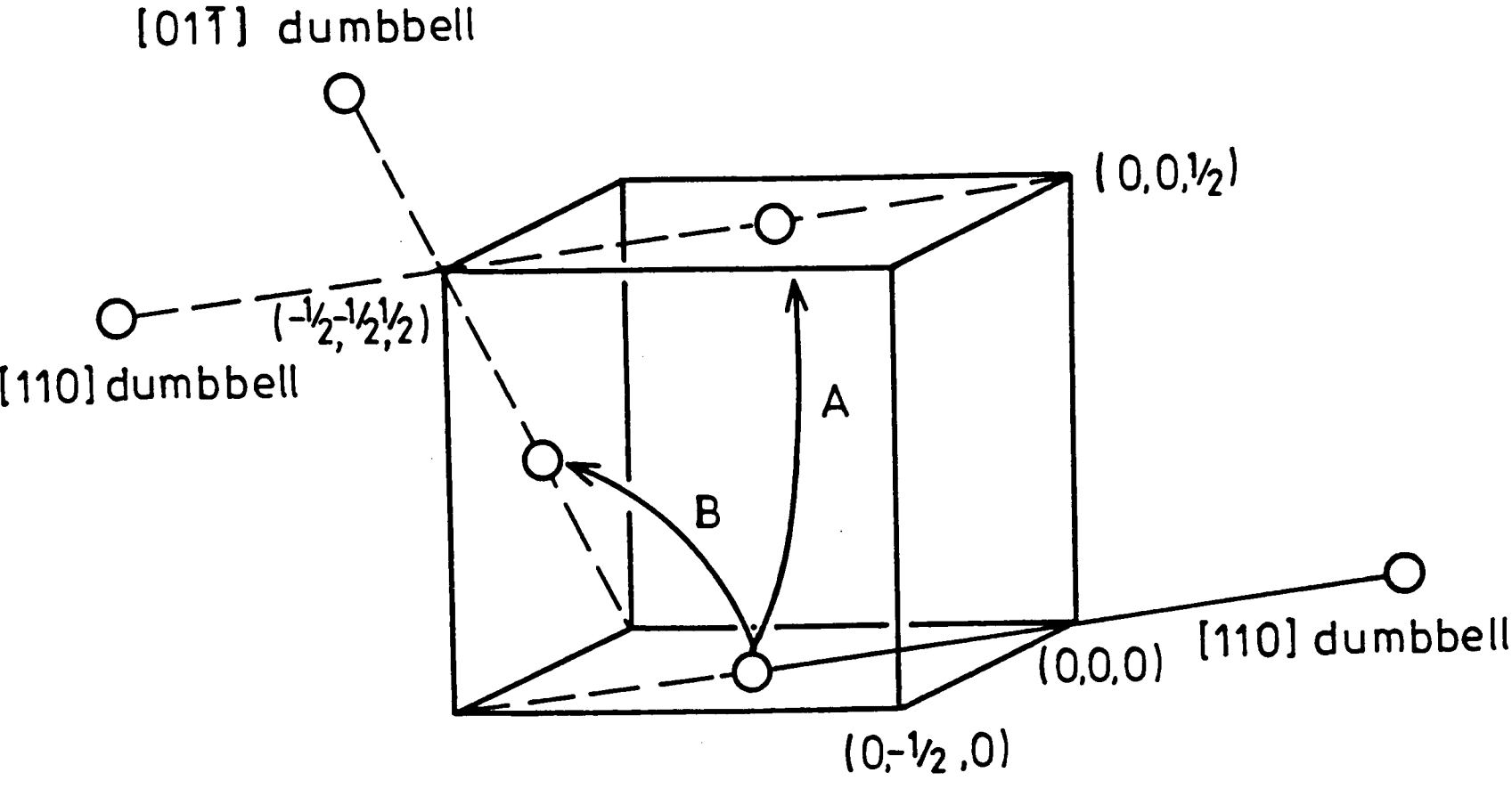

Figure 16. Possible migration paths for the [110] split interstitial.

Robrock [1981] have suggested that an interstitial moving in this manner will remain on one ⟨110⟩ plane for many migration steps: all four such ⟨111⟩ jumps from the new site are coplanar with the old jump. The length of a step A jump is $0.502a$.

Step B in figure 16 involves a rotation of the dumbbell, and is therefore known as the 'reorientation jump'. The dumbbell centre moves as before, but the dumbbell itself is now pointing along a different ⟨110⟩ direction. Using once more a typical dumbbell separation of $0.755a$, the migrating atom moves from (–0.267, –0.267, 0.0) to (–0.50, –0.233, 0.233). This step has length $0.331a$, and its direction is very close to [101].

The nomenclature used here for the migration steps is the same as that used by Harder and Bacon [1986].

5.2 Calculational Procedure

The method of §3.2.1 enables DEVIL to freeze the interstitial on various planes along the migration path, permitting energies of migration to be calculated. To step an atom i by a distance δ in the direction of unit vector $\mathbf{n}$, the position $\mathbf{x}_i$ at the end of one relaxation is simply replaced by

$$\mathbf{x}_i' = \mathbf{x}_i + \delta\,\mathbf{n} \tag{5.1}$$

The migrating atom itself may relax on the plane perpendicular to $\mathbf{n}$, as discussed in §3.2.1. Stepping to the next position involves moving only the

migrating atom; the rest of the lattice then relaxes from the position occupied at the end of the previous step. This process should mirror what happens in a real migration, but it does introduce some hysteresis: the energy saddle points for migration steps forward and backward do not necessarily lie at the same place. This is unimportant physically, but will tend to complicate the description of what is happening.

I performed all of the interstitial migration calculations in the block to be used for the dislocation modelling: block edges [111], [1$\bar{1}$0] and [11$\bar{2}$], of size 24×12×24 lattice planes. The block has fixed boundaries in the first two directions, and a periodic boundary condition is applied in the third direction. There are 1152 atoms in the free region, plus another 1872 in the fixed boundaries. The periodic boundary layers contain 2268 images of free and fixed atoms. The periodic boundaries in the [11$\bar{2}$] direction mean that the block really contains an infinite line of defects migrating; they are separated by sufficient distance though that any interaction should be negligible.

I have already described calculations of vacancy formation energy in molybdenum (§2.4.1). Prior to studying vacancy migration, I needed formation energies for the other metals. These were calculated just as in §2.4.1, in a 10×10×10 block (250 free atoms) with periodic boundary conditions. The block edges are all parallel to the basis cube: i.e. [100], [010] and [001].

Vacancy migration is easily dealt with: I define a pair of vacancies, put an interstitial in one and migrate it by the above method towards the other. To allow room for any relaxations associated with the migration, the migration calculations themselves have been performed in a 12×12×12 block. This block must have **fixed** boundaries: otherwise, when the interstitial atom is pushed in its migration direction, the whole of the rest of the lattice will translate with it! The block contains 432 free atoms, plus 1026 atoms in the boundary layers.

5.3 Interstitial Migration Results

Table 5.2 summarises the results obtained, and the subsections below discuss the calculations in more detail. Although the detail above has related to steps in the [101] and [001] directions, the calculations have actually used steps along [10$\bar{1}$] and [00$\bar{1}$]. The introduction uses the positive steps merely so that figure 16 is easier to relate to figure 19.

metal	$E_i^{m,3D}$/eV, jump B (0.25[10$\bar{1}$] step)	$E_i^{m,2D}$/eV, jump A ($\frac{1}{2}$[00$\bar{1}$] step)
V	0.29	0.38
Nb	0.22	0.37
Ta	0.37	0.36
Mo	0.23	0.25

Table 5.2 Calculated interstitial migration energies.

5.3.1 Niobium: reorientation jump favoured

When I started doing the interstitial migration calculations, I expected the 'reorientation jump', path B in figure 16, to be favoured over path A. The niobium calculation bears out this expectation rather well. The curves of energy against distance along migration direction (figure 17) have similar shapes and are nicely symmetrical. The longer migration path A has a correspondingly higher migration energy. There are no shocks here.

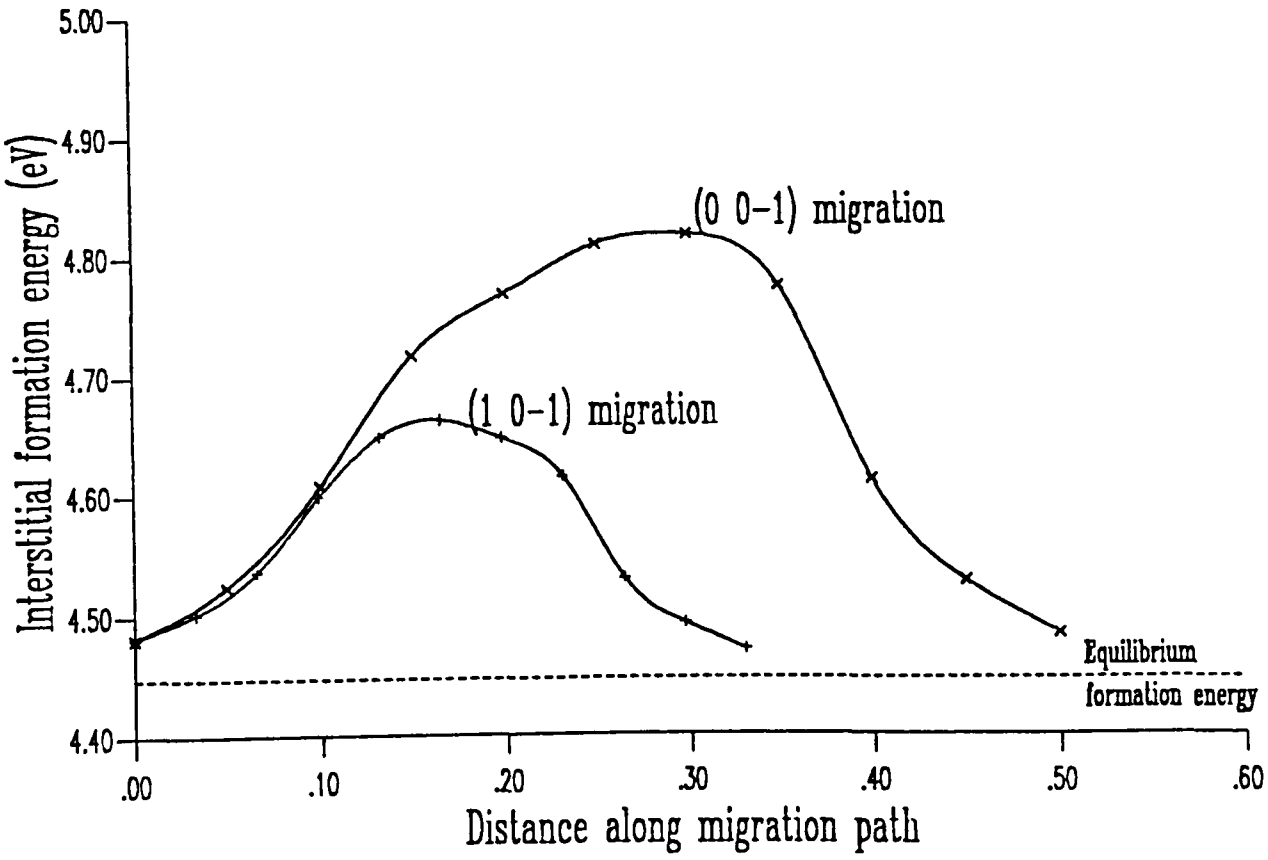

Figure 17. Niobium: interstitial energy against migration distance.

5.3.2 Vanadium: a second-neighbour jump

The [10$\bar{1}$] migration in vanadium goes as expected. The migration step has a fairly small energy, the migrating atom follows the obvious path and the

curve of energy against distance along the forced migration direction is symmetric. Figure 18 shows this curve.

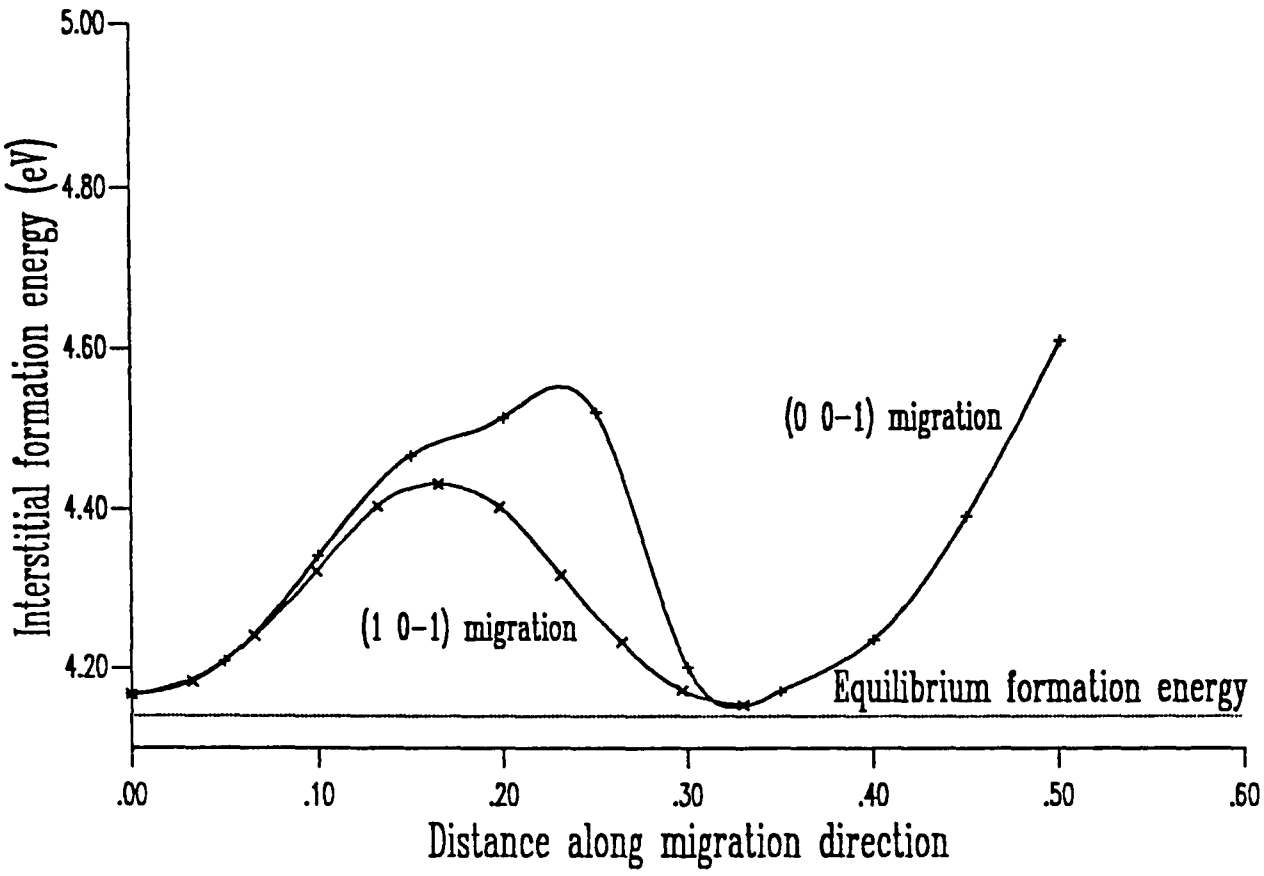

Figure 18. Vanadium: interstitial energy against migration distance.

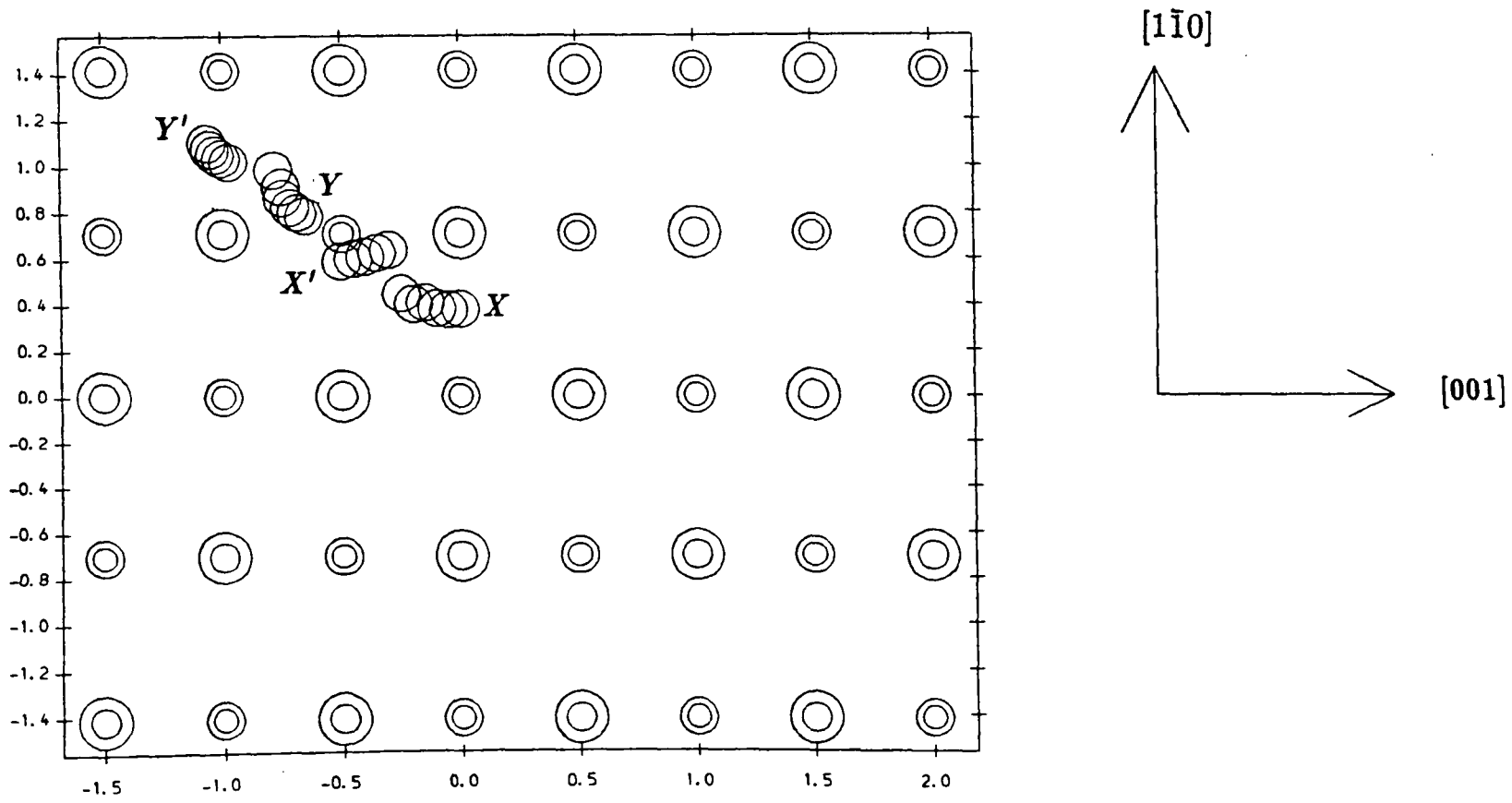

Figure 19. Vanadium: paths of migrating atoms in the 'double jump'.

However, the results for the $\frac{1}{2}[00\bar{1}]$ step were not what I had expected. Instead of the dumbbell going from being centred at (0, 0, 0) to $(\frac{1}{2}, \frac{1}{2}, -\frac{1}{2})$,

the final split interstitial is centred at (1, 1, −1). This migration step has been proposed by Johnson [1985] as a possible mechanism for 2-d migration (the dumbbell always migrates in the ⟨110⟩ plane that is coplanar with its two atoms). I did not expect to see this step favoured over the shorter jump though, particularly when I was pushing the migrating atom in the correct direction for it to make the short jump.

Figure 19 shows the path of the migrating atom ($X-X'$), starting from the relaxed dumbbell position of (0.26, 0.26, 0.0). The positions of the atoms on the perfect lattice are shown as a background reference: these are **not** the relaxed positions.

The z–coordinate is reduced in steps of $0.1a$, with relaxation allowed in the (001) plane, and for the first five steps, everything goes smoothly. But the relaxed position for the next step is a long way from the previous path, and the closest pair of atoms in the solid is no longer centred at $(\frac{1}{2}, \frac{1}{2}, -\frac{1}{2})$ but at (1, 1, −1). The migration path ($Y-Y'$) of the atom originally at $(\frac{1}{2}, \frac{1}{2}, -\frac{1}{2})$ is also plotted, and it too shows the jump: from being part of the dumbbell centred at $(\frac{1}{2}, \frac{1}{2}, -\frac{1}{2})$ to being part of the dumbbell centred at(1, 1, −1). Pushing the 'migrating' atom further in the z–direction merely upsets the equilibrium of the newly-formed dumbbell, raising the energy as shown in figure 18.

5.3.3 Tantalum: 2-d migration possible

In tantalum, the short migration step (path B) once more behaves as expected (figure 20). The path A migration seems to find a flat energy plateau with a wide saddle, before descending into the expected minimum, a jump by $(\frac{1}{2}, \frac{1}{2}, -\frac{1}{2})$. This phenomenon appears to be connected with the relatively flat portion of figure 5: the interstitial formation energy changes only slowly as the dumbbell rotates from ⟨110⟩ to ⟨111⟩. There are no unusual features in the plot of the atom paths.

5.3.4 Molybdenum: complicated by the bent interstitial

Self-interstitial migration in molybdenum is less straightforward, mainly because the ⟨110⟩ dumbbell is not the lowest-energy configuration. The 'bent interstitial', first mentioned in §2.4.2 and examined in more detail in §3.2.2, is rotated away from ⟨110⟩ by some 15°. Figure 3 shows that a rotation very nearly in the (001) plane has the lowest energy, but rotation in any direction will reduce the interstitial formation energy by about 0.04 eV. Starting from a [110] split dumbbell therefore means that the energy will drop slightly to start with, and will rise at the end of the migration paths.

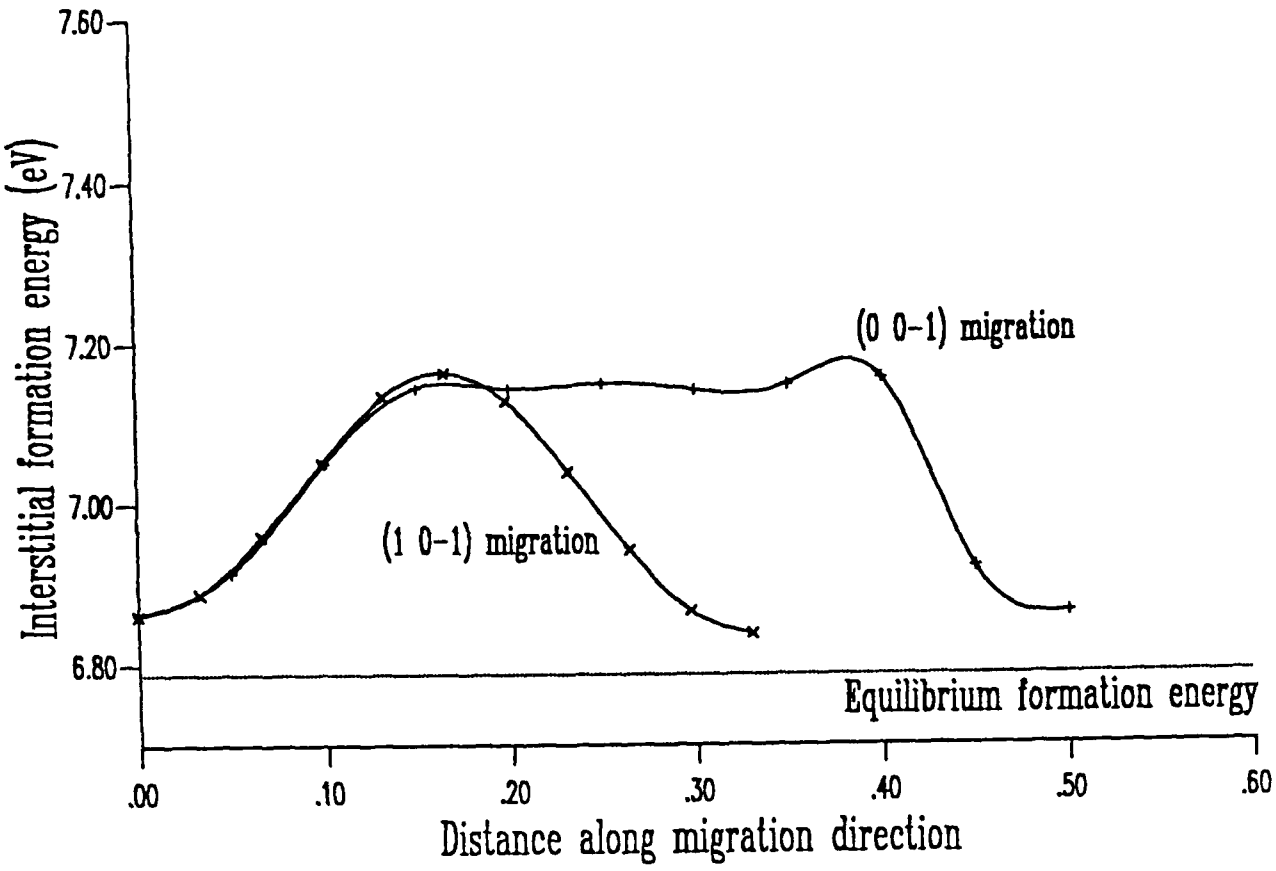

Figure 20. Tantalum: interstitial energy against migration distance.

Both the $[10\bar{1}]$ (path B) and the $[00\bar{1}]$ (path A) migrations in figure 21 show this nicely.

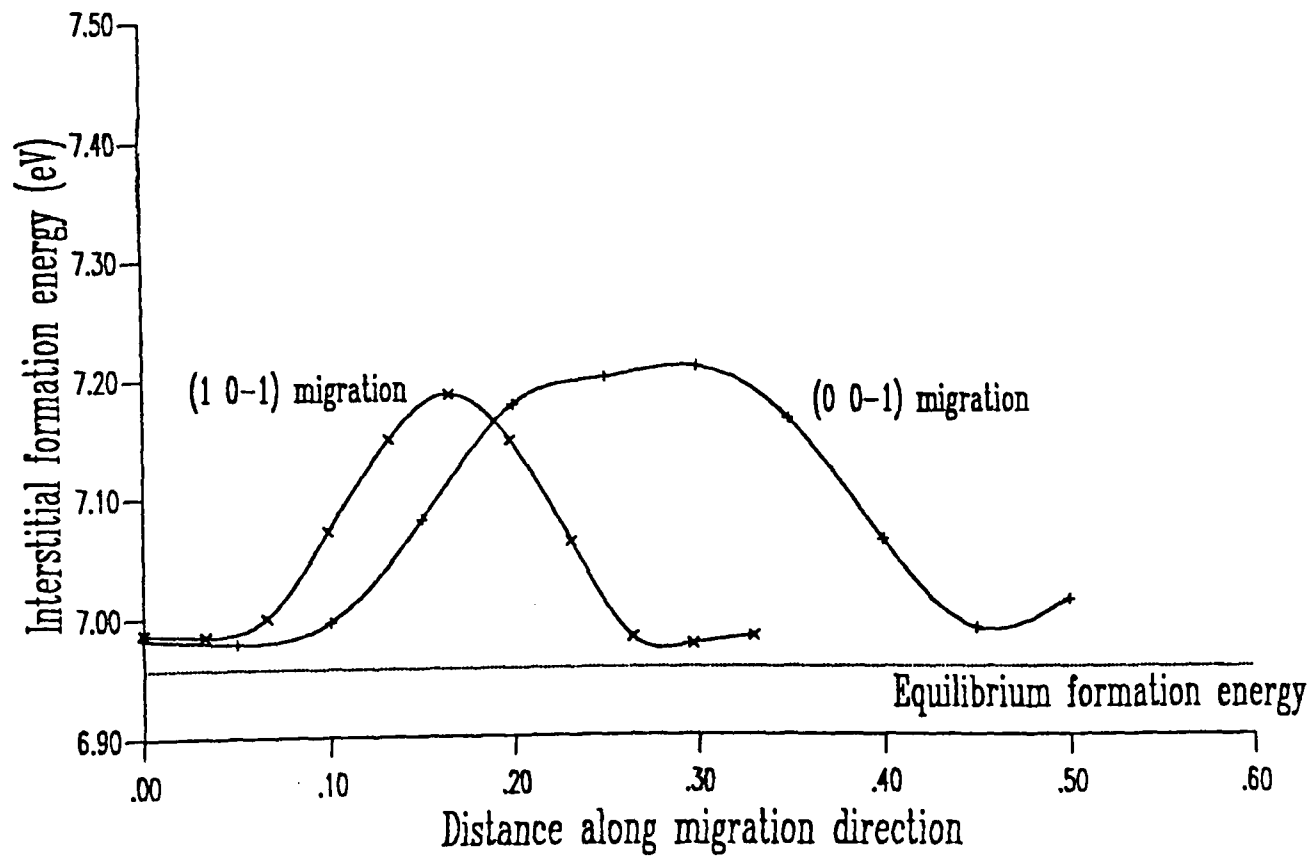

Figure 21. Molybdenum: interstitial energy against migration distance.

Both curves are close to being symmetric, upset only by the interstitial striving to attain its minimum-energy bent position. The path B migration

has a slightly lower energy than the longer step A, so while 2-d migration is not strongly favoured, neither is it (energetically) excluded.

Again, the plots of the paths of the migrating atoms show nothing unexpected.

5.3.5 Tungsten: 1-d migration

When testing the new core potential in §3.2.5, I noticed that the energies of the tungsten ⟨111⟩ crowdion and the ⟨111⟩ dumbbell interstitial were very close. The positions of the atoms involved are also very similar, so the result obtained in that section (a low migration energy along ⟨111⟩) was not a surprise.

The stability of the ⟨111⟩ crowdion and dumbbell in tungsten seems to be an artefact of the potential: as far as I am aware, all the experimental evidence is that the interstitial adopts a ⟨110⟩ split dumbbell configuration, as in all the other b.c.c. transition metals.

The calculations described here are for a block with edges in directions [111], [1$\bar{1}$0] and [11$\bar{2}$]. (This apparently strange choice arises because the survey of interstitial migration in perfect crystals described in this chapter leads on to migration in crystals containing dislocations. As periodic boundary conditions in the dislocation line direction are required to get the infinite dislocation, one of the block edges must be parallel to this direction.) This block is rather different from the [100] [010] [001] block used in chapter 3, and it has some surprising effects on the defect energies.

The effect of block size on the behaviour of the ⟨111⟩ interstitial in tungsten has already been described in §3.2.5: as the defect has an extended nature it can run up against the fixed boundaries if the block is not large enough. Every time I started with a [111] crowdion in the middle of the block, and pushed it along [111], the energy increased. There was no sign of the expected maximum in energy at the split interstitial configuration, and no decrease to the corresponding crowdion centred at $(\frac{1}{2}, \frac{1}{2}, \frac{1}{2})$. In fact, the deformation round the defect was interacting with the boundary of the block. (I observed the same effect in the molybdenum interstitial migration calculation.)

This problem required me to use a 'diagonal' of the block: instead of using the [111] direction, which has length $4a\sqrt{3}$, I used a [11$\bar{1}$] crowdion and a [11$\bar{1}$] migration direction. Although not a true diagonal, this gives me a distance of $6a\sqrt{3}$ which is enough to avoid a strong interaction with the fixed boundaries, changing qualitatively the outcome. The results then show the

expected behaviour, with a maximum for the split dumbbell and a minimum for the crowdion centred at the next lattice site. I have not reproduced the curve of energy against migration distance calculated with the new block shape, as it is virtually identical to figure 7: some slight differences are due to the different block sizes. The difference between the ⟨111⟩ crowdion energy and the ⟨111⟩ dumbbell energy is just 0.026 eV, so this is my value for the interstitial migration energy in tungsten.

5.4 Vacancy Migration Results

The simulations of vacancy migration do not show the same richness of behaviour as those of interstitial migration. In all cases, the interstitial that is migrating between the two declared vacancies follows a straight path, and the lattice relaxes round it in the expected manner.

Section 2.4.1, while investigating the effect of block size on the DEVIL results, calculated vacancy formation energies for molybdenum. Calculated formation energies for the other metals are given here in table 5.3, and compared with experimental results. Agreement is good, though the theoretical values tend to be at the low end of the experimental range. The calculation used a 10×10×10 block with periodic boundary conditions, as in §2.4.1. The block edges are all parallel to the basis cube: i.e. [100], [010] and [001].

The migration calculations require a slightly larger (12×12×12) block. This block must have fixed boundaries, as explained in §5.2.

I have calculated migration energies for each of the five metals, and for migration jumps to both first and second neighbours. The jumps to second neighbours have activation energies larger by factors of 3.3 (Mo) to 4.4 (V) times the jumps to nearest neighbours, and are not tabulated. Table 5.4 compares the DEVIL results for the shortest jump with calculations by Harder and Bacon [1986] and Rebonato *et al.* [1987], and with various experimental values. No experimental result seems to be available for vanadium, due apparently to the difficulty of obtaining pure specimens, but the experimental values agree magnificently for the other metals.

metal	DEVIL	experiment
V	1.85	2.1
Nb	2.51	2.7 to 3.0
Ta	2.91	2.8 to 3.1
Mo	2.55	3.0 to 3.25
W	3.63	3.6 to 4.0

More recent measurements (for example Ziegler and Schäfer [1986] and Mundy, Ockers and Smedskjaer [1986]) are not significantly different.

Table 5.3 Calculated energies (E_v^f) and experimental enthalpies (H_v^f) of vacancy formation (eV). [compilation of Herzig and Köhler 1981]

	E_v^m / eV			H_v^m/eV
metal	DEVIL	Harder[a]	Rebonato[b]	experiment
V	0.69	0.76	0.72	0.8[c]
Nb	0.85	0.91	0.87	0.95 ± 0.15[d]
Ta	1.13	1.22	1.12	1.1 ± 0.2[d]
Mo	1.30	1.32	1.32	1.3 ± 0.2[d]
W	1.45	—	—	1.5 ± 0.3[e]

[a] Harder and Bacon [1986]

[b] Rebonato *et al.* [1987]

[c] deduced by subtracting H_v^f=2.1 eV (table 5.3) from Q_1=2.9 eV [Siegel, 1981].

[d] by electron microscopy [Phillipp, Saile and Urban, 1981]

[e] from positron experiments [Tietze, Takaki, Schwirtlich and Schultz, 1981]

Table 5.4 Calculated and experimental vacancy migration energies

5.5 Discussion

I had three reasons for doing the perfect-lattice migration calculations described in this chapter.

Firstly, I wanted to be sure that the migration algorithm in DEVIL was working properly, before I tried to apply it to the complicated environment around a dislocation. The experience gained here on the best way to present the results and to plot the migration paths was also valuable.

Secondly, although experimental values for migration enthalpies are clouded with uncertainty, they are important physically. They offer a useful comparison point between experiment and theory, and also between different theories.

Thirdly, details of the migration may influence other properties of the metal lattice. Following the original suggestion of Foreman [1972] (who invoked one-dimensional migration), Evans [1983] has proposed a theory for the formation of void lattices in molybdenum that is based upon 2-d migration of interstitials. Computer simulation [Evans, 1985] shows that in a crystal where interstitials are constrained to move on certain planes, an initially random distribution of voids will turn into a regular void lattice. (Further implications of anisotropic migration of interstitials are discussed by Evans and Foreman [1985].) Had the migration step A from figure 16 been favoured over step B, or even had the double jump seen in vanadium (§5.3.2) been energetically favoured over the step B single jump, then the migrating interstitial would tend always to have its dumbbell lined up in the same ⟨110⟩ direction. It would then move in the {110} plane defined by this direction, giving the 2-d migration required for the Evans theory.

In all these DEVIL interstitial migration calculations, the energy for the planar step has at least as high an energy as that for the alternative 'reorientation jump'. This fact suggests that the ⟨111⟩ migration will tend to have a 3-dimensional character. (But note that two-dimensional migration can still arise, even if it is not favoured energetically: work by Lucasson, Maury and Lucasson [1986] on vibrational modes of interstitials suggests that the ⟨110⟩ dumbbell vibrates on its site with a motion that encourages planar migration.)

An alternative theory of void lattice formation has been proposed by Woo and Frank [1985]. Being advocates of the two-interstitial model (TIM), they suggest that interstitial migration takes place in a two-stage process, the first stage of which is anisotropic. (See §5.1 for a detailed description of the one- and two-interstitial models.) Low-temperature migration is due to a metastable excited ⟨111⟩ crowdion state, which has a higher formation energy than the 'ground state' ⟨110⟩ dumbbell. This crowdion migrates along the ⟨111⟩ direction, via the ⟨111⟩ dumbbell, and provides the required anisotropy. The tungsten calculation in §5.3.5 shows just how easy this ⟨111⟩ migration can be. Only at higher temperatures are the ground state ⟨110⟩ dumbbells able to move.

This theory requires that the ⟨111⟩ crowdion is more stable than the ⟨111⟩ dumbbell. Table 3.2 shows that in vanadium and tantalum the two forms of

interstitial have essentially equal energy, while the dumbbell is more stable in niobium and the crowdion in molybdenum. As all of the four metals have energy-orientation diagrams similar to figure 5 — i.e. with no maximum between ⟨111⟩ and ⟨110⟩ — an unstable crowdion scotches the two-interstitial model immediately, for the ⟨111⟩ dumbbell is unstable with respect to the ⟨110⟩ dumbbell. Hence the TIM is unlikely to apply to niobium. (The results here do not quite spell doom for the TIM, as the important quantity is not the energy as calculated here (internal energy, at constant volume) but the Gibbs free energy G, which takes into account changes in volume and entropy.)

Consider now the cases where the crowdion *is* stable with respect to the ⟨111⟩ dumbbell: molybdenum, and perhaps vanadium and tantalum. The instability of the ⟨111⟩ dumbbell with respect to the ⟨110⟩ dumbbell interstitial has further consequences for the TIM. As the ⟨111⟩ dumbbell configuration is the saddle point on the ⟨111⟩ migration path, the crowdion migration energy is just

$$E_c^m = E_i^{m,1D} = |E_c^f - E_{\langle 111\rangle}^f| \tag{5.2}$$

But the energy to convert the crowdion to a ⟨110⟩ dumbbell cannot be any higher (and could be lower), as the ⟨111⟩ dumbbell is a saddle point for a conversion path too! One must therefore invoke entropy and dynamic effects to explain the long-range migration of crowdions without conversion to dumbbells in stage I_E of recovery.

metal	$E_i^{m,3D}$ /eV	$E_i^{m,2D}$ /eV	E_{act} /eV	$E_i^{m,1D}$ /eV
V	0.29	0.38	0.45	0.008
Nb	0.22	0.37	0.39	0.062
Ta	0.37	0.36	0.31	0.001
Mo	0.23	0.25	0.24	0.036
W	—	—	—	0.026

Table 5.5 Energies for 3-dimensional, 2-dimensional and 1-dimensional interstitial migration.

The possibility of migration along ⟨111⟩ directions still remains. Table 5.2 gives the energies of migration for the three-dimensional reorientation jump (B) and the two-dimensional jump A. But rotation of a ⟨110⟩ dumbbell to ⟨111⟩, followed by motion along ⟨111⟩, is a possible migration route,

particularly if the energies for ⟨111⟩ migration are small. Assuming that there are no maxima in energy between the ⟨111⟩ crowdion and the ⟨111⟩ dumbbell, table 3.2 gives enough information to determine the migration energies for this process. The activation energy E_{act} is just the difference between the ⟨110⟩ dumbbell and the greater of E_c^f and $E_{\langle 111\rangle}^f$, while the migration energy is just the crowdion migration energy defined in equation (5.2). Table 5.5 lists these results, and reproduces the earlier values for $E_i^{m,3D}$ and $E_i^{m,2D}$ from table 5.2. A comparison of these values shows that the ⟨111⟩ migration does indeed have lowest activation energy in tantalum, and is very little different in energy from the other two mechanisms in molybdenum.

The migration along ⟨111⟩ need not be one-dimensional though. Unless one such step, driven by momentum or the excitation of a suitable phonon, favours another in the same direction, the saddle-point ⟨111⟩ dumbbell configuration will soon relax to a ⟨110⟩ dumbbell. And as this dumbbell interstitial may well be excited to a different ⟨111⟩ direction next time, long-range one-dimensional migration in unlikely. (In tungsten, of course the ⟨111⟩ crowdion is the DEVIL ground state and ⟨111⟩ migration ought to be very easy.)

Although the migration energies $E_i^{m,1D}$ in table 5.5 are very low, they are not quite low enough to explain the apparent long-range migration of interstitials seen during the stage I_E recovery. Even down towards liquid helium temperatures, self-interstitial defects produced by radiation damage seem to be able to migrate in vanadium, niobium and tantalum. Table 5.6 gives the temperatures obtained by Schultz [1981] for the stage I_E recovery of the b.c.c. transition metals, and the corresponding enthalpies of migration. Note that these enthalpies are in meV, not eV! Even the apparently tiny migration energies calculated by DEVIL are too high to explain self-diffusion at these extremely low temperatures. So even if the ⟨111⟩ dumbbell interstitial *is* stable against conversion to a ⟨110⟩ dumbbell, the experimental results remain unexplained.

Finally, consider thermally-activated self-diffusion. Vacancies have lower formation energies than self-interstitials, but higher migration energies. Comparing $E_v^f+E_v^m$ with $E_i^f+E_i^m$ should give an indication as to whether self-diffusion is due to interstitials or vacancies. Taking the minimum of $E_i^{m,3D}$ $E_i^{m,2D}$ and E_{act} from table 5.5 for the value of E_i^m gives table 5.7. Vacancy migration is favoured every time, and seems in accord with experimental results Q^{SD} for the heat of self-diffusion.

Despite the adverse implications of the above result for the two-interstitial

metal	T_{I_E} /K	H_{mig} /meV
V	<5	<0.4
Nb	<8	<0.7
Ta	<8	<0.7
Mo	35	3.0
W	27	2.3

Table 5.6 Temperatures and corresponding enthalpies for stage I_E recovery [Schultz, 1981].

model, 1-d migration of ⟨111⟩ crowdions does seem to be the more likely mechanism for any anisotropic diffusion.

5.6 Conclusions

In this chapter I have investigated the migration of point defects in perfect lattices. Some interesting phenomena occur, fully justifying the inclusion of a separate chapter on these migrations, free from the complications introduced by dislocations.

Tungsten remains an anomaly. I can see no obvious reason why the Finnis-Sinclair potential should predict that the stable form of the interstitial is a ⟨111⟩ crowdion, but given that it does, DEVIL predicts ⟨111⟩ migration with a very low activation energy. The tungsten system thus has value as a model for what may happen if the crowdion is after all metastable in any of these b.c.c. metals.

The most striking result is that stage I_E diffusion in radiation-damaged metals is unlikely to be due the migration of a metastable, frozen-in, ⟨111⟩ interstitial. Ignoring the effects of configurational entropy and of the different attempt frequencies, table 5.5 implies that migration of an excited interstitial state is a possibility in tantalum and molybdenum, but this migration will be wholesale: all the interstitials in the material can migrate in this manner. There seems little chance of a small fraction of metastable interstitials being responsible for stage I_E recovery, because the proposed ⟨111⟩ interstitials are simply unstable! In coming to the conclusion that stage I_E migration is due to stable interstitials, I join most of the rest of the world outside Stuttgart in accepting that the one-interstitial model for resistivity recovery is correct.

I do not suggest that the idea of interstitials in non-equilibrium states

metal	$E_v^f+E_v^m$ /eV	$E_i^f+E_i^m$ /eV	exptl. Q^{SD} /eV
V	2.54	4.45	3.2[a]
Nb	3.36	4.69	3.62[b]
Ta	4.04	7.14	4.0±0.2[c]
Mo	3.85	7.20	4.53[d]
W	5.08	8.90	5.45[e]

[a] Maier, Peo, Saile, Schäfer and Seeger [1979]

[b] Einziger, Mundy and Hoff [1978]

[c] Hönes [1979]

[d] Maier, Mehrer and Rein [1979]

[e] Mundy, Rothman, Lam, Hoff and Nowicki [1978]

Table 5.7 Calculated activation energies for migration of monovacancies and ⟨111⟩ crowdions, compared with experimental values of heat of self-diffusion Q^{SD}.

migrating should be abandoned. A more rigorous calculation, working with Gibbs free energy rather than internal energy *may* come to a different conclusion. And the self-diffusion seen at extremely low temperatures in metals that have undergone radiation damage below 5K suggests an extremely low migration energy, in a range seen here only for ⟨111⟩ migration. Perhaps the ⟨111⟩ crowdion *is* somehow stabilised after all?

Another fundamental result is that the total energy for vacancy migration (i.e. $E_v^f+E_v^m$) is always considerably less than the energy required to excite and migrate an interstitial dumbbell. This suggests that normal thermal self-diffusion is due to vacancies.

6 Dislocations and Point Defects

6.1 Introduction

Although point defect migration in perfect crystals is interesting in its own right, more important in radiation damage theory is the ultimate fate of the point defects.

In a nuclear reactor, fission fragments, neutrons and α particles can all produce cascades of displaced atoms when they hit metal objects. These objects could be the fuel cans or subassembly wrappers, or part of the structure of the reactor. Typically a 'cascade' consists of a vacancy-rich core surrounded by an interstitial-rich shell.

As in the previous chapters, all these calculations use a block of atoms with constant volume. The results are therefore *energies* rather than *enthalpies;* I have used the symbol E throughout. Experimental results tend to measure enthalpies, and are denoted H.

The migration energy of the interstitials is much lower than that of the vacancies (compare tables 5.3 and 5.4), so the interstitials will tend to migrate rapidly to the various 'sinks' (voids, surfaces, grain boundaries, interstitial loops, vacancy loops and dislocations) that exist in the metal. A vacancy is also a sink: an interstitial atom and a vacant site can recombine, leaving a region of perfect lattice. The sinks can all emit point defects as well as absorb them; emission of an interstitial by the perfect lattice, leaving behind a vacancy, is just the well-known Frenkel pair production. At typical temperatures, the equilibrium interstitial production rate is negligible and only the thermal emission of vacancies need be considered.

Most sinks are 'neutral': they have no preference for interstitials or vacancies. Although the equilibrium concentration c_i of interstitials is much lower than the equilibrium vacancy concentration c_v, the interstitial diffusion coefficient is much higher than that for vacancies ($D_i \gg D_v$). In fact, the products $c_i D_i$ and $c_v D_v$ are just about equal: hence the net flux of the two defects at a neutral sink, *in a block of material where all other sinks are also neutral,* is zero.

In the treatment of radiation damage problems using elasticity theory, the point defects are modelled using misfitting elastic shapes inserted into a continuous elastic medium. An interstitial is represented by an inclusion, possibly with different elastic constants, embedded into a hole that is too small for it. Similarly a vacancy is modelled by a sphere of material of smaller equilibrium radius than the hole into which it fits, but the boundaries are

forced to coincide by 'gluing' them together. The mismatch in volume is larger for an interstitial than for a vacancy, leading to the so-called 'size effect': through its long-range stress field, a dislocation has a stronger interaction with an interstitial than with a vacancy. The dislocation attracts interstitials more strongly than it attracts vacancies, and this 'bias' leaves an excess of vacancies in the lattice. The vacancy flux to the neutral sinks will exceed the interstitial flux, and as the voids attract more vacancies than interstitials so they grow in size, leading to swelling [Cawthorne and Fulton, 1966] with all its attendant problems for reactor operation.

The absorption of interstitials at dislocations is therefore crucial in the theory of radiation damage in metals.

Before continuing, I ought to define the concept of 'sink strength'. The sink strength defines how strongly a sink of type L attracts point defects (for the sake of illustration, say vacancies) normalised to remove the effect of the defect diffusivity (D_v). More precisely, Brailsford and Bullough [1981] in equation (7) define

$$J^v_{Ll} = D_v k^2_{Ll,v} \int_{V_M} c_v \, dV - K_{Ll,v} V_M \tag{6.1}$$

Here, J^v_{Ll} is the vacancy flux to a sink of type L at a location l, integrated over the boundary of the cell volume V_M, containing the sink; $k^2_{Ll,v}$ is the sink strength for vacancies of the sink Ll; c_v is the local concentration of vacancies; and $K_{Ll,v}$ is a measure of the ability of the sink to emit vacancies. Although equation (6.1) is attempting to define two quantities ($k^2_{Ll,v}$ and $K_{Ll,v}$) at once, requiring $K_{Ll,v}/D_v$ to go to zero at absolute zero (i.e. no thermal production of vacancies at zero temperature) separates the two parameters successfully.

Summing over all the locations l,

$$k^2_{Lv} = \sum_l k^2_{Ll,v} \tag{6.2}$$

and

$$K_{Lv} = \sum_l K_{Ll} \tag{6.3}$$

define the sink strength and emission rate, for vacancies, of sinks of type L.

Quasi-chemical rate theory has been used for some time [Damask and Dienes, 1963, Harkness and Li, 1971, Wiedersich, 1972] to model radiation damage. The introduction of the 'effective medium approach' by Brailsford and Bullough [1972] allowed the calculation of sink strengths in more complicated systems, and a detailed theoretical study of void swelling

[Brailsford and Bullough, 1973 and many papers since] has been built around the various sink strengths.

Much work has been done using elasticity theory, modelling point defects with misfitting spheres embedded in a continuum. To avoid the infinities that arise in the elasticity calculation at the dislocation core, most models assume that any point defect inside a certain radius migrates spontaneously to the core. Not only can atomistic simulation provide a value for this radius, but the models can also illuminate diffusion in the core itself, and give an idea of the activation energy required to enter the zone of spontaneous absorption. Atomistic modelling aims to produce a value for the all-important dislocation bias for interstitials.

This chapter considers the behaviour of an interstitial when near to the core of a dislocation: what the formation energy of an interstitial is in the core, where its zone of spontaneous absorption is, and how it can migrate into the centre of the core.

6.2 Further Capabilities of DEVIL

To carry out migration calculations, I needed to extend DEVIL to perform some more tasks.

6.2.1 Extensions to plotting options

Interactions of interstitials with dislocations are hard to visualise; DEVIL has evolved more sophisticated plotting routines to help the user see what is happening. The first development was to plot out some of the atom positions at the end of every run, rather than dumping all the coordinates and running a separate job to do the plotting as described in §4.2.3 and Appendix 1.

One vital piece of information in migration calculations is not just where the atoms end up, but how they are moving. Hence I added a piece of code to draw in displacement vectors, from a set of positions read in from one dump (typically that produced for a block containing just a dislocation) to a new set of positions read from another dump. Having the displacement vectors proved to be so useful that this option rapidly became standard: at the end of every run, DEVIL plots the relaxed positions, with lines from the positions occupied by the atoms before the interstitial was added.

The various paths through the program can be controlled via a parameter (ISTORT) that is read in from the input dataset. No expensive recompilation of subroutines is necessary, and the parts of DEVIL that set up the lattice can be used by each type of calculation.

To illustrate the range of cases that DEVIL can handle, table A1.2 in Appendix 1 lists the permissible values of ISTORT and the corresponding behaviour of DEVIL.

6.2.2 Two-stage relaxation

Calculations to determine the zone of spontaneous absorption of interstitials by dislocations start with the relaxed structure of a single edge dislocation. A problem soon appeared when I inserted an interstitial at some place in the lattice and watched to see whether or not it would be absorbed. The act of inserting the interstitial distorts the lattice, and can provide enough potential energy to overcome migration barriers: the unrelaxed energy after insertion is typically 20 to 30 eV above the relaxed dislocation energy.

Kirsanov and Turkebaev [1986] also encountered this problem, when modelling defect absorption using pair potentials. Their solution was first to relax the block of atoms, keeping the interstitial stationary, then to release the interstitial and let the whole structure come to equilibrium. Although the intermediate position will still contain some potential energy, this approach looks to be the best and I have adopted it for DEVIL. To save on computer time, the accuracy ACC1 (see Appendix 1) input by the user is somewhat arbitrarily multiplied by four for the first stage of the relaxation. This first stage need not give a relaxed energy correct to a fraction of an eV: all we desire is a reduction in the strain energy, and relaxing to a wider tolerance seems to be the best way to do this.

6.2.3 Migrating interstitials

The activation energies for the absorption of defects by dislocations are important parameters in radiation damage theory. We wish to calculate these energies by atomistic simulations. Section 3.2.1 discusses the ability of DEVIL to apply constraints: either to the direction of a dumbbell interstitial or to keep a particular atom in a given plane. The calculational procedure has already been mentioned in §5.2.

The interstitial is inserted outside the zone of spontaneous absorption, and a two-stage relaxation (see §6.2.2) carried out. However, the interstitial is not allowed to move along the line joining it to the dislocation core: all forces in this direction are zeroed. After the energy of the block of atoms in this configuration has been noted (and the atom positions dumped), the interstitial is stepped towards the dislocation core and the two-stage relaxation repeated. Mimicking the behaviour of a real metal, the atoms are

relaxed in the next step from their positions at the end of the previous one. This procedure has the advantage (over a restart from the 'dislocation-only' position) that many of the atoms will already be in relaxed positions, enabling the calculation to converge faster.

The stepping can be repeated until absorption occurs, giving a set of energy values along the migration path. This path should be close to the one followed in the real material.

6.3 The Binding of Interstitials to Dislocations

6.3.1 Theory

If the energy obtained by relaxing a block containing an interstitial and a dislocation is E_{i+d}, the energy of the block with just the dislocation E_d and the cohesive energy of the perfect lattice U_{coh} per atom, then the formation energy of the interstitial in the core of the dislocation is

$$E^f_{i,d} = E_{i+d} - E_d + U_{coh} \tag{6.4}$$

U_{coh} must be added when the extra atom is introduced, just as it was subtracted when considering vacancy formation energy in §2.4.1. The binding energy of the interstitial to the dislocation can also be deduced, and is simply

$$E^b_{i,d} = E^f_i - E^f_{i,d} \tag{6.5}$$

where E^f_i is just the formation energy in perfect crystal calculated in §3.2.

6.3.2 Calculational procedure

Section 3.2 has already considered interstitial formation energies in perfect crystals. After using the method described in chapter 4 to set up and relax a dislocation, I wrote the relaxed coordinates into a file. DEVIL reads this file at the start of a second run (see §4.2.3 and Appendix 1), then inserts an extra interstitial into the centre of the dislocation core and relaxes the block. This procedure gives the formation energy of an interstitial in the core; it should be lower than that in the perfect crystal because the interstitial will sit in the tensile region just above the extra half plane of atoms.

All the calculations are on the stable $\frac{1}{2}\langle 111\rangle$ edge dislocations, and all use a block with 1152 free atoms. The fixed boundaries of the block contain a further 1872 atoms, and the areas forming the periodic boundaries contain the images of another 2268 atoms.

6.3.3 Results

Table 6.1 gives the results obtained for the five metals under study. The second column gives the energy of formation of the interstitial plus the dislocation, E^f_{i+d}. The next three columns come from calculations in chapter 4 (the dislocation energy E_d), the original Finnis and Sinclair [1984] paper (the cohesive energy U_{coh}) and table 3.2 (the interstitial formation energy E^f_i). Using these three values and equations (6.4) and (6.5), I have calculated the formation energy of the interstitial in the dislocation core ($E^f_{i,d}$) and the binding energy ($E^b_{i,d}$) of the interstitial to the dislocation. The values have been rounded after subtraction, and appear in the last two columns of table 6.1. The fraction $E^b_{i,d}/E^f_i$ is almost constant, varying from 0.673 (Nb) to 0.742 (Ta): an interstitial is bound to a dislocation by about 70% of its formation energy.

Metal	E_{i+d}/eV	E_d/eV	U_{coh}/eV	E^f_i/eV	$E^f_{i,d}$/eV	$E^b_{i,d}$/eV
V	44.20	48.28	5.31	4.16	1.23	2.93
Nb	52.11	58.22	7.57	4.47	1.46	3.01
Ta	70.59	76.93	8.10	6.83	1.76	5.07
Mo	77.61	82.26	6.82	6.97	2.17	4.80
W	101.81	108.11	8.90	8.88	2.61	6.27

Table 6.1 Calculated interstitial formation ($E^f_{i,d}$) and binding ($E^b_{i,d}$) energies in the presence of a $\frac{1}{2}\langle 111\rangle$ dislocation.

This result is in contrast to that obtained by Kirsanov and Turkebaev [1986]. They found a binding energy of about 4 eV for self-interstitials in iron, 87% of the interstitial formation energy of 4.6 eV.

6.4 The Binding of Vacancies to Dislocations

6.4.1 Theory

This is very similar to the theory developed for interstitials in §6.3.1. The only difference is that the cohesive energy U_{coh} of the lattice must now be subtracted rather than added, as one fewer atom is present. The equations for the formation energy of the vacancy in the dislocation core $E^f_{v,d}$ and the binding energy $E^b_{v,d}$ of the vacancy to the dislocation are

$$E^f_{v,d} = E_{v+d} - E_d - U_{coh} \tag{6.6}$$

and

$$E^b_{v,d} = E^f_v - E^f_{v,d} \tag{6.7}$$

6.4.2 Calculational procedure

The block size and general procedure are the same for vacancies as for interstitials, but one extra wrinkle is required. Section mentions that when setting up a dislocation, I needed to redefine some of the ordinary atoms in the most distorted regions as interstitials. This involved creating a vacancy at that site, and inserting an interstitial. All of the atoms that were right on the dislocation line (at the edge of the extra half-plane) got this treatment; and these are precisely the core atoms that I now want to define as vacancies.

Once an atom has been defined to DEVIL as an interstitial, there is no easy way to remove this appellation. And as I am restarting from a dump, all the core atoms are already set to be interstitials. I do not really want to rerun the dislocation relaxation, nor to modify the DEVIL code. The quickest way to avoid the problem is to use the DEVIL input dataset to create a vacancy at a site near to the core, then to edit the dumped coordinates to move the required core atom into this vacancy.

The site selected for each of the metals was that of the atom originally (pre-dislocation) at (0, 0, 0). With the distortion round the dislocation, this atom moves to approximately (0.13, 0.13, 0.04), varying by about $0.02a$ from metal to metal. This site is not necessarily the one nearest to the dislocation line, and does not necessarily have the lowest vacancy formation energy, but it is a good approximation.

6.4.3 Results

Table 6.2 presents the DEVIL results for vacancies in the core of dislocations. Once again I have calculated the ratio of binding energy to the formation energy in the perfect lattice, $E^b_{v,d}/E^f_v$. And once more, this ratio (see final column of table 6.2) varies very little between the metals: from 0.418 (Nb) to 0.459 (V), implying that a vacancy is bound to a dislocation by about 44% of its formation energy.

Again, Kirsanov and Turkebaev [1986] disagree. Their calculation for iron gives a binding energy of 1 eV, compared to the vacancy formation energy of 1.37 eV: a ratio of 0.73. Although there is no *a priori* reason for iron to be the same as the metals dealt with above, the discrepancy may well be due to the difference between their Johnson pair potential and the Finnis-Sinclair many-body potential.

Metal	E_{v+d}/eV	$E_d+U_{coh}+E_v^f$/eV	$E_{v,d}^f$/eV	$E_{v,d}^b$/eV	$E_{v,d}^b/E_v^f$
V	54.59	55.44	1.00	0.85	0.459
Nb	67.25	68.30	1.46	1.05	0.418
Ta	86.61	87.94	1.58	1.33	0.457
Mo	90.56	91.63	1.48	1.07	0.420
W	119.11	120.64	2.10	1.53	0.421

Table 6.2 Calculated vacancy formation ($E_{v,d}^f$) and binding ($E_{v,d}^b$) energies in the presence of a $\frac{1}{2}\langle 111\rangle$ dislocation.

6.5 Zone of Spontaneous Absorption for Interstitials

6.5.1 Method

The region round a dislocation from which an interstitial will spontaneously be absorbed is clearly of interest to anybody modelling radiation damage. Kirsanov and Turkebaev [1986] have investigated this zone using pair potentials in α–iron and quenched molecular dynamics. I have studied the area round the dislocation core using their two-stage relaxation method (see §6.2.2).

The extra interstitial atom cannot simply be introduced at random in the neighbourhood of the dislocation. Unless it is inserted in a position of relatively low energy, the distortion introduced in the first stage of the relaxation will make the calculation meaningless. For example, if one of the lattice atoms was at (0.5, 0.5, 0.5) and the interstitial was introduced at (0.5, 0.5, 0.6), the first atom would be pushed unrealistically close to the expected absorbed position of (0.5, 0.5, 0.0). Instead, I take care to add the interstitial as part of a dumbbell. Suppose that $\mathbf{d}_j$ is the vector between the two atoms in one of the split dumbbell configurations. (The suffix j describes which configuration.) I select one of the sites around a fully-relaxed dislocation, say atom i at $\mathbf{x}_i$; I then define this site as a vacancy and introduce a pair of interstitials at $\mathbf{x}_i \pm \frac{1}{2}\mathbf{d}_j$.

Typically, introducing the interstitial leads to an energy increase of 20 to 30 eV, and the first relaxation (with the defect held stationary) will get to within 1 eV of the final energy. An excess of 1 eV, shared between all of the free atoms in the block, is not enough seriously to affect the behaviour when the interstitial atoms are released.

6.5.2 Results

From some positions, the interstitial is absorbed straight away into the core. The edge dislocation then has an adatom on its extra half-plane (or equivalently, a pair of jogs); in real life the extra atom will presumably diffuse rapidly along the dislocation core until it is absorbed by a jog. From other start positions, the interstitial may displace a neighbouring atom from its lattice site, and the displaced atom may then be absorbed in the core. Replacement chains involving three lattice atoms occur often, particularly along close-packed directions. Finally, if the interstitial is inserted far enough away from the dislocation core, it will not be absorbed but will relax *in situ* to form either a dumbbell or a crowdion.

Figure 22 shows an interstitial being absorbed in two steps along the [111] direction. Just two $(11\bar{2})$ atom planes are plotted, and the interstitial *I* was originally created on the site at about (1.5, 0.7) in the coordinates of the figure. Each atom from the free region has a line joining its relaxed position to the position it occupied before the interstitial was inserted. The interstitial itself can be identified as it has no displacement vector. The relaxations of the atoms round the interstitial are perhaps surprisingly small, indicating the amount of space in the dislocation core that is available to accommodate the interstitial.

More dramatic replacement chains can occur, particularly if the interstitial is inserted on the compressive side of the dislocation glide plane. The extra strain energy can be large enough to feed processes such as that shown in figure 23. The figure shows all six of the $(11\bar{2})$ layers that form one repeat of the lattice. The interstitial dumbbell was originally centred at (1.5,–0.7) in the units of the diagram; one of the dumbbell atoms (*A*) has moved to the next $(1\bar{1}0)$ plane, pushing another (*B*) in turn into the tensile region. From there, absorption takes place along the close-packed [111] direction.

If the interstitial is inserted further away from the core, it can form a stable structure such as a split dumbbell or a crowdion. Figure 24 portrays a relaxed position with the interstitial as part of a $[10\bar{1}]$ dumbbell (*A* and *B*), while figure 25 shows a $[1\bar{1}1]$ crowdion centred at *C*. Enough of the $(11\bar{2})$ layers have been included in each case to demonstrate what is happening in the relaxed crystal.

The orientation in which the interstitial dumbbell is created can determine whether or not absorption takes place. Tables 6.4 and 6.5 give the results of a survey of the boundary of the absorption zone in niobium. Table 6.3 goes through the situation on the tensile side of the dislocation glide plane (the

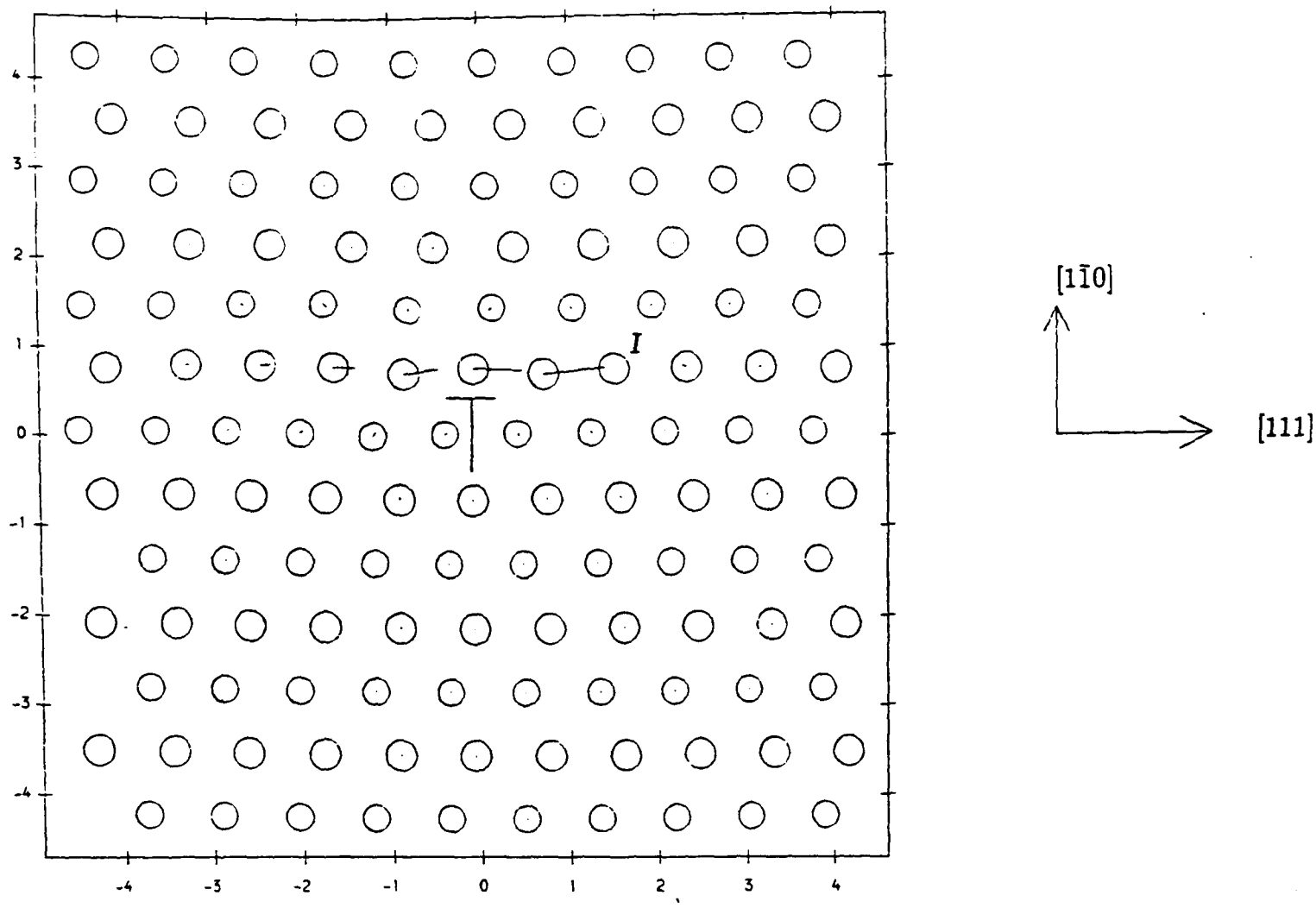

Figure 22. Absorption of an interstitial in two [111] steps.

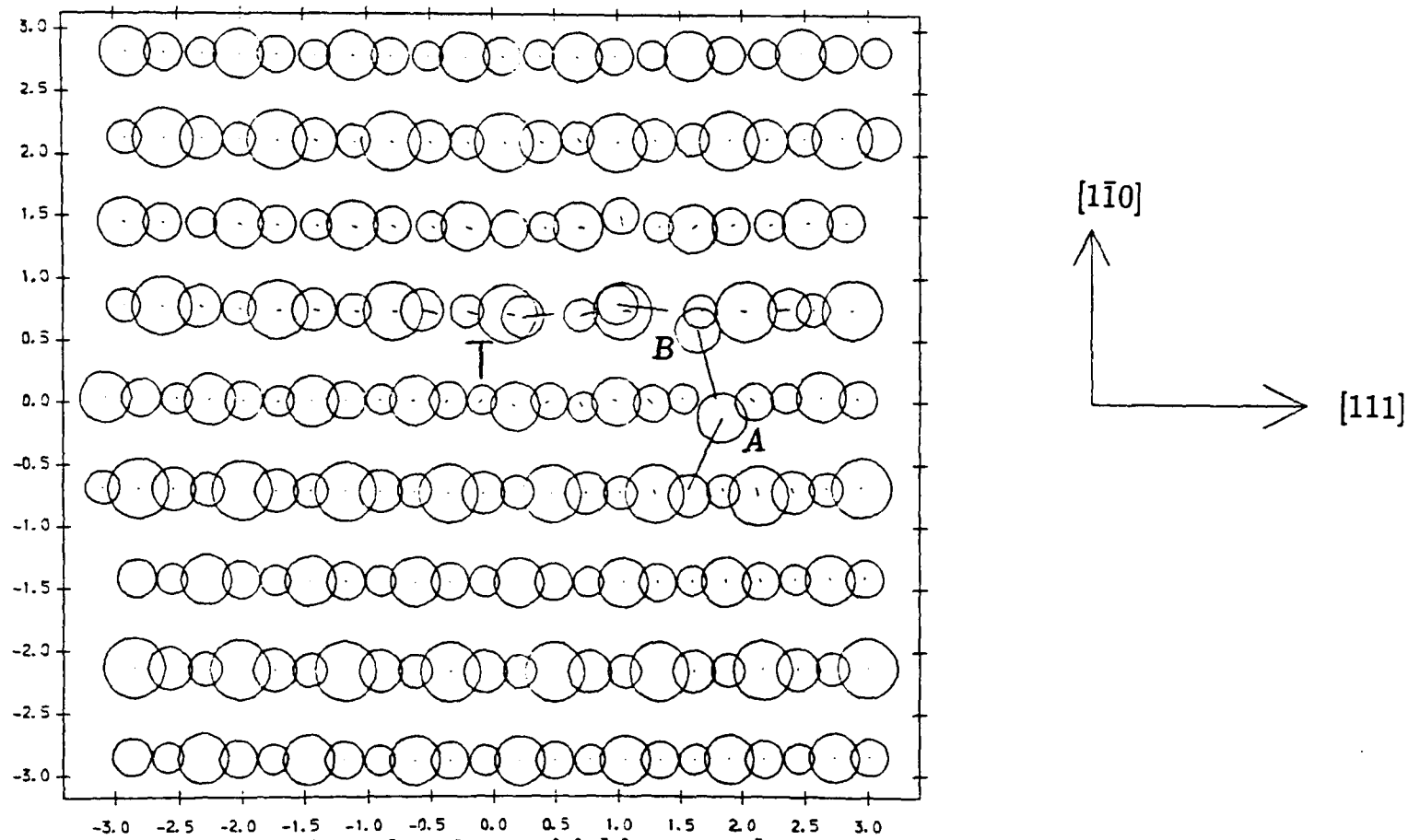

Figure 23. Absorption of an interstitial in several steps.

upper half of the plots showing atom positions). Of the four sites listed, two will support a stable interstitial dumbbell in any of the six ⟨110⟩ orientations. One site is unstable for all of the six dumbbells, while the fourth site is stable for two interstitial orientations but not for the other four.

The interstitial formation energy varies between orientations at any given site; as expected, the dumbbells with a component in the direction of highest tension (i.e. [111]) have the lowest formation energies. Interestingly, at the site where only two of the dumbbells are stable, the unstable ones are the

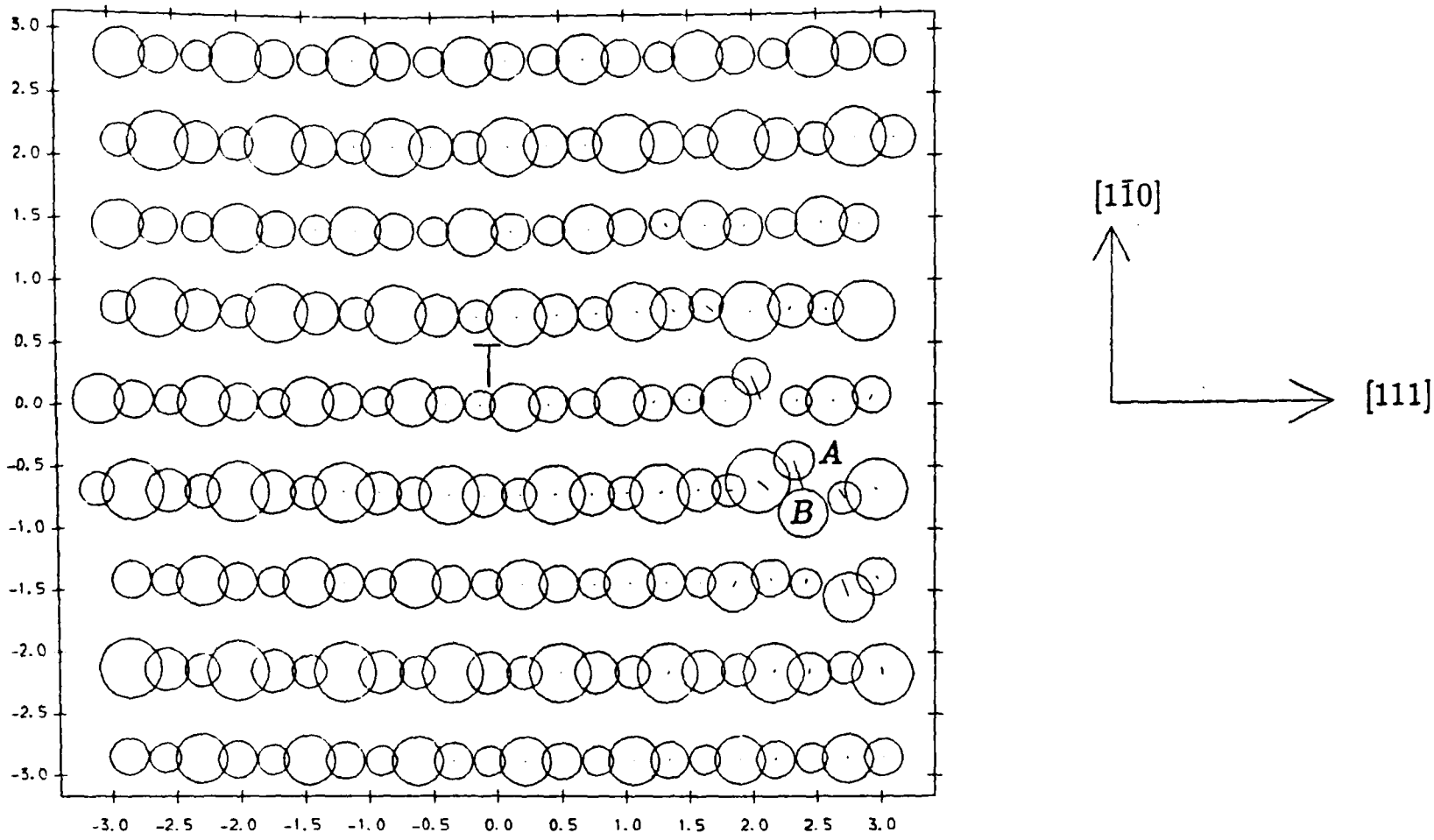

Figure 24. Interstitial forming [10$\bar{1}$] dumbbell near ½[111] dislocation in niobium.

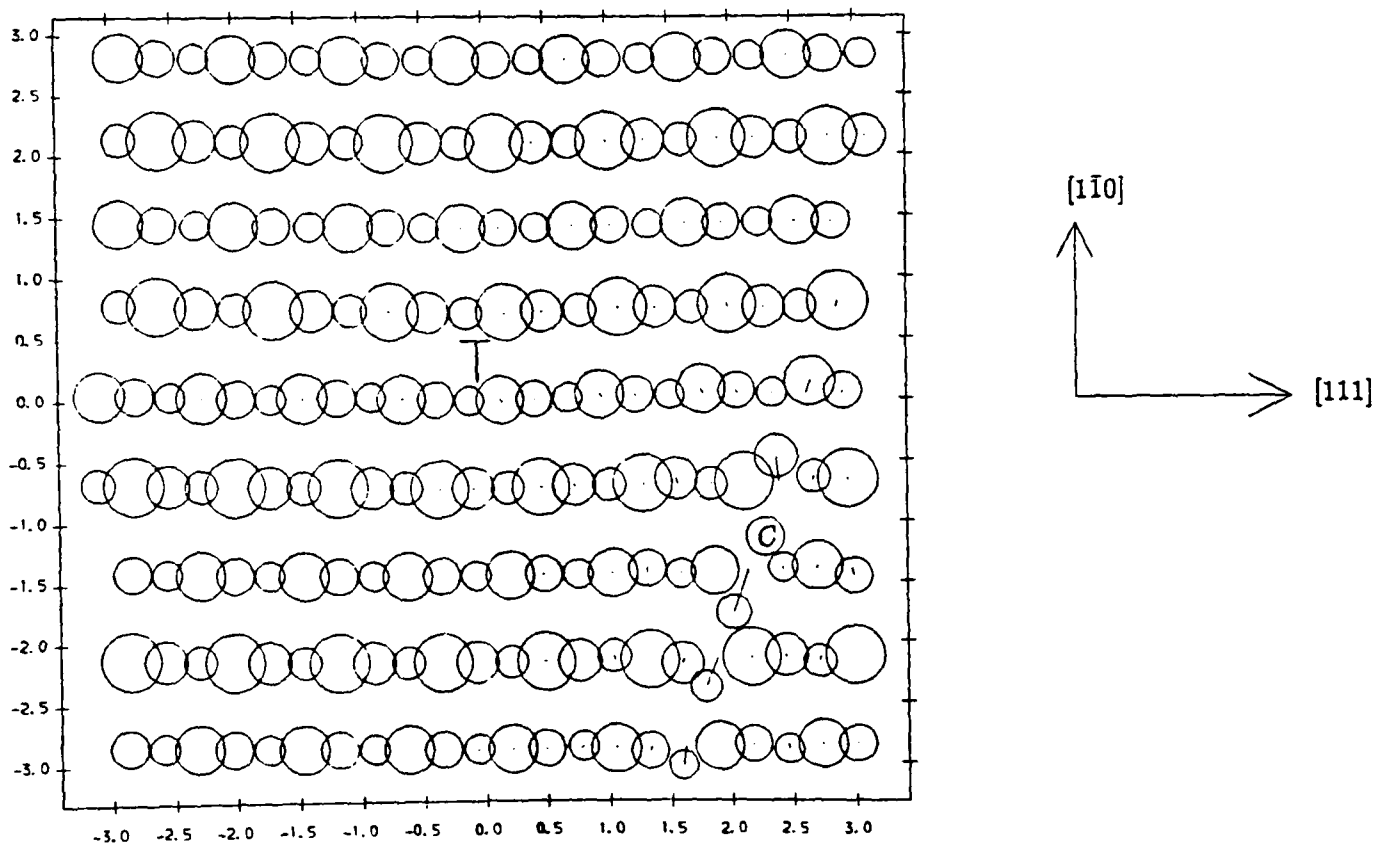

Figure 25. Interstitial forming [1$\bar{1}$1] crowdion near ½[111] dislocation in niobium.

lower-energy configurations. This must be due to the fact that they are aligned so as to make migration along −[111] easy, and are absorbed by the dislocation. The [1$\bar{1}$0] and [10$\bar{1}$] interstitials are stuck in high-lying minima. In fact, these last two dumbbells are rotated away from their original orientations. They tend to line up with the local distortion of the [1$\bar{1}$0] direction, as the (111) planes are distorted round the end of the extra half-plane.

Some of the calculations have not been carried through to convergence:

Dumbbell centred at[a]	Dumbbell orientation	E_i^f/eV	Comments
(2.0,–1.0, 0.0)	[1$\bar{1}$0]	4.40	stable all other orientations also stable
(2.5,–0.5, 0.5)	[1$\bar{1}$0]	4.51	stable
(2.5,–0.5, 0.5)	[110]	4.07	stable
(2.5,–0.5, 0.5)	[10$\bar{1}$]	4.51	stable
(2.5,–0.5, 0.5)	[101]	4.09	stable
(2.5,–0.5, 0.5)	[011]	4.32	stable
(2.5,–0.5, 0.5)	[01$\bar{1}$]	4.42	stable
(2.0, 1.0, 1.0)	[1$\bar{1}$0]	4.85	stable
(2.0, 1.0, 1.0)	[110]	1.46	absorbed
(2.0, 1.0, 1.0)	[10$\bar{1}$]	4.58	stable
(2.0, 1.0, 1.0)	[101]	—	absorbed; E<2.20eV
(2.0, 1.0, 1.0)	[011]	—	absorbed; E<2.21eV
(2.0, 1.0, 1.0)	[01$\bar{1}$]	—	absorbed; E<3.38eV
(1.5, 0.5, 0.5)	[1$\bar{1}$0]	—	absorbed; E<2.35eV all other orientations also absorbed

[a]These positions are approximate, and refer to the coordinates in the undistorted (pre-dislocation) crystal. They are correct to within 0.1 though.

Table 6.3 Calculated interstitial formation energies at various positions on tensile side of a $\frac{1}{2}\langle 111\rangle$ edge dislocation in niobium.

when absorption is taking place via a displacement chain, the relaxation can be quite slow. In some cases where the energy is already below the formation energy for an interstitial outside the core, I have stopped the calculation. If the energy at termination is E_0, the 'Comments' column contains '$E<E_0$'. The fully-converged 'absorbed' value of 1.46 eV agrees with the formation energy $E_{i,d}^f$ of an interstitial in the dislocation core quoted in table 6.1.

Table 6.4 deals with interstitials on the compressive side of the edge dislocation. As before, some sites lead to absorption of all dumbbells, some are stable for all orientations and others show mixed behaviour. One feature not seen on the tensile side is migration of an interstitial away from the glide plane. The formation energy of an interstitial is clearly higher in the regions of high compressive stress than where the stress is lower; this is enough to overcome the migration barrier in a couple of cases and the interstitial moves downwards to an area of lower stress.

Dumbbell centred at[a]	Dumbbell orientation	E_i^f/eV	Comments
(0.5, 1.5, 0.5)	$[1\bar{1}0]$	—	absorbed; E<3.13eV all other orientations also absorbed
(1.0, 2.0, 1.0)	$[1\bar{1}0]$	—	absorbed; E<4.52eV
(1.0, 2.0, 1.0)	[110]	3.46	absorbed in 4 steps
(1.0, 2.0, 1.0)	$[10\bar{1}]$	4.88	stable
(1.0, 2.0, 1.0)	[101]	5.06	migrates away from dislocation, to crowdion configuration
(1.0, 2.0, 1.0)	[011]	—	absorbed; E<4.34eV
(1.0, 2.0, 1.0)	$[01\bar{1}]$	5.09	stable
(−1.0, 2.0, 0.0)	$[1\bar{1}0]$	5.01	stable
(−1.0, 2.0, 0.0)	$[10\bar{1}]$	5.05	stable
(−1.0, 2.0, 0.0)	[101]	—	migrates away from dislocation; E<5.14eV
(−0.5, 2.5, 0.5)	$[1\bar{1}0]$	4.92	stable
(−0.5, 2.5, 0.5)	$[10\bar{1}]$	4.95	stable
(−0.5, 2.5, 0.5)	[101]	5.04	stable
(0.0, 3.0, 1.0)	$[1\bar{1}0]$	4.98	stable
(0.0, 3.0, 1.0)	$[10\bar{1}]$	5.00	stable
(0.0, 3.0, 1.0)	[101]	4.99	migrates away from dislocation to form $[1\bar{1}0]$ dumbbell
(0.0, 3.0, 1.0)	[110]	—	migrates away from dislocation; E<5.09eV

[a] These positions are approximate, and refer to the coordinates in the undistorted (pre-dislocation) crystal. They are correct to within 0.1 though.

Table 6.4 Calculated interstitial formation energies at various positions on compressive side of a $\frac{1}{2}\langle 111\rangle$ edge dislocation in niobium.

To assist the interpretation of figure 28, and similar pictures plotted on the same axes, figure 26 shows the six dumbbell orientations as they appear on the axes of the calculational block: [111] and $[1\bar{1}0]$. Each dumbbell is centred at (0, 0, 0), and the labels on each cross give the third coordinate: the distance in the $[11\bar{2}]/\sqrt{6}$ direction. Two of the dumbbells ($[10\bar{1}]$ and $[01\bar{1}]$) lie on top of one another in this diagram, and are suitably labelled.

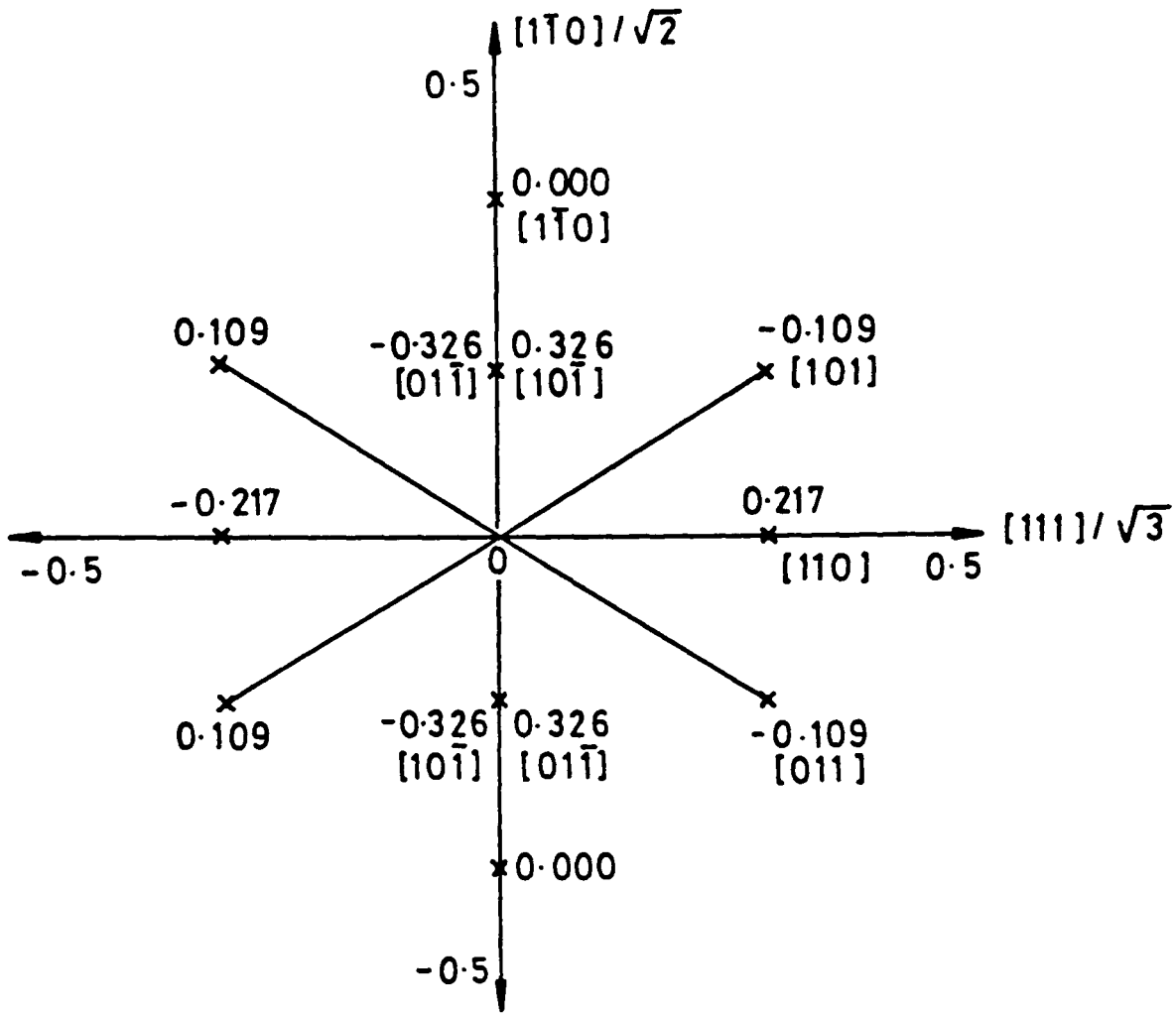

Figure 26. Dumbbell positions plotted on block axes.

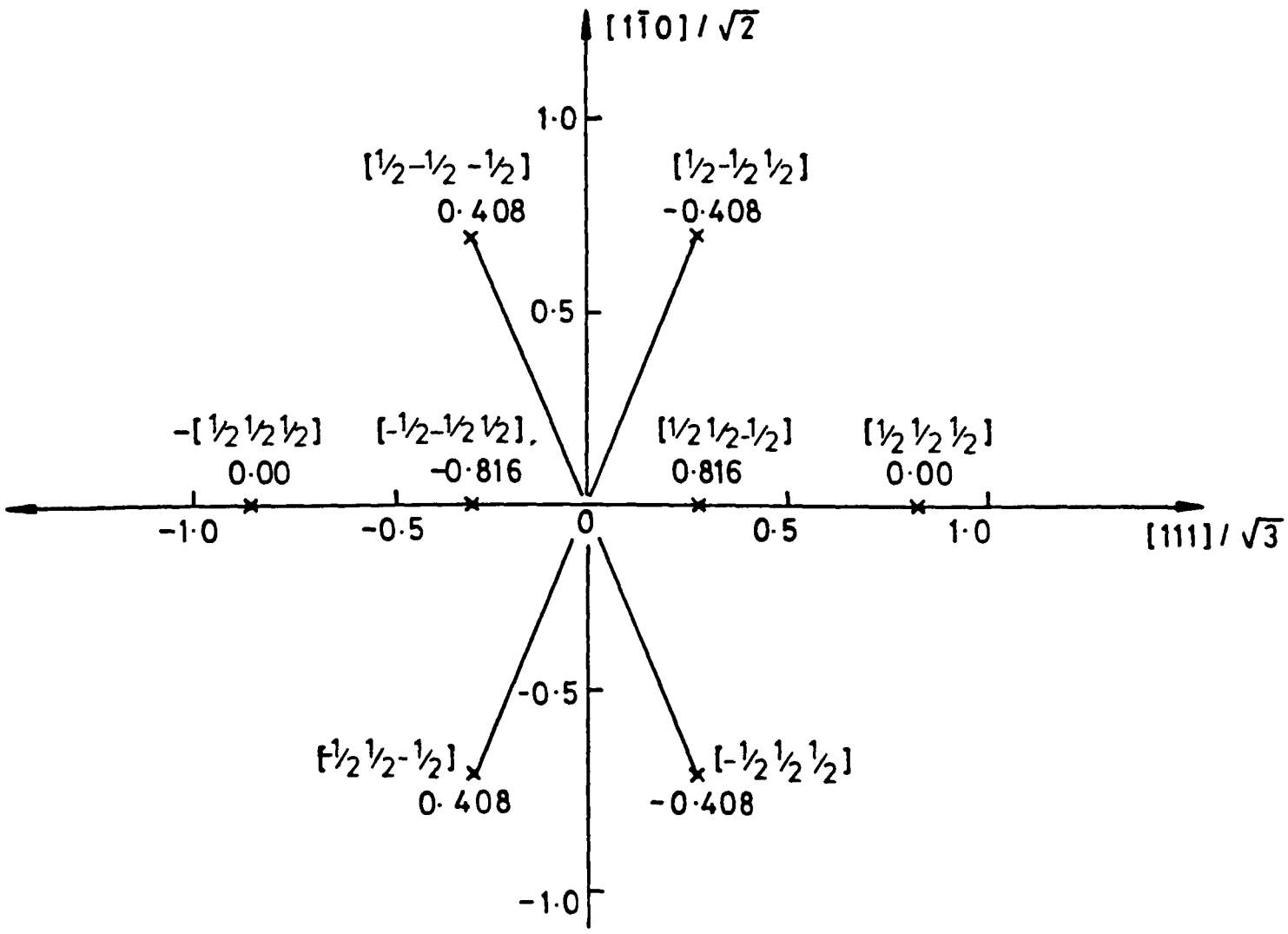

Figure 27. Nearest neighbour positions plotted on block axes.

Figure 27 may also be useful: this shows, again on the block axes, the positions of the nearest neighbours of an atom at (0, 0, 0) in a perfect lattice. The nearest neighbour directions also serve, naturally, to identify the ⟨111⟩ directions for plots on block axes. Note particularly those that are angled at about 70° to the horizontal, and have a component out of the plane of the paper: one of them is the direction of the crowdion in figure 25.

All the interstitial absorption information is difficult to represent graphically, but figure 28 makes an attempt. Like the plots of atom positions, this figure uses the block edges as the directions for its axes. The circles show atoms around a fully-relaxed dislocation, with no point defects present. These are the potential interstitial dumbbell sites.

The triangles indicate the starting positions of those dumbbells that end up absorbed; straight lines join the two atoms of each dumbbell. The linked crosses show the final configuration for the stable dumbbells. Each pair is labelled with the interstitial formation energy.

Finally, the squares show the starting positions of those dumbbells that migrate away from the glide plane. Each pair is labelled with the formation energy in its final configuration, and is further identified as a migrating interstitial by the arrow. Not all of the dumbbells are in the plane of the paper: where some ambiguity may arise, they are labelled with their direction.

All of the information in tables 6.4 and 6.5, as well as figure 28, relates to a single $(11\bar{2})$ plane. There are six of these planes before the lattice repeats in the $[11\bar{2}]$ direction, and ideally all six should be investigated, on both sides of the extra half-plane. I have concentrated on one side only; and although the figures and tables above relate to only one plane of atoms, I have done enough calculations on the other planes to locate the boundary of the zone of spontaneous absorption. Table 6.5 summarises the results for the other planes, and figure 29 brings together all the absorption calculations: it indicates how many of the six dumbbell orientations are absorbed from various atom positions round a dislocation. A comprehensive set of calculations is unnecessary: if an interstitial in a particular orientation is absorbed from one lattice site, I have assumed that it would also be absorbed from one closer to the core on the same $(1\bar{1}0)$ plane.

6.5.3 Discussion

Elasticity calculations (with misfitting inclusions representing interstitials and vacancies) rely on capture radii to avoid difficulties at the dislocation core. To make an estimate of the equivalent capture radius of the core,

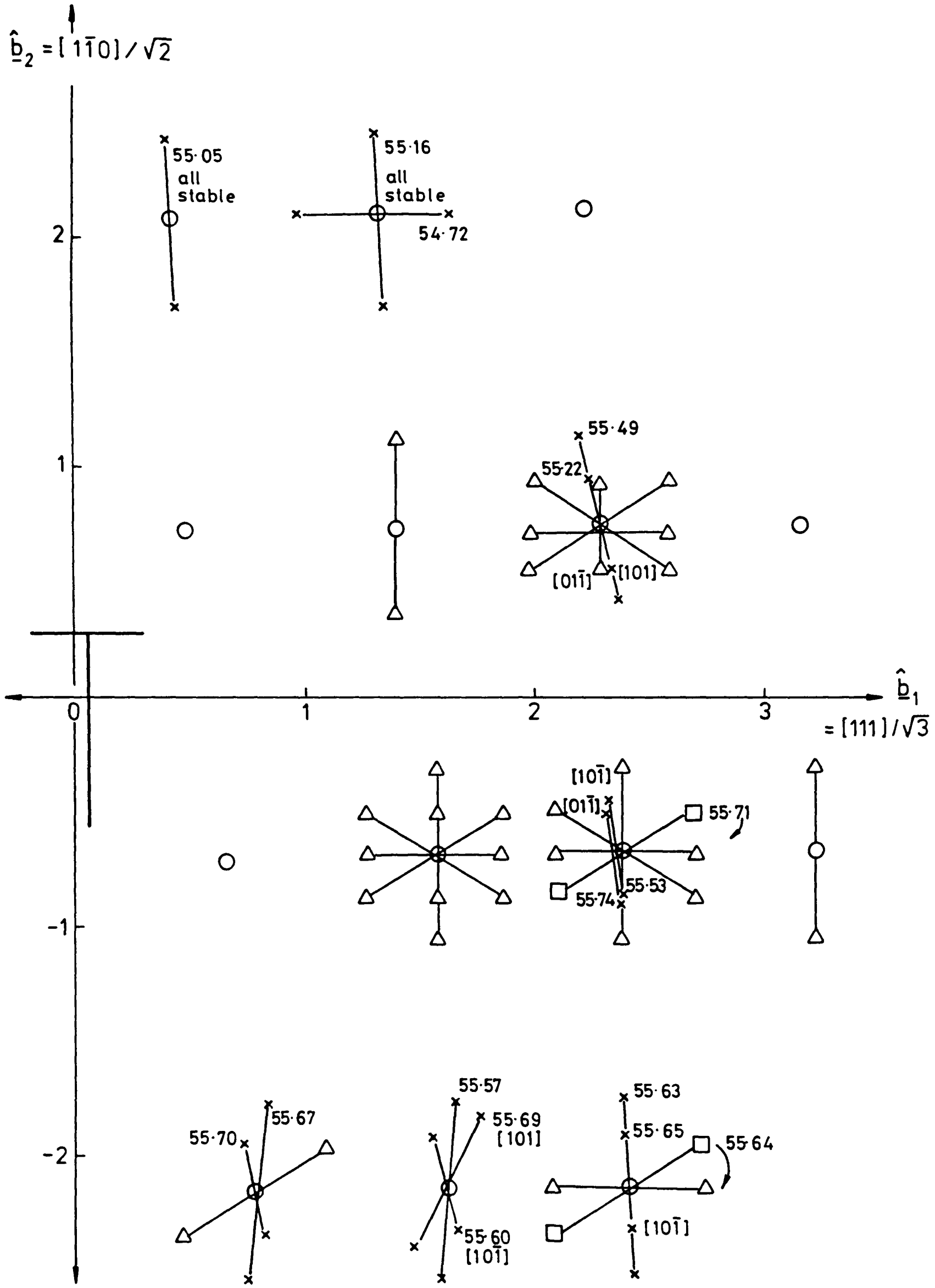

Figure 28. Stability of niobium interstitials near a dislocation.

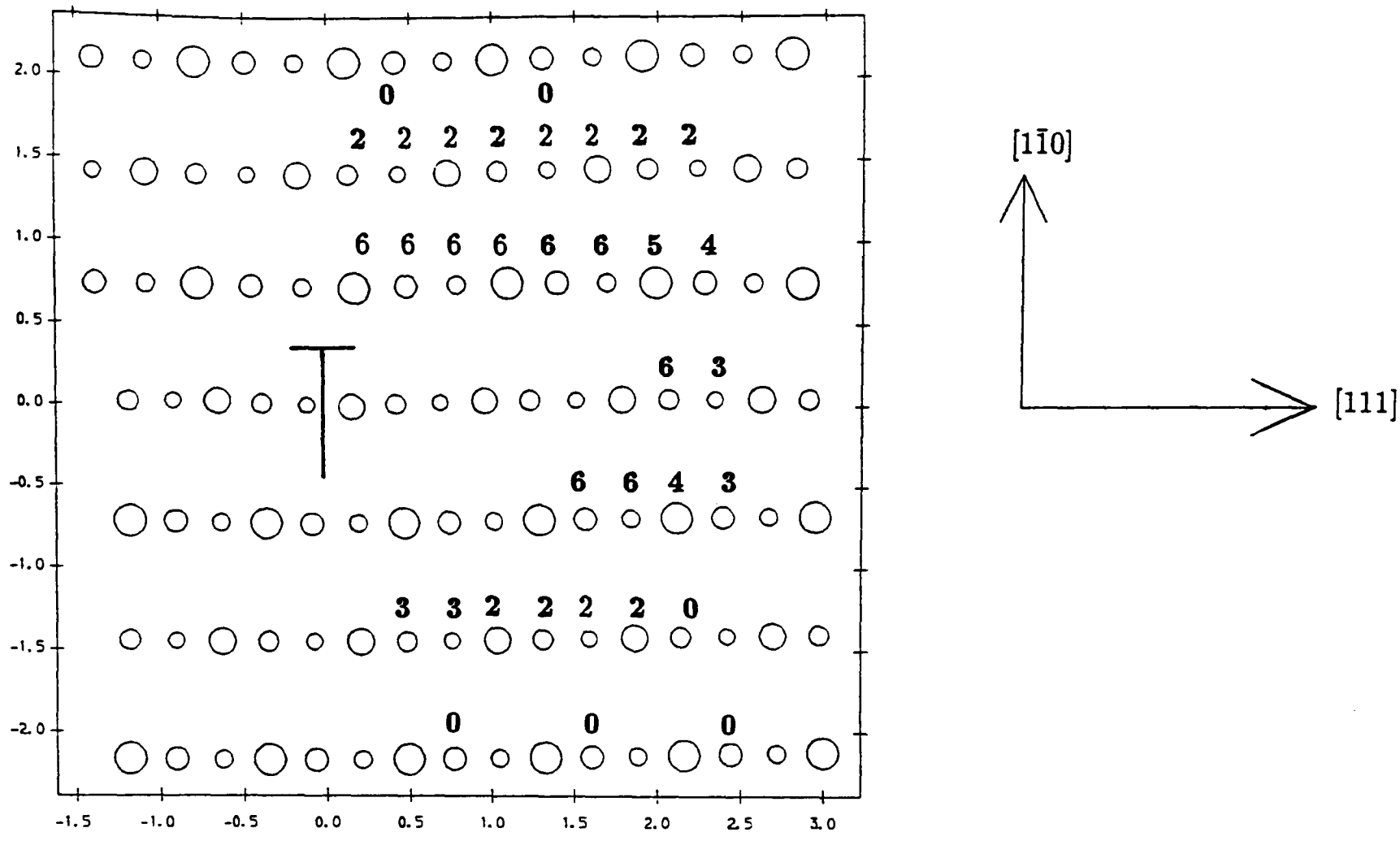

Figure 29. Spontaneous absorption of interstitials by a ½[111] dislocation.

Positions of atoms around the dislocation are marked with the number of the six interstitial dumbbell orientations that are spontaneously absorbed.

assume that interstitials are equally likely to be created in any of the dumbbell orientations on any site. The sum of all the digits in figure 29 (plus the implied values inside the absorption zone) divided by six, is then the number of sites from which capture would occur: this comes to 27.667, or 55.333 when the other side of the extra half-plane is included. In the figure, each site is associated with an area of $\frac{1}{6}a\sqrt{3} \times \frac{1}{2}a\sqrt{2} = 0.204a^2 = \omega$ say. Equating 55.333ω with $\pi r_{i,cap}^2$ gives a capture radius $r_{i,cap}$ of $1.900a$, or 0.626nm.

Kirsanov and Turkebaev [1986] use pair potentials to investigate the zones of spontaneous absorption in α–iron. Although they consider only two dumbbell orientations ([1$\bar{1}$0] and [01$\bar{1}$]), they find results similar to those presented here: that absorption depends on orientation and is most extensive in the first compressive (1$\bar{1}$0) plane. They also find absorption via replacement chains of three or more atoms, and their absorption regions are similar in size to those calculated here. However, their calculations of absorption radii (for use in elasticity calculations) are based upon equating the measured *perimeter* of the absorption zone with $2\pi r$. Given the rather jagged shape of this zone, it is not surprising that their quoted radius

Dumbbell centred at[a]	Comments
(2.0, 1.0, 0.0)	all six orientations absorbed
(1.5, 0.5, 1.5)	all six orientations absorbed
(2.0, 2.0, 0.0)	$[1\bar{1}0]$, $[10\bar{1}]$, [101] absorbed [110], [011], $[01\bar{1}]$ stable
(0.5, 2.5, 0.5)	$[1\bar{1}0]$, $[10\bar{1}]$, $[01\bar{1}]$ stable; [110], [101], [011] move to other orientations or locations
(–0.5, 1.5,–0.5)	$[1\bar{1}0]$, [110], $[01\bar{1}]$ stable; $[10\bar{1}]$, [101], [011] absorbed
(1.5,–0.5,–0.5)	[110], $[10\bar{1}]$, [101], [011] stable; $[1\bar{1}0]$, $[01\bar{1}]$ absorbed
(1.5, 1.5, 0.5)	[110], [011], $[01\bar{1}]$ absorbed
(0.5, 1.5, 1.5)	$[01\bar{1}]$, [101] stable; $[10\bar{1}]$ absorbed
(2.0, 0.0, 0.0)	$[1\bar{1}0]$, $[01\bar{1}]$ absorbed
(1.0, 2.0, 0.0)	[101], $[01\bar{1}]$ absorbed
(0.0, 2.0, 0.0)	[101] stable (as crowdion); $[10\bar{1}]$, [011] absorbed
(2.5, 0.5, 0.5)	$[1\bar{1}0]$, $[01\bar{1}]$ absorbed
(–0.5, 1.5, 0.5)	[101] stable
(–0.5, 2.5, 1.5)	$[10\bar{1}]$ stable; [011] absorbed
(0.0, 2.0, 1.0)	$[10\bar{1}]$, [011] absorbed
(0.0, 2.0,–1.0)	$[10\bar{1}]$ absorbed
(3.0, 1.0, 0.0)	$[1\bar{1}0]$, $[01\bar{1}]$ absorbed

[a]These positions are approximate, and refer to the coordinates in the undistorted (pre-dislocation) crystal. They are correct to within 0.1 though.

Table 6.5 Calculations defining zone of spontaneous absorption for interstitials near a $\frac{1}{2}\langle 111 \rangle$ edge dislocation in niobium.

(1.185nm) is larger than my niobium value, despite the smaller lattice parameter of α–iron.

6.6 Spontaneous Absorption of Vacancies

6.6.1 Results

Vacancies are rather easier to treat than interstitials. As they have no orientation, I need to make only one calculation at any lattice site; presenting the results is also easier.

Using the same method as for the interstitials, I define vacancies near to the core of a dislocation, relax the lattice and see what happens. In *none* of the cases studied does the vacancy migrate to the core of the dislocation. This fact must be due to the binding energy of the niobium vacancy to the dislocation: just 1.05 eV (table 6.1), compared to 3.01 eV for interstitials. The very limited distortion round a vacancy, and its relatively low formation energy, give little opportunity for the vacancy to escape from its energy minimum.

The results are better plotted (figure 30) than tabulated. The circles correspond to the positions of atoms round a pure dislocation, and are the sites selected to be defined as vacancies. The sites are labelled with the formation energy of a vacancy at that position.

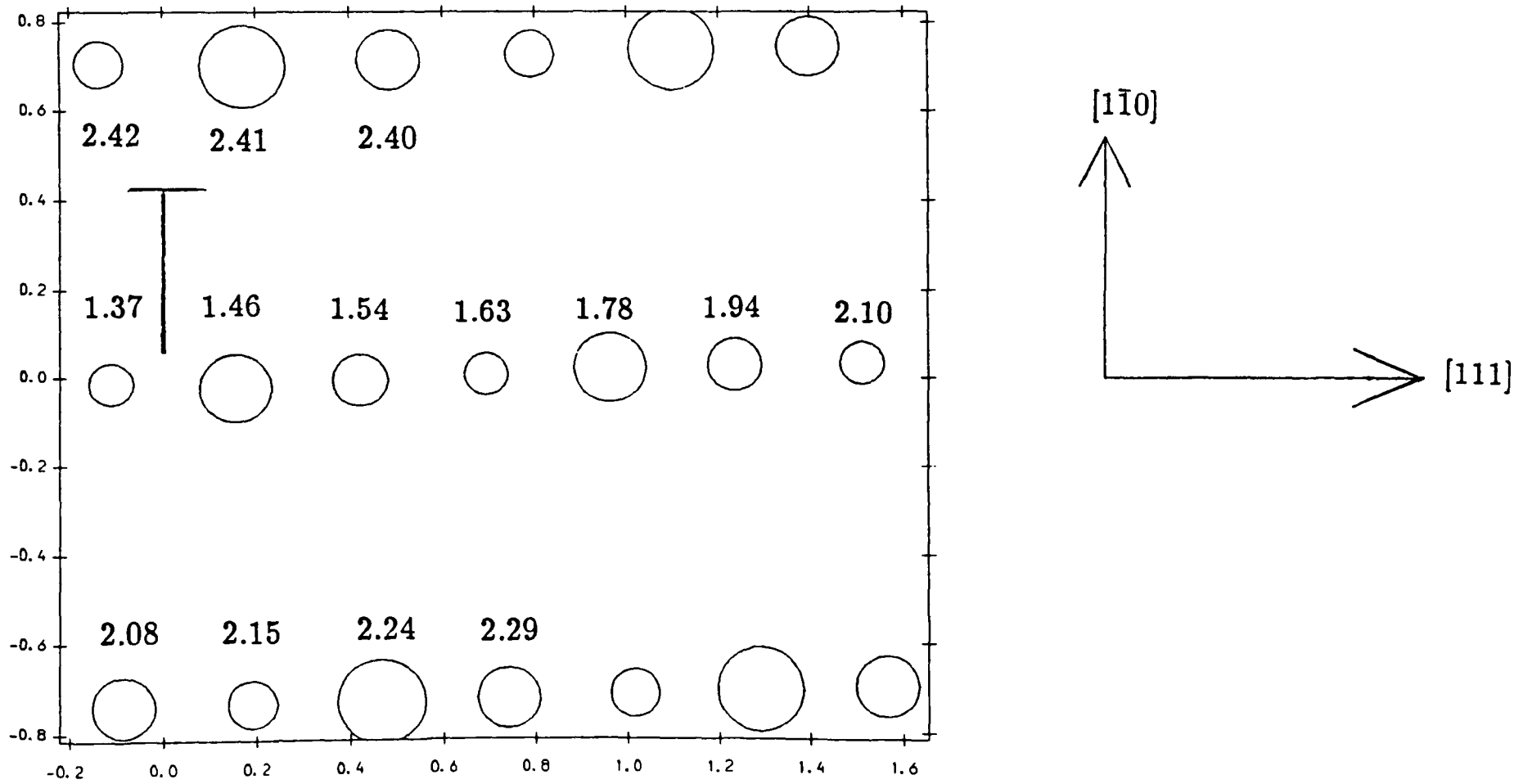

Figure 30. Formation energies of a niobium vacancy near to a ½[111] dislocation.

6.6.2 Discussion

In the absence of any vacancy migration into the core, the only vacancies that can be treated as 'absorbed' are those that are already in the core, namely those with formation energies of 1.37 and 1.46 eV. On this assumption, an analysis along the lines of that for the capture radius of interstitials (§6.5.3) gives $r_{v,cap} = 0.360a = 0.119$nm.

Alternatively, one can argue that although nearby vacancies have not been spontaneously absorbed, some of them will not escape into the lattice because they would require a significant fraction of their formation energy to do so. For the interstitials, the situation is clear-cut: either the interstitial formation energy is close to its perfect-lattice value, or a replacement chain is initiated and absorption is obvious. The vacancy formation energy varies much more smoothly with distance from the dislocation core, and judging the capture region is not easy. Drawing a somewhat arbitrary boundary halfway between the formation energy in the core and that in the perfect lattice, any vacancy with a formation energy of 1.94 eV or less can be treated as 'bound'. This then gives five bound sites in the half-plane under consideration, which implies a capture radius $r_{v,cap} = 0.806a = 0.266$nm.

Kirsanov and Turkebaev [1986] also find no replacement chains for vacancies, and consider vacancies at just two sites to be absorbed. Once more, their capture radius (0.340nm) is greater than mine, owing to the slightly odd definition they employ. Their results that the vacancy formation energy is (predictably) smaller in the compressive than in the tensile region, and that the binding energy falls off as the vacancy-dislocation distance increases, are confirmed here. Using many-body potentials instead of pair potentials does seem to make some difference, as even on the tensile side of the dislocation glide plane I find a vacancy formation energy less than the perfect-lattice value: i.e. a positive binding energy. This reduction in formation energy seems to be due to a slight relaxation of the first compressive $(1\bar{1}0)$ plane of atoms (the glide plane).

6.7 Dislocation Bias

Brailsford and Bullough [1981] define the 'bias' Z of a dislocation via the relation

$$k_d^2 = Z\rho_d \tag{6.3}$$

where ρ_d is the dislocation density, and k_d^2 the sink strength of dislocations for the point defect in question. The biases for vacancies and interstitials, Z_v and Z_i will be different, with Z_i being larger. They also define a 'relative

bias' as $1-Z_v/Z_i$, for the purposes of their figure 10, and find that it typically lies in the range 0.3 to 0.45, depending on the dislocation density ρ_d and the strength of the internal sinks k_c^2.

The above results for capture of interstitials and vacancies can provide a crude estimate of the relative bias of dislocations. The ratio of the areas of the absorption zones is 1:28 (or 1:5.5 if the 'bound' vacancies are treated as absorbed). Using this ratio as an estimate of Z_v/Z_i [Bullough, 1989], gives a relative bias of 0.96 (or 0.82). Assuming that the capture radii given by Kirsanov and Turkebaev [1986] can be used to calculate a similar ratio, their results give a capture area ratio of $r_i^2/r_v^2 = 12.15$, and hence a relative bias of 0.92.

All of these values seem very high, suggesting that the absorption zone for vacancies does in fact include the 'bound' region. Section 6.9 covers vacancy migration into the core, and finds that migration barriers into the spontaneous absorption region are indeed lowered considerably.

6.8 Interstitial Migration to the Dislocation Core

Having found the boundaries of the zone of spontaneous absorption, I was interested in the migration of point defects into this region. The height of the migration barrier for the final step into the absorption zone may have a significant effect on point defect absorption.

I first defined the centre of the dislocation core as the position of an absorbed atom: about (0.0, 0.5) on the block axes $[111]/\sqrt{3}$ and $[1\bar{1}0]/\sqrt{2}$. The interstitial then migrates from its inserted position towards the dislocation core. Constraints as described in §3.2.1 keep it at a fixed distance from the core on each migration step.

The migration energies calculated this way differ only very slightly from the perfect lattice values. There is thus no significant difference between the last migration step into the absorption zone, and the previous steps through nearly-perfect lattice.

6.9 Vacancy Migration to the Dislocation Core

Contrariwise, vacancy migration is considerably affected by the presence of the dislocation. The method of calculation is identical to the calculation in the perfect lattice (see §5.2). The results obtained are close to those expected if a migration energy of 0.85 eV (table 3.3) is superposed on a formation energy curve that drops by 0.3 to 0.4 eV between near-neighbours along the [111] direction (see figure 30).

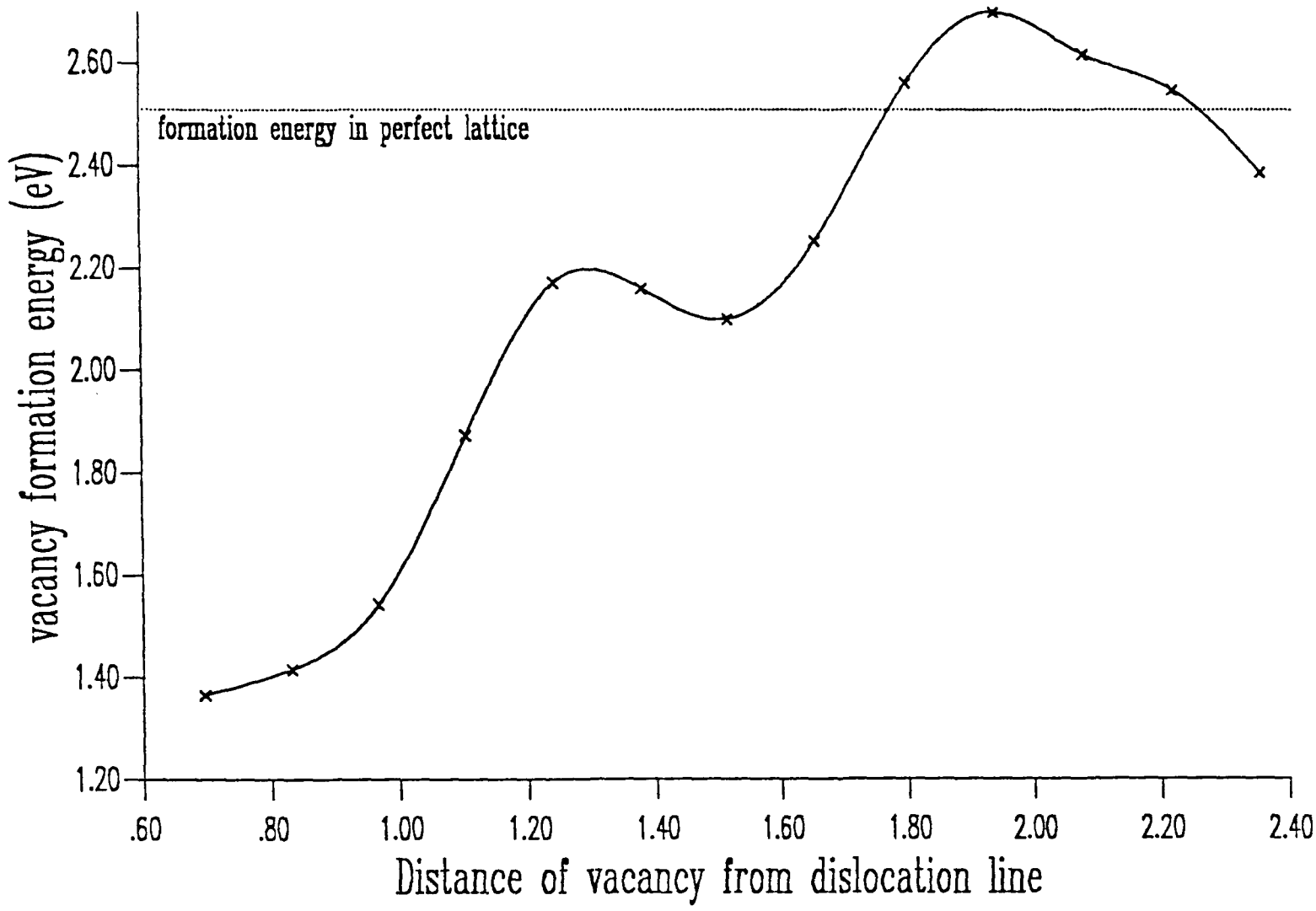

Figure 31. Niobium vacancy migrating towards a $\frac{1}{2}$[111] dislocation: energy against distance from dislocation line.

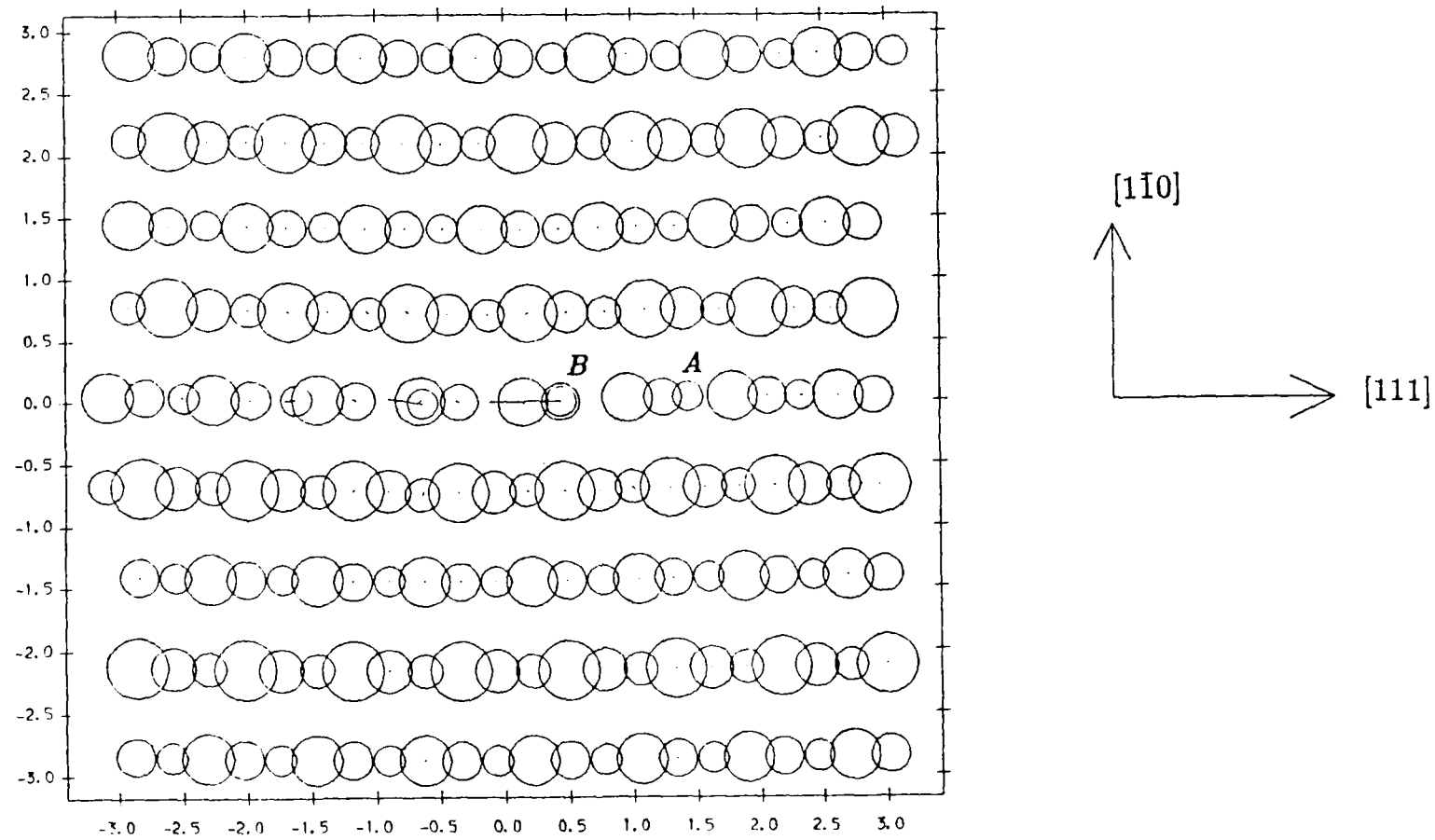

Figure 32. Migration of a niobium vacancy towards a $\frac{1}{2}$[111] dislocation: final position.

Figure 31 plots the vacancy formation energy as the vacancy moves along [111] towards the dislocation line. During the first step (from 2.3475 to 1.5119) the migration is well behaved. In the second stage, the interstitial that is migrating between the two 'vacant' sites moves as prescribed in six equal steps, ending up in the position labelled *A* in figure 32. However, the distortion produced at the saddle point is sufficient for the $-(\frac{1}{2}, \frac{1}{2}, \frac{1}{2})$ neighbour (labelled *B*) of the migrating interstitial to move into the supposed vacancy. The vacancy thus moves further into the dislocation core, and the formation energy falls from 1.63 eV (expected) to 1.36 eV.

The abscissa of figure 31 (distance of the vacancy from the dislocation line) is hard to define. In the scheme used here (one interstitial migrating between two vacant sites), the interstitial moves from one site to the other in six steps. The interstitial end positions are not quite the vacant sites themselves (if such a concept has a meaning), because of the inward relaxation due to the vacancy at the other end of the path. I have simply taken the vacant site to occupy the position of the removed atom from the dislocation-only state; as the vacancy moves (courtesy of the interstitial coming in the opposite direction), its distance from (0, 0, 0) decreases in six equal steps until it reaches the site at the end of the path.

Although this procedure is well-defined for the first migration step, the second step causes trouble as the vacancy is absorbed. Defining the position of the vacancy is by no means trivial when two or more neighbouring atoms are in motion. Taking moments about the dislocation line is one possible solution, but for the sake of simplicity (it's only a diagram!) I have taken the same approach as for the first step and pretended that the vacancy ends up at its intended site.

6.10 Conclusions

For the five metals studied, the results in tables 6.2 and 6.3 suggest that an interstitial is bound to a dislocation by 70% (±4%) of its formation energy, while the binding energy for a vacancy is 44% (±2%) of its formation energy.

Dislocations absorb interstitials spontaneously from a sizable volume of the lattice, over twice the nearest-neighbour separation on average. The absorption zone for vacancies is much smaller. No vacancy inserted away from the dislocation core is truly spontaneously absorbed.

The formation energy of a vacancy decreases steadily as the vacant site approaches the dislocation core. The migration energy required to move

from one site to the next down this 'hill' is small, and a moderate disturbance can be sufficient to trigger absorption of the vacancy.

The static zones of spontaneous absorption are not good guides to the relative bias of interstitials. Very high values of the relative bias arise from taking a simple ratio of absorption areas; the enhanced migration of vacancies into the core should be taken into account.

7 Summary

7.1 Significant Progress

The static minimisation code DEVIL is now up-to-date. Using a double pass through the lattice, DEVIL can handle *N*–body potentials. The algorithm for evaluating the energy of the lattice has a new form: at the expense of storage space, most of the inner loops will be vectorised by a vectorising compiler. DEVIL now has many more options for plotting the positions of atoms, reading in dumped sets of coordinates, setting up dislocations, constraining defects and controlling the motion of migrating atoms.

New repulsive terms at small interatomic separations enable Finnis-Sinclair potentials to model situations where metals are in compression. Calculations with the new cores produce realistic values of self-interstitial formation energies in vanadium, niobium, tantalum, molybdenum and tungsten. As observed experimentally, the stable interstitial configuration for the self-interstitial in vanadium, niobium, tantalum and molybdenum is the ⟨110⟩ split dumbbell. In tungsten, the Finnis-Sinclair potential predicts that the ⟨111⟩ crowdion is stable, with the ⟨111⟩ split interstitial at a very slightly higher energy. Although not in accord with experiment, this stability does facilitate study of one-dimensional migration in the ⟨111⟩ direction.

My discovery of a stable skew position for the self-interstitial dumbbell in molybdenum has prompted many workers to be more careful with symmetry when making relaxation calculations. The detailed survey of interstitial formation energy against dumbbell direction leads to a better understanding of the behaviour of interstitial on its lattice site; in particular, how free it is to rotate to another orientation.

Formation and migration enthalpies for interstitials and vacancies in perfect crystals compare well with experimental measurements (where available), engendering confidence in the form of the potentials used. I see no evidence for two-dimensional migration of the lowest-energy ⟨110⟩ interstitial dumbbell configuration.

With the exception of tungsten, the ⟨111⟩ dumbbell turns out to be unstable with respect to conversion to ⟨110⟩. This means that long-range migration of 'metastable' ⟨111⟩ crowdions without converting to ⟨110⟩ dumbbells is unlikely, lending support to the one interstitial model against the two interstitial model. Moreover, the ⟨111⟩ crowdion itself is unstable in niobium, and seems to have neutral stability in tantalum and vanadium.

Even the low energy barrier to ⟨111⟩ migration seems too high to explain the self-diffusion seen at very low temperatures in some metals.

Results for the total energy of migration (formation plus migration) imply that vacancies migrate at a lower temperature than interstitials, and are therefore responsible for thermally-activated self-diffusion.

Calculations of binding energies of interstitials and vacancies to dislocations can provide input into the chemical rate theory of radiation damage. The work on zones of spontaneous absorption indicates that although they are sharply defined for interstitials, vacancies can migrate easily towards a dislocation from an extended region around the absorption zone proper. This fact complicates the procedure of estimating the relative bias of dislocations from the ratio of volumes of absorption zones: molecular dynamics calculations would give a better answer in this case.

7.2 Future Developments

This section lists those things I would like to have done, given unlimited time and money, or things that I would do as a follow-up to this doctorate. Possible improvements to the methods used here are followed by further interesting (and important) problems.

Although I have vectorised much of the minimisation algorithm in DEV3, FORTRAN compilers evolve continually and more work could well improve the vectorising still further.

The minimisation algorithm itself is rather old. Using modern numerical methods, I suspect that an improved algorithm, tailored for the Cray, could be found. A first step in this direction could well be the method used by Sabochick, Yip and Lam [1986]. More rapid minimisation would permit the study of larger blocks of atoms. A larger block would not only give more accurate results for all the quantities calculated here, but would eliminate some of the 'edge effect' problems with the interstitial absorption calculations in §6.5.

DEVIL, as a static relaxation code, is always relaxing the metals to absolute zero. As the relaxation proceeds, the potential energy in the lattice is gradually reduced; in some sense, so is the temperature. There is a problem in interpreting the spontaneous absorption calculations, as the motion may be driven by the unrelaxed potential energy. The two-stage procedure adopted in §5.2 tries to overcome this problem by relaxing the rest of the lattice before letting the migrating atom move, but doubts will always remain about whether the motion is truly a zero-temperature phenomenon.

Molecular dynamics (MD) calculations are rather easier to interpret. Even with quenched MD, a lattice temperature is always available; and the best way to investigate both spontaneous absorption of point defects at dislocations and defect migration is probably with finite-temperature molecular dynamics.

The DEVIL calculations are also performed at constant volume, while experiments tend to measure quantities at constant pressure. Simulations with the MD program MOLDY (see §3.2.6) can allow the size and shape of the block to alter. Although a factor of six slower, an MD calculation at finite temperature and constant pressure avoids some of the problems that beset static relaxations. A calculation that goes beyond simple internal energy, to enthalpy and Gibbs free energy would be particularly interesting for the calculations of migration in perfect lattices.

Rebonato's recent correction [1989] to the Finnis-Sinclair potentials, to reproduce the correct behaviour under increased temperature, looks to be worth making.

A subject that is important and easily investigated by the methods used here is 'stress-induced preferential absorption', or SIPA. In a crystal under tension, edge dislocations with their Burgers vector parallel to the applied stress will have an increased affinity for interstitials. The higher bias of these dislocations makes them climb more than others, which leads to the phenomena of growth and irradiation creep. Applying the stress is straightforward: elasticity theory gives the displacements for atoms in the fixed boundary regions, and applying these displacements will produce a simulation of a block under stress.

The construction of improved repulsive cores to the Finnis and Sinclair potentials, described in chapter 3, ought to be extended to the ferromagnets iron and chromium. Iron, of course, is of enormous technological importance.

In my spontaneous absorption calculations, I have considered only niobium. Calculations for the other metals would give valuable input into sink strength calculations.

Migration of point defects along dislocation cores is another interesting area. The speed of this pipe diffusion determines how rapidly an interstitial (or vacancy) finds a jog to which to bind.

Finally, Car and Parrinello [1985] have shown the way forward for *ab initio* electronic structure calculations. I feel that such calculations (see Car [1989] and Gillan [1989] for some impressive examples) will overtake simulations based on empirical potentials in the not-too-distant future.

Appendix 1: The DEVIL Program

A1.1 Introduction

The DEVIL code was written in the early 1970's at Harwell, to undertake static relaxation of crystals containing defects. No information about the code was published until 1985 [Thetford, 1985]; since that document, DEVIL has continued to evolve. In the course of working on this thesis, I have prepared a new version, DEVIL-2, which is different in many ways from Norgett's original DEVIL: little remains other than the routines for locating lattice sites and performing the minimisation. I have vectorised the calculation of energies and gradients, and have added routines to set up dislocations, perform migration calculations, plot out results and draw displacement vectors.

Figure 33 shows the relationships of the DEVIL subroutines. All of the routines called by PLOT are from the GHOST library, while F02AGF is a NAG routine and MA23BD is from the Harwell subroutine library.

In this appendix, I intend to put on record information on the current capabilities of the code, how to use it, and a brief description of how it works. Some of the text is reproduced directly from chapter 2.

A1.2 General Description

A1.2.1 Setting up the block

The atoms over which calculation takes place are divided into two regions: 'inner' and 'outer'. The size of the inner or 'free' region is specified by the user. The atoms in this region will be free to relax. The boundary layers compose the outer region, which can be either fixed or cyclic (i.e. a translated image of the main crystal). The size of this boundary region is determined by the input value of SERCH: the neighbour list of one atom will include only those atoms that are closer to it than SERCH in the undistorted lattice. Hence SERCH must exceed the range of the potential by by an amount sufficient to cope with the largest distortion in the block.

DEVIL uses the three lattice vectors $\mathbf{l}_1$, $\mathbf{l}_2$ and $\mathbf{l}_3$ and the three block edge vectors $\mathbf{b}_1$, $\mathbf{b}_2$ and $\mathbf{b}_3$ input by the user to define the block of atoms to be modelled. The block is built from planes of atoms lying perpendicular to the vector products $\mathbf{b}_2 \times \mathbf{b}_3$, $\mathbf{b}_3 \times \mathbf{b}_1$ and $\mathbf{b}_1 \times \mathbf{b}_2$. The routine LATTIS calculates all the required vector products, reciprocal lattices, *et cetera*. REGION builds the block of atoms, using sizes specified in the input dataset, and sets up the boundary layers.

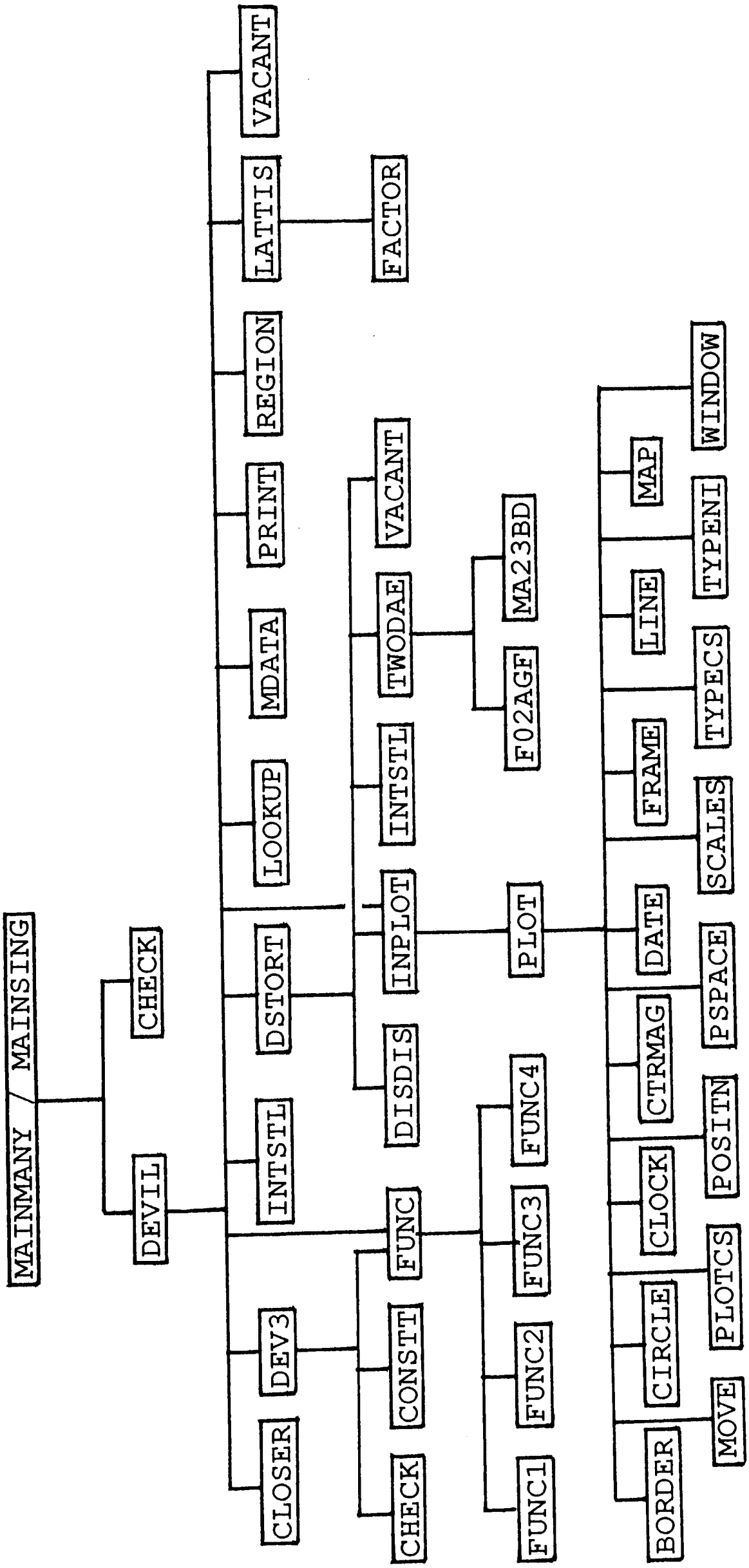

Figure 33. DEVIL calling tree.

Each atom in the whole block (free plus boundary regions) is indexed by the numbers of the planes in which it appears. An additional index copes with the possibility (found only when skew blocks are used) of more than one atom in each 'unit cell'. The x, y and z coordinates of the mth atom in the cell where planes i, j and k meet are stored as ATOM(1,I,J,K,M), ATOM(2,I,J,K,M) and ATOM(3,I,J,K,M). Coordinates of the *JINT*th interstitial atom are found in ATOMI(n,JINT), with n=1,2,3.

Vestiges of Norgett's index function method remain in the allocation to each atom of a characteristic index number Z, which is equal to $(i-1)+25(j-1)+625(k-1)+31250(m-1)$. An array KNV is constructed to act as a look-up table: KNV(1,Z) contains i, KNV(2,Z)=j, KNV(3,Z)=k, KNV(4,Z)=m. In this way, the indices i,j,k and m are easily obtainable from Z.

The atoms in the periodic boundaries are counted as they are found. One or more of the vectors spanning the block edges is subtracted from the position of the cyclic atom, until it falls inside the free region. The total vector subtracted for the Lth cyclic atom is stored in ACYC(n,L), and the indices of the atom of which it is an image are held as MCYC(n,L) (n=1,2,3 as before). The coordinates of the Lth cyclic atom are thus

$$\text{ATOM}(n,\text{MCYC}(1,L),\text{MCYC}(2,L),\text{MCYC}(3,L)) + \text{ACYC}(n,L)$$

In addition, each atom has a 'type', stored in LCO(I,J,K,M). This type, call it L, defines the atom thus:

l<0: atom is the Lth cyclic atom.

l=0: atom is a vacancy.

l=1: atom is in the free region.

l=2: atom is in a fixed boundary

Interstitial atoms, though not having an entry in array LCO, are indicated in various pieces of output by l=3.

The subroutine LOOKUP calculates which atoms are within a distance SERCH of each atom in the lattice, and constructs the neighbour array. In this array, NBR(INBR,I,J,K,M) contains the Z-value pertaining to the *INBR*th neighbour of atom i,j,k,m. The old method of applying a series of shifts in the index function to find the set of neighbours (see §2.2.1) no longer applies: the coordinates are available immediately.

A1.2.2 Computing the energy of the block

The conjugate gradients method demands both energies and forces. With the Finnis-Sinclair many-body potential, the energy of a particular atom can be split up into a cohesive part E_c and a repulsive part E_r, defined by equations (4.3) and (4.4). Before the vectorisation work mentioned in §4.2.1, both energy and forces were provided by a user subroutine (POTEN). However, any loop that contains a subroutine call cannot be vectorised, so POTEN was copied inside FUNC and there it remains. In fact, four copies of POTEN are required: to assist the compiler, FUNC is now split into four sections.

The first (FUNC1) calculates the contributions to the E_c's from interactions between 'regular' (free and fixed) atoms; the second (FUNC2) completes the calculation of the E_c's by considering interactions between interstitials and free atoms and among interstitials. With all of the E_c's calculated, FUNC3 can accumulate the repulsive interactions E_r for 'regular' atoms and calculate the forces on them, and FUNC4 deals once more with the interstitials.

Interstitial atoms fall outside the method used to construct the neighbour list, which works on regions of perfect crystal. FUNC treats them separately, and assumes that they may in principle interact with any other atoms in the crystal — though of course only those within the range of the potential will actually contribute. A vacancy is modelled simply by flagging an atomic site as vacant, setting all of its interactions to zero, and thereafter ignoring it.

Unlike the original case, some calculation needs to be done for atoms in any fixed boundary region. For atoms in this boundary, a flag is set when POTEN is called. This flag results in only the value of $\phi(R_{ik})$ being calculated; f_i is then accumulated (see equations (1.3) and (1.4)). The value of f_i is needed because as the inner atoms move, the sum of cohesive potentials for the boundary atoms will vary, and this in turn affects the forces on the 'free' atoms via equation (1.9). Problems can arise in calculating the total cohesive energy at a boundary atom, as some of its neighbours may not lie in the calculation region at all. For example, if an atom is in the $+x$ boundary layer, no information is likely to be available on its [100] neighbour. In this case DEVIL uses the equilibrium separation for a [100] neighbour in the perfect crystal, which is stored by LOOKUP in array STDSEP.

A1.2.3 The relaxation calculation

DEVIL relaxes the lattice by using the method of conjugate gradients. The original minimisation routine, DEV3, is a slightly modified version of the Harwell subroutine VA08A. I have tuned DEV3 to suit the problems studied in this thesis.

The method of conjugate gradients [Fletcher and Reeves, 1964] moves downhill in an N–dimensional space, in directions which are orthogonal to each other. Let $\mathbf{x}=\{\mathbf{x}_i\}$ be the $3N_{free}$ vector of atom coordinates, $\mathbf{g}=\{\mathbf{g}_i\}$ be the vector $\partial E/\partial \mathbf{x}$ and $\mathbf{s}$ be the search direction for a particular step. The three-vector $\mathbf{g}_i$ representing the gradient of energy of atom i has Cartesian coordinates, $g_{i,\mu}$ with $\mu=1,2,3$. The first 'search direction' is just the steepest descent from the starting point: i.e. $\mathbf{s}=-\mathbf{g}$. The atom positions $\mathbf{x}$ will be altered to $\mathbf{x}+\alpha\mathbf{s}$, and a call to FUNC evaluates the new energy of the lattice and the new gradient vector $\mathbf{g}$. DEV3 then aims to find the value of α such that the condition

$$\mathbf{g}\cdot\mathbf{s} = 0 \qquad \text{(A1.1)}$$

holds. Rather than waste a lot of time trying to satisfy this equation precisely, the search is deemed satisfactory if $\mathbf{g}\cdot\mathbf{s}$ is reduced to less than a tenth of its value at the start of the step: that is, if

$$\mathbf{g}\cdot\mathbf{s} < 0.1(\mathbf{g}\cdot\mathbf{s})_{initial} \qquad \text{(A1.2)}$$

When restarting in the direction of steepest descent, the first guess made for α is $0.05/g_{\max}$, where

$$g_{\max} = \max_{i,\mu}(g_{i,\mu}) \qquad \text{(A1.3)}$$

Thereafter, the first step in a new search direction s just uses the value of α that was successful in satisfying relation (A1.2) on the previous step. This method seems to work well, often satisfying (A1.2) at the first attempt.

If the inequality (A1.2) is not satisfied by the first guess for α, a new estimate is required. We now have several pieces of information: the value of $\mathbf{g}\cdot\mathbf{s}$ from the first guess, call it $(g\cdot s)_1$; the guess α_1 and the initial value $(\mathbf{g}\cdot\mathbf{s})_{init}$ If the energy is varying quadratically with α, then $\mathbf{g}\cdot\mathbf{s}$ should be varying linearly: hence a linear interpolation should get very close to finding the zero of $\mathbf{g}\cdot\mathbf{s}$. This interpolation is nearly always successful.

In cases where the interpolated value of α still fails to give a gradient $\mathbf{g}$ that satisfies (A1.2), DEV3 can make further interpolations. The code keeps track of the values of α that have given the smallest positive and negative values of $\mathbf{g}\cdot\mathbf{s}$ (or just the two most recent values if all evaluations of $\mathbf{g}\cdot\mathbf{s}$ are on

the same side of zero) and uses these for the interpolation (or extrapolation). Up to five interpolations are allowed before the code gives up the search in that search direction and restarts once more with a steepest-descent step.

Finally, because the conjugate gradient algorithm never quite satisfies equation (A1.1), some 'slack' develops in the method: after a certain number of iterations, a greater decrease in energy can be obtained by returning to the steepest descent rather than continuing in yet another conjugate direction. The number of iterations made before restarting with a steepest descent is controlled by ISTEEP: I have found that ISTEEP=10 seems to be roughly optimum for block containing dislocations, and ISTEEP=20 appropriate for blocks without.

A1.2.4 Distorting the block

Chapter 4 discusses how a dislocation can be modelled by setting up displacements in the fixed boundaries of a block of atoms. DSTORT is the subroutine that strains the lattice in this way, and offers diverse other possibilities for manipulating the lattice. The operation of DSTORT is controlled by the parameter ISTORT; table A1.1 lists the possible values of ISTORT and the effect they have.

ISTORT	Effect
0	return immediately from DSTORT
1	read in a new set of coordinates
2	set up a dislocation
3	fix an atom in a particular position
4	set up a dislocation and read a set of coordinates
5	read a set of dumped coordinates and plot out
6	set up dislocation; read in coordinates of free atoms
7	plot displacement from old to new set of coordinates
8	read in a set of coordinates; then relax in two stages, around defect and with defect
9	do plotting without displacement vectors
10	freeze all free atoms and relax only interstitials

Table A1.1 Various modes of DEVIL operation.

Sinclair provided subroutines TWODAE and DISDIS that DEVIL uses for setting up dislocations. TWODAE uses two-dimensional anisotropic elasticity theory to set up matrix elements required for DISDIS; DSTORT

calls DISDIS with old atom positions and receives the distorted positions in return.

The large relative displacements of atoms on the glide plane will often disturb the neighbour lists that have been set up for the perfect lattice. After some experimentation with redefining the neighbour lists, I have settled for simply extending the search distance SERCH. To ensure that no interactions are being missed, the new subroutine CHECK simply goes through the whole lattice to see whether any pairs of atoms that are not defined as neighbours are interacting. To prevent the wastage of large amounts of Cray time on invalid runs, DEV3 calls CHECK periodically (every IPRINT iterations), and CHECK aborts the run if any errors are found. A useful extension to CHECK would be a block of code that automatically redefined the neighbour lists, then carried on the minimisation.

A1.2.5 Restarting from a dump

A feature of DSTORT referred to in table A1.1 is that it can pick up a set of atom coordinates from a dump. The block has to be set up in the normal way, with each atom allocated a neighbour list and a set of indices i, j, k and m. DSTORT calls subroutines VACANT and INTSTL to set up the vacancies and interstitials that are present in the dump, and then reads in a set of values as

$$i \;\; j \;\; k \;\; m \;\; x \;\; y \;\; z \;\; l$$

Here, x, y and z are the new Cartesian coordinates for atom (i,j,k,m). If the type l does not match the declared type LCO(I,J,K,M) of the atom, DSTORT prints an error message and stops. The nth interstitial is indicated by $i=j=m=0$, $l=3$ and $k=n$. A line with $i=j=k=m=-1$ acts as a terminator; control returns to the DEVIL subroutine which can call VACANT and INTSTL again to set up more vacancies and interstitials (if required); relaxation can then proceed.

A1.2.6 Plotting

DSTORT also initiates plotting by calling INPLOT. INPLOT assembles the coordinates of the atoms lying within certain limits into arrays X1, X2, X3, X4, X5 and X6. These arrays are currently set to hold all of the atoms in each of the six atom planes that make up one repeat of the b.c.c. lattice in the $[11\bar{2}]$ direction. A full plot will produce pictures of the lattice two layers at a time (X1 and X2, *etc.),* but often one plot with all six layers is sufficient.

INPLOT calls Sinclair's routine PLOT, a GHOST80-based plotting

routine, with a large array XX of atom positions, and information on what part of XX should be plotted. PLOT draws circles at the positions in XX (which may be Cartesians but are often defined in terms of the normalised block edge vectors $\mathbf{b}_1$, $\mathbf{b}_2$ and $\mathbf{b}_3$). PLOT will size the circles representing the atoms according to how close to the 'eye' they are, giving some impression of depth: the position of the eye on the z–axis and the base size of the circle are both set in PLOT. INPLOT also sets up BX, an array containing the 'previous' positions of all the atoms in XX: PLOT draws lines from the positions in BX to the centre of the circles representing the new atom positions. As default BX contains the perfect lattice positions of the atoms, but a restart from a set of dumped coordinates will fill BX with the dumped values. The displacement vectors give a very useful picture of what has happened in a relaxation.

A1.2.7 Applying constraints

Section 3.2.1 discusses how DEVIL applies constraints to the motion of atoms: essentially, forces in one or more directions are zeroed and the atoms move under the remaining forces. Atoms can be fixed completely, allowed to relax on one particular plane, constrained to keep a certain distance from a fixed point, *et cetera*. The reference point used in these calculations has coordinates (REF1,REF2,REF3) and is set in routine DEVIL.

The constraint facility has proved to be most useful for migration calculations as in chapter 5, and for the calculations on dumbbell interstitials in various orientations in chapter 3.

A1.2.8 Multiple calculations

To avoid the expense of repeatedly setting up a new lattice, finding all the neighbours, *etc.*, DEVIL can perform multiple relaxations in one run. Using MAINMANY instead of MAINSING as the main program, two DO loops are available. The dumbbell orientation calculations in chapter 3 were done in just one run per metal, letting the DO loops cover the orientation plane. Starting a minimisation from the perfect lattice position each time would cause a considerable increase in running time.

Calculations of migration energies *need* to start one relaxation from the relaxed position at the end of the previous one, as this mimics the situation in real life. One of the DO loops in MAINMANY is disabled; the other reduces the distance from the fixed point by an increment set in MAINMANY.

data	read by	description
IPRINT MAXFN IDUMP ACC1 ISTORT	DEVIL	printing flag, max. no. of function evaluations, dumping flag, accuracy, flag controlling DSTORT
METAL	DEVIL	name of metal to be modelled
XLAT(1,1) XLAT(2,1) XLAT(3,1) XLAT(1,2) XLAT(2,2) XLAT(3,2) XLAT(1,3) XLAT(2,3) XLAT(3,3)	LATTIS	lattice vectors
XBLK(1,1) XBLK(2,1) XBLK(3,1) XBLK(1,2) XBLK(2,2) XBLK(3,2) XBLK(1,3) XBLK(2,3) XBLK(3,3)	LATTIS	block edge vectors: must not be coplanar
NFX NFY NFZ	REGION	number of planes parallel to each face (negative values imply periodic boundary conditions in that direction)
SERCH	REGION	search distance in terms of lattice parameter
DISLX DISLY[a]	*DSTORT*	*Cartesian coordinates of point where dislocation line cuts z=0 plane*
NVAC[b]	*VACANT*	*no. of vacancies*
X1 Y1 Z1[b] *...NVAC lines...*	*VACANT*	*vacancy coordinates in lattice to be read in from dump*
NINT[b]	*INTSTL*	*no. of interstitials*
X1 Y1 Z1[b] *...NINT lines...*	*INTSTL*	*interstitial coordinates in lattice to be read in from dump*
NVAC	VACANT	no. of vacancies
X1 Y1 Z1 L1 ...NVAC lines...	VACANT	vacancy coordinates
NINT	INTSTL	no. of interstitials
X1 Y1 Z1 ...NINT lines...	INTSTL	interstitial coordinates
TITLE ...one line per relaxation...	INPLOT	title (format 9A8) for plot

[a] only for ISTORT=2 or ISTORT=6
[b] for ISTORT=4,5,6,7,8

Table A1.2 Explanation of DEVIL input data.

A1.3 How to use DEVIL

A1.3.1 Input data

I shall assume that any potential user is sufficiently familiar with his or her computer to know how to run jobs, and cope with input and output on multiple channels (streams).

DEVIL reads the standard input data in free format, from stream 5 (FT05F001 in IBM JCL; *stdin* in Unix). Table A1.2 gives the values required, in the lines in which they should be input. Some of the items are optional, depending on the mode that the code is in (which is in turn controlled by ISTORT). The optional data are given in italic script, and the footnotes indicate for what values of ISTORT they are required.

The following notes amplify the descriptions in table A1.2. Every IPRINT iterations, DEVIL will print the current interstitial coordinates and gradients. IDUMP set to 1 enables the dumping of the solution, on FORTRAN stream 16. DEV3 will call FUNC a maximum of MAXFN times (in any single minimisation if a number are being made). A relaxation terminates once the average value of the gradient reaches ACC1. ($\mathbf{g}\cdot\mathbf{g}$ is compared with $NV \times ACC1^2$ where $\mathbf{g}$ is the gradient vector and NV the total number of atomic coordinates.) The coordinates are given in terms of the lattice parameter. In a run (e.g. a migration) with several relaxations, INPLOT will usually be called once for each relaxed position and therefore a title line needs to be supplied for each plot. (Few things are more annoying than finding that a relaxation has been completed but then a job crashes (without plotting the results) because INPLOT had tried to read beyond the end of the input file!)

The abbreviation for the metal required (V, Nb, Ta, Mo or W) must start in the first column, and is passed to a new routine MDATA. MDATA sets the parameters of the potentials, the elastic moduli C_{11}, C_{12} and C_{44} (used to set up the dislocation strain field), and the lattice constant a.

```
 0   200   0   5.E-5 0
Mo
-0.5   0.5   0.5
 0.5  -0.5   0.5
 0.5   0.5  -0.5
 1.0   0.0   0.0
 0.0   1.0   0.0
 0.0   0.0   1.0
 -14   -14   -14
 1.4   1.4   1.4
 1
 0.0   0.0   0.0
 2
 0.31   0.20    0.01
-0.30  -0.19    0.00
Single split dumbbell interstitial
```

Data to model a dumbbell interstitial in a 14×14×14 block of a b.c.c. lattice with periodic boundary conditions.

Table A1.3 First example of DEVIL input data.

Table A1.3 shows an example of the input required to model a dumbbell interstitial in a 14×14×14 block of a b.c.c. lattice, with periodic boundary

```
100 200  1  5.E-4  8
Nb
-0.5  0.5  0.5
 0.5 -0.5  0.5
 0.5  0.5 -0.5
 1.0  1.0  1.0
 1.0 -1.0  0.0
 1.0  1.0 -2.0
  24   12  -24
 1.5
 12
-2.00 -2.00  4.00
-1.50 -1.50  3.50
-1.50 -1.50  2.50
-1.00 -1.00  2.00
-0.50 -0.50  1.50
-0.50 -0.50  0.50
 0.00  0.00  0.00
 0.50  0.50 -0.50
 0.50  0.50 -1.50
 1.00  1.00 -2.00
 1.50  1.50 -2.50
 1.50  1.50 -3.50
 12
-2.00 -2.00  4.00
-1.50 -1.50  3.50
-1.50 -1.50  2.50
-1.00 -1.00  2.00
-0.50 -0.50  1.50
-0.50 -0.50  0.50
 0.00  0.00  0.00
 0.50  0.50 -0.50
 0.50  0.50 -1.50
 1.00  1.00 -2.00
 1.50  1.50 -2.50
 1.50  1.50 -3.50
 1
 2.50 -0.50  0.50
 2
 2.64  -0.832  0.41
 2.19  -0.300  0.409
(1-1 0) interstitial near (111) dislocn (centred at (2.5-0.5 0.5))
```

Data to model an interstitial near core of $\frac{1}{2}\langle 111\rangle$ dislocation previously set up in a 24×12×24 block.

Table A1.4 Second example of DEVIL input data.

conditions. Table A1.4 reproduces the dataset needed to model an interstitial near to a dislocation. The relaxed positions round the dislocation will be read in on stream 17, and the run used to produce this dump had 12 atoms redefined as interstitials. These are the first vacancies and interstitials defined; the last vacancy and last two interstitials set up the interstitial which is going to have its stability investigated.

A1.3.2 Output

The input information is reproduced at the beginning of a run, and the output (on stream 6) also gives some indication of how the calculation is progressing (energy, number of function evaluations, value of **g**.**g**). Coordinates and gradients are printed at the interval specified by IPRINT

and at the end of the run. In a run with several relaxations, this is true for the first relaxation only: subsequently, just a summary is produced.

DEVIL prints a summary of the interstitial positions at the end of each minimisation, with information on the energy, $\mathbf{g}\cdot\mathbf{g}$ and the number of function evaluations required. DEVIL also calls a routine CLOSER, which goes through the lattice to find the nearest pair of atoms: having the indices and positions of the closest pair printed helps enormously when one is trying to follow a complicated absorption of an interstitial.

INPLOT is set up to print the position of every atom it finds in the slice selected for plotting, but I usually disable the printing for standard lattice atoms and leave it active only for interstitials. The printing is useful because it gives not only Cartesian coordinates, but also the atom positions in terms of the normalised block vectors $\hat{\mathbf{b}}_1$, $\hat{\mathbf{b}}_2$ and $\hat{\mathbf{b}}_3$.

The plotting output is written to stream 2 (FT02F001 or fort.2), and is in the form of a GHOST trangridfile (a set of integers). At the end of each successful step (iteration), DEV3 writes the number of iterations, the number of function calls, the energy and the latest value of $\mathbf{g}\cdot\mathbf{g}$ to stream 18. Stream 20 output contains the desired and actual distances of the last interstitial (which is usually the migrating atom) from the reference point, plus the energy at the end of each minimisation. Importing this file directly into the IBM Interactive Chart Utility (ICU) provides a quick way to plot graphs of energy against distance along migration direction (like figure 18).

Appendix 2: Formation, binding and migration energies

A2.1 Introduction

This appendix draws together results from earlier chapters of this thesis, so that they are all in one place for easy reference. The first table gives energies of formation, migration and binding to a $\frac{1}{2}\langle 111 \rangle$ dislocation for a vacancy in the five metals studied. The second table provides the same details for interstitials, with additional information on the stable interstitial configurations and the lowest-energy migration paths.

A2.2 Vacancies

The calculation of the vacancy formation energies E_v^f (table 5.3) used a 10×10×10 block (250 free atoms) with periodic boundary conditions. The migration calculations need a slightly larger 12×12×12 block with fixed boundaries (432 free atoms, 1026 fixed atoms); values of E_v^m are taken from table 5.4. In both cases, the block edges are all parallel to the basis cube: i.e. [100], [010] and [001].

The calculation of the binding energy of a vacancy to a dislocation (table 6.2) uses the standard dislocated block: 24×12×24 atom planes, with fixed boundaries in the $\mathbf{b}_1$ [111] and $\mathbf{b}_2$ [$1\bar{1}0$] directions, and periodic boundary conditions applied in the $\mathbf{b}_3$ [$11\bar{2}$] direction. This block contains 1152 free atoms, 1872 fixed atoms and 2268 periodic images.

metal	E_v^f / eV	E_v^m / eV	$E_{v,d}^b$ / eV
V	1.85	0.69	0.85
Nb	2.51	0.85	1.05
Ta	2.91	1.13	1.33
Mo	2.55	1.30	1.07
W	3.63	1.45	1.53

Table A2.1 Calculated vacancy formation, binding and migration energies.

A2.3 Interstitials

The larger relaxations associated with interstitials require larger blocks. The binding energy calculation ($E^b_{i,d}$, table 6.1) takes place in the same sized block as the corresponding vacancy calculation. The migration calculations (E^m_i, table 5.5) also use this block, while the formation calculations (E^f_i, table 3.2) use at least 1024 atoms in a 16×16×16 block with edges parallel to the basis cube: [100], [010] and [001].

Table A2.2 also shows the configuration of the stable interstitials. The 'bent dumbbell' is exhaustively covered in §3.2.2; 'step B' refers to figure 16; and the lowest-energy migration route for a tantalum interstitial is rotation to the ⟨111⟩ split dumbbell, followed by migration along ⟨111⟩ through the crowdion position.

metal	E^f_i / eV	configuration	E^m_i / eV	path	$E^b_{i,d}$ / eV
V	4.16	⟨110⟩ dumbbell	0.29	step B	2.93
Nb	4.47	⟨110⟩ dumbbell	0.22	step B	3.01
Ta	6.83	⟨110⟩ dumbbell	0.31	via ⟨111⟩	5.07
Mo	6.97	bent dumbbell	0.23	step B	4.80
W	8.88	⟨111⟩ crowdion	0.03	⟨111⟩	6.27

Table A2.2 Calculated interstitial formation, migration and binding energies.

References

Ackland, G.J. and Finnis, M.W., 1986, 'Semi-empirical calculation of solid surface tensions in body-centred cubic transition metals', *Phil.Mag.A* **54** 301.

Ackland, G.J. and Thetford, R., 1987, 'An improved *N*–body semi-empirical model for body-centred cubic transition metals', *Phil.Mag.A* **56** 15-30.

Ackland, G.J., 1987, 'Non-pairwise Potentials and Defect Modelling for Transition Metals', D.Phil. Thesis, University of Oxford, 1987.

Ackland, G.J., Finnis, M.W. and Vitek, V., 1988, 'Validity of the second moment tight binding model', *J.Phys.F* **18** L153.

Ackland, G.J. and Vitek, V., 1989, 'Application of Many-body potentials to Noble Metal Alloys', to be published.

Balluffi, R.W., 1978, 'Vacancy defect mobilities and binding energies obtained from annealing studies', *J.Nucl.Mater.* **69/70** 240.

Brailsford, A.D. and Bullough, R., 1972, 'The rate theory of swelling due to void growth in irradiated metals', *J.Nucl.Mater.* **44** 121.

Brailsford, A.D. and Bullough, R., 1973, 'The stress dependence of high temperature swelling', *J.Nucl.Mater.* **48** 87.

Brailsford, A.D., Bullough, R. and Hayns, M.R., 1976, 'Point defect sink strengths and void swelling', *J.Nucl.Mater.* **60** 246.

Brailsford, A.D. and Bullough, R., 1981, 'The theory of sink strengths', *Philosophical Transactions of the Royal Society of London* **302** 87.

Bristowe, P.G., Crocker, A.G. and Norgett, M.J., 1974, 'The Structure of Twin Boundaries in Body Centred Cubic Metals', *J.Phys.F* **4** 1859.

Bullough, R. and Perrin, R.C., 1968, 'The morphology of interstitial aggregates in iron', *Proc.Roy.Soc.A* **305** 541.

Bullough, R. and Willis, J.R., 1984, 'Interactions of point defects and dislocations', *Proc. Eshelby Memorial Symposium,* Sheffield, April 1984 (Cambridge University Press, 1985).

Bullough, R., 1989, private communication.

Car, R., 1989, 'First-principles molecular dynamics simulation of materials', Proc.Int. Workshop on Many-atom Interactions in Solids, Pajulahti, Finland, June 1989, to be published.

Car, R. and Parrinello, M., 1985, 'Unified approach for molecular dynamics and density-functional theory', *Phys.Rev.Lett.* **55** 2471.

Catlow, C.R.A., Corish, J., Jacobs, P.W.M. and Lidiard, A.B., 1981, 'The thermodynamics of characteristic defect parameters', *J.Phys.C* **14** L121.

Damask, A.C. and Dienes, G.J., 1963, 'Point Defects in Metals', chapter 2, Gordon and Breach, New York.

Cawthorne, C. and Fulton, E.J., 1966, 'Voids in irradiated stainless steel', *Nature* **216** 575.

Daw, M.S. and Baskes, M.I., 1984, 'Embedded-atom method: Derivation and application to impurities, surfaces and other defects in metals', *Phys.Rev.B* **29** 6443.

Daw, M.S., 1989, 'Many-atom description of metallic cohesion', *Phys.Rev.B* **39** 7441.

Dederichs, P.H., Lehmann, C., Schober, H.R., Scholz, A. and Zeller, R., 1978, 'Lattice theory of point defects', *J.Nucl.Mater.* **69/70** 176.

Einziger, R.E., Mundy, J.N. and Hoff, H.A., 1978, 'Niobium self-diffusion', *Phys.Rev.B* **17** 440.

Ercolessi, F., Tosatti, E. and Parrinello, M., 1986, 'Au (100) Surface Reconstruction', *Phys.Rev.Lett.* **57** 719.

Ercolessi, F., Parrinello, M. and Tosatti, E., 1988, 'Simulation of gold in the glue model', *Phil.Mag.A* **58** 213.

Ehrhart, P., 1978, 'The configuration of atomic defects as determined from scattering studies', *J.Nucl.Mater.* **69/70** 200.

Evans, J.H., 1983, 'Void and bubble lattice formation in molybdenum: a mechanism based on two-dimensional self-interstitial diffusion', *J.Nucl.Mater.* **119** 180.

Evans, J.H., 1985, 'A computer simulation of the two-dimensional SIA diffusion model for void lattice formation', *J.Nucl.Mater.* **132** 147.

Evans, J.H. and Foreman, A.J.E., 1985, 'Some implications of anisotropic self-interstitial diffusion on void swelling in metals', *J.Nucl.Mater.* **137** 1.

Field, G.J., 1987, 'Problems caused by irradiation deformation in CANDU reactors', Proc.Int.Conf. on Fundamental Mechanisms of Radiation-Induced Creep and Growth, Hecla Island, Manitoba, Canada, June 1987, published as *J.Nucl.Mater.* **159** (1988) 3.

Finnis, M.W. and Sinclair, J.E., 1984, 'A simple empirical *N*–body potential for transition metals', *Phil.Mag.A* **50** 45.

Fletcher, R. and Reeves, C.M., 1964, 'Function minimisation by conjugate gradients', *Comput.J.* **7** 149.

Foiles, S.M., Baskes, M.I., and Daw, M.S., 1986, 'Embedded-atom-method functions for the fcc metals Cu, Ag, Au, Ni, Pd, Pt, and their alloys', *Phys.Rev.B* **33** 7983.

Foreman, A.J.E., 1972, 'A mechanism for the formation of a regular void array in an irradiated metal', Harwell Report AERE-R.7135, HMSO, London.

Frank, W., 1981, 'Point defects and radiation effects in b.c.c. metals', *Proc.Yamada Conf. on Point Defects and Defect Interactions in Metals,* Kyoto, Japan, 1981. Eds. J. Takamura, M. Doyama and M. Kiritani (Univ. of Tokyo Press, 1982) p.203.

Frank, W. and Seeger, A., 1986, 'The role of radiation damage in b.c.c. metals in the point-defect model controversy', Proc.Int.Conf. on Vacancies and Interstitials in Metals and Alloys, Berlin, 1986, published as *Materials Science Forum* **15-18** (1987) 57.

Gillan, M.J., 1989, 'The validity of perturbation theory for simple metals', Proc.Int. Workshop on Many-atom Interactions in Solids, Pajulahti, Finland, June 1989, to be published.

Girifalco, L.A. and Weizer V.G., 1959, 'Application of the Morse Potential Function to Cubic Metals', *Phys.Rev.* **114** 687.

Guinan, M.W., Stuart, R.N. and Borg, R.J., 1977, 'Fully dynamic computer simulation of self-interstitial diffusion in tungsten', *Phys.Rev.B* **15** 699.

Harder, J.M. and Bacon, D.J., 1986, 'Point-defect and stacking-fault properties in body-centred-cubic metals with *n*–body interatomic potentials', *Phil.Mag.A* **54** 651.

Harder, J.M. and Bacon, D.J., 1988, 'The structure of small interstitial clusters in b.c.c. metals modelled with *N*–body potentials', *Phil.Mag.A* **58,** 165.

Harkness, S.D. and Li, C.–Y., 1971, 'A Study of Void Formation in Fast Neutron-Irradiated Metals', *Metall.Trans.,* **2** 1457.

Herzig, C. and Köhler, U., 1986, 'Atomic-defect mechanisms for diffusion in refractory b.c.c. metals', Proc.Int.Conf. on Vacancies and Interstitials in Metals and Alloys, Berlin, 1986, published as *Materials Science Forum* **15-18** (1987) 451.

van Heughten, W.F.W.M., Berg, F.V.D., Caspers, L.M. and van Veen, A., 1978, 'Relaxation of Lattice Atoms around Defects in V, αFe and Mo', *Delft Progress Report* **3** 97.

Hirth, J.P. and Lothe, J., 1968, 'Theory of Dislocations', (McGraw-Hill, New York).

Hönes, D., 1979, Diplomarbeit (dissertation) Stuttgart.

Jacques, H. and Robrock, K.–H., 1981, 'Mechanical relaxation effects of self-interstitial atoms in molybdenum', *Proc.Yamada Conf. on Point Defects and Defect Interactions in Metals,* Kyoto, Japan, 1981. Eds. J. Takamura, M. Doyama and M. Kiritani (Univ. of Tokyo Press, 1982) p.159.

Johnson, R.A., 1964, 'Interstitials and Vacancies in α Iron', *Phys.Rev. A* **134** 1329.

Johnson, R.A., 1972, 'Relationship between Two-Body Interatomic Potentials in a Lattice Model and Elastic Constants', *Phys.Rev.B* **6** 2094.

Johnson, R.A., 1985, 'Two dimensional interstitial migration in the bcc lattice', *J.Nucl.Mater.* **135** 283.

Jurewicz, L.S., 1987, 'Remote repositioning of fuel channels in Bruce A reactors', Trans. 9th Int. Conf. on Structural Mechanics in Reactor Technology, Lausanne, Switzerland, August 1987 (A.A. Balkema, Rotterdam/Boston), volume D pp317-322.

Kirsanov, V.V. and Turkebaev, T.E., 1986, 'Zones of spontaneous absorption of point defects by the edge dislocation', *J.Nucl.Mater.* **140** 264.

Köhler, J.S., 1981, 'Unsolved Problems concerning Point Defects', *Proc.Yamada Conf. on Point Defects and Defect Interactions in Metals,* Kyoto, Japan, 1981. Eds. J. Takamura, M. Doyama and M. Kiritani (Univ. of Tokyo Press, 1982) p.143.

Lidiard, A.B. and Norgett, M.J., 1972, *Computational Solid State Physics* eds. F. Herman, N.W. Dalton and T.R. Köhler (Plenum, New York) pp385-412.

Lucasson, P., Maury, F. and Lucasson, A., 1986, 'On the migration of interstitial defects in irradiated cubic metals', Proc.Int.Conf. on Vacancies and Interstitials in Metals and Alloys, Berlin, 1986, published as *Materials Science Forum* **15-18** (1987) 231.

Maarleveld, P.R., Kaars, P.B., Weeber, A.W. and Bakker, H., 1986, 'Application of the embedded atom method to the calculation of formation enthalpies and lattice parameters of Pd-Ni alloys', *Physica* **142B** 328.

Maier, K., Mehrer, H. and Rein, G., 1979, 'Self-diffusion in molybdenum', *Z.Metallk.* **70** 271.

Maier, K., Peo, M., Saile, B., Schaefer, H.–E. and Seeger, A., 1979, 'High-temperature positron annihilation and vacancy formation in refractory metals', *Phil.Mag. A* **40** 701.

Marchese, M., Jacucci, G. and Flynn, C.P., 1988, 'Isotope effect of vacancy diffusion in b.c.c. α–Fe', *Phil.Mag.Lett.* **57** 25.

Matthai, C.C. and Bacon, D.J., 1985, 'Relaxed vacancy formation and surface energies in the bcc transition metals', *Phil.Mag.A* **52** 1.

Matthews, J.R., 1989, 'The importance of understanding irradiation damage in alloys used in the construction of nuclear power plant components', to be presented to a seminar on the Role of R&D in the Nuclear Industry, 7-8 December, 1989, Institute of Mechanical Engineers (London).

Maysenhölder, W., 1986, 'Lowest-order approximations to relaxation volumes of monovacancies in cubic metals from pair potentials and Finnis-Sinclair potentials', *Phil.Mag.A* **53** 783.

Miller, K.M., 1981, 'Point defect-dislocation interactions in molybdenum', *J.Phys.F* **11** 1175.

Mizubayashi, H. and Okuda, S., 1981, 'Elastic after-effect studies of self-interstitials in tungsten after fast neutron irradiation at 5K', *Rad.Effects* **54** 201.

Mundy, J.N., Ockers, S.T and Smedskjaer, L.C., 1986, 'Vacancy migration enthalpy in tungsten at high temperatures', Proc.Int.Conf. on Vacancies and Interstitials in Metals and Alloys, Berlin, 1986, published as *Materials Science Forum* **15-18** (1987) 199.

Mundy, J.N., Rothman, S.J., Lam, N.Q., Hoff, H.A. and Nowicki, L.J., 1978, 'Self-diffusion in tungsten', *Phys.Rev. B* **18** 6566.

Norgett, M.J., Perrin R.C. and Savino, E.J., 1972, 'Computer Simulation of Edge and Screw Dislocations in Copper', *J.Phys.F* **2** L73.

Nørskov, J.K. and Lang, N.D., 1980, 'Effective-medium theory of chemical binding: Application to chemisorption', *Phys.Rev.B* **21** 2130.

Nørskov, J.K., 1982, 'Covalent effects in the effective-medium theory of chemical binding: Hydrogen heats of solution in the 3*d* metals', *Phys.Rev.B* **26** 2875.

Okuda, S. and Mizubayashi, H., 1981, 'Elastic modulus change in Mo due to Frenkel defects', *Proc.Yamada Conf. on Point Defects and Defect Interactions in Metals,* Kyoto, Japan, 1981. Eds. J. Takamura, M. Doyama and M. Kiritani (Univ. of Tokyo Press, 1982) p.163.

Phillipp, F., Saile, B. and Urban, K., 1981, 'Investigation of vacancy diffusion in niobium, molybdenum and tantalum by means of high-voltage electron microscopy', *Proc.Yamada Conf. on Point Defects and Defect Interactions in Metals,* Kyoto, Japan, 1981. Eds. J. Takamura, M. Doyama and M. Kiritani (Univ. of Tokyo Press, 1982) p.261.

Rebonato, R., Welch, D.O., Hatcher, R.D. and Bilello, J.C., 1987, 'A modification of the Finnis-Sinclair potentials for highly deformed and defective transition metals', *Phil.Mag.A* **55** 655.

Rebonato, R., 1989, 'Adaptation of the Finnis-Sinclair potentials for conditions of extension and for b.c.c. transition metal alloys', *Phil.Mag.B* **60** 325.

Sabochick, M.J., Yip, S. and Lam, N.Q., 1986, 'Calculation of the properties of vacancy clusters in copper using a new, efficient energy minimisation scheme', Proc.Int.Conf. on Vacancies and Interstitials in Metals and Alloys, Berlin, 1986, published as *Materials Science Forum* **15-18** (1987) 857.

Schober, H., Taylor, R., Norgett, M.J. and Stoneham, A.M., 1975, 'Theory of the Diffusion of Heavy Impurities in Alkali Metals', *J.Phys.F* **5** 673.

Schober H.R., 1977, 'Single and multiple interstitials in FCC metals', *J.Phys.F* **7** 1127.

Schultz, H., 1981, 'Atomic defects in b.c.c. metals', *Proc.Yamada Conf. on Point Defects and Defect Interactions in Metals,* Kyoto, Japan, 1981. Eds. J. Takamura, M. Doyama and M. Kiritani (Univ. of Tokyo Press, 1982) p.183.

Schüle, W., 1981, 'On the validity of the One- and the Two-Interstitial Models', *Proc.Yamada Conf. on Point Defects and Defect Interactions in Metals,* Kyoto, Japan, 1981. Eds. J. Takamura, M. Doyama and M. Kiritani (Univ. of Tokyo Press, 1982) p.209.

Siegel, R.W., 1981, 'Atomic defects and diffusion in metals', *Proc.Yamada Conf. on Point Defects and Defect Interactions in Metals,* Kyoto, Japan, 1981. Eds. J. Takamura, M. Doyama and M. Kiritani (Univ. of Tokyo Press, 1982) p.533.

Stott, M.J. and Zaremba, E., 1980, 'Quasiatoms: An approach to atoms in nonuniform electronic systems', *Phys.Rev.B* **22** 1564.

Stroh, A.N., 1962, 'Steady State Problems in Anisotropic Elasticity', *J.Math. and Phys. (Cambridge, Mass., U.S.A.)* **41** 77-103.

Sutton, A.P., 1989, to be published in *Phil.Mag.*

Thetford, R., 1985, 'Application of the DEVIL program to *N*–body potentials', Harwell report AERE-M.3507, HMSO, London.

Thetford, R., 1988, 'Modelling dislocations with DEVIL and *N*–body potentials', Harwell report AERE-M.3697, HMSO, London.

Tietze, M., Takaki, S., Schwirtlich, I.A. and Schultz, H., 1981, 'Quenching investigations on b.c.c. transition metals', *Proc.Yamada Conf. on Point Defects and Defect Interactions in Metals,* Kyoto, Japan, 1981. Eds. J. Takamura, M. Doyama and M. Kiritani (Univ. of Tokyo Press, 1982) p.265.

van Veen, A., 1986, 'Thermal helium desorption spectroscopy (THDS) as a tool for the study of vacancies and self-interstitials', Proc.Int.Conf. on Vacancies and Interstitials in Metals and Alloys, Berlin, 1986, published as *Materials Science Forum* **15-18** (1987) 3.

Vitek, V., Perrin, R.C. and Bowen, D.K., 1970, 'The Core Structure of ½[111] Screw Dislocations in B.C.C. Crystals', *Phil.Mag.* **21** 1049.

Wiedersich, H., 1972, 'On the theory of void formation during irradiation', *Rad.Effects,* **12** 111.

Wollenberger, H.J., 1983, 'Point Defects', in *Physical Metallurgy* eds. R.W. Cahn and P. Haasen (North-Holland, Amsterdam, 1983) pp1139-1221.

Woo, C.H. and Frank W., 1985, 'A Theory of Void-Lattice Formation', *J.Nucl.Mater.* **137** 7.

Young, F.W., Jr., 1978, 'Interstitial mobility and interactions', *J.Nucl.Mater.* **69/70** 310.

Zeper, W.B., 1986, 'Computersimulatie van defekten in molybdeen m.b.v.de 'embedded atom'-methode', dissertation, Technische Hogeschool Delft (in Dutch).

Ziegler, R. and Schaefer, H.E., 1986, 'Vacancy formation in molybdenum and tungsten investigated by positron lifetime measurements', Proc.Int.Conf. on Vacancies and Interstitials in Metals and Alloys, Berlin, 1986, published as *Materials Science Forum* **15-18** (1987) 145.

INDEX